CNWRA *A center of excellence in earth sciences and engineering*

A Division of Southwest Research Institute™
6220 Culebra Road • San Antonio, Texas, U.S.A. 78228-5166
(210) 522-5160 • Fax (210) 522-5155

August 27, 2002
Contract No. NRC–02–97–009
Account No. 20.01402.571

U.S. Nuclear Regulatory Commission
ATTN: Tamara Bloomer
Two White Flint North
11545 Rockville Pike
Mail Stop T7 F3
Washington, DC 20555

Subject: Submittal of Intermediate Milestone—Stress Corrosion Cracking and Hydrogen Embrittlement of Container and Drip Shield Materials, IM 01402.571.240

Dear Ms. Bloomer:

Enclosed is the subject report which documents environmentally assisted cracking of container and drip shield materials, including stress corrosion cracking and hydrogen embrittlement. This report provides a review of the DOE model abstractions and laboratory data on the subject and presents results of experimental work conducted at CNWRA. The CNWRA investigations indicate that Alloy 22 is resistant to stress corrosion cracking in both concentrated chloride solutions and extremely aggressive lead-containing solutions. However, Titanium Grade 7 appears to be susceptible to environmentally assisted cracking in the presence of fluoride. This report also identifies several deficiencies and limitations in the DOE approach and technical bases that are the subjects of existing DOE and NRC agreements.

If you have any questions regarding this report, please feel free to contact Yi-Ming Pan at (210) 522-6640.

Sincerely yours,

Vijay Jain
Element Manager
Corrosion Science & Process Engineering

VJ:jg
Enclosure

cc:	J. Linehan	K. Stablein	A. Campbell	S. Brossia	Y. Pan	D. Gute
	D. DeMarco	B. Leslie	J. Andersen	W. Patrick	L. Yang	
	B. Meehan	S. Wastler	J. Thomas	B. Sagar	D. Dunn	
	E. Whitt	D. Brooks	C. Trottier	G. Cragnolino	O. Pensado	
	W. Reamer	T. McCartin	A. Henry	CNWRA EMs (cvr only)	P. Maldonado	
	J. Greeves	T. Ahn	J. Schlueter	CNWRA Dirs. (cvr only)	T. Nagy (contracts)	

Washington Office • Twinbrook Metro Plaza #210
12300 Twinbrook Parkway • Rockville, Maryland 20852-1606

CNWRA 2002-xx

STRESS CORROSION CRACKING AND HYDROGEN EMBRITTLEMENT OF CONTAINER AND DRIP SHIELD MATERIALS

Prepared for

U.S. Nuclear Regulatory Commission
Contract NRC–02–97–009

Prepared by

Y.-M. Pan
C.S. Brossia
G.A. Cragnolino
D.S. Dunn
G.D. Gute
L. Yang

Center for Nuclear Waste Regulatory Analyses
San Antonio, Texas

August 2002

PREVIOUS REPORTS IN SERIES

Number	Name	Date Issued
CNWRA 91-004	A Review of Localized Corrosion of High-Level Nuclear Waste Container Materials—I	April 1991
CNWRA 91-008	Hydrogen Embrittlement of Candidate Container Materials	June 1991
CNWRA 92-021	A Review of Stress Corrosion Cracking of High-Level Nuclear Waste Container Materials—I	August 1992
CNWRA 93-003	Long-Term Stability of High-Level Nuclear Waste Container Materials: I—Thermal Stability of Alloy 825	February 1993
CNWRA 93-004	Experimental Investigations of Localized Corrosion of High-Level Nuclear Waste Container Materials	February 1993
CNWRA 93-014	A Review of the Potential for Microbially Influenced Corrosion of High-Level Nuclear Waste Containers	June 1993
CNWRA 94-010	A Review of Degradation Modes of Alternate Container Designs and Materials	April 1994
CNWRA 94-028	Environmental Effects on Stress Corrosion Cracking of Type 316L Stainless Steel and Alloy 825 as High-Level Nuclear Waste Container Materials	October 1994
CNWRA 95-010	Experimental Investigations of Failure Processes of High-Level Radioactive Waste Container Materials	May 1995
CNWRA 95-020	Expert-Panel Review of the Integrated Waste Package Experiments Research Project	September 1995
CNWRA 96-004	Thermal Stability and Mechanical Properties of High-Level Radioactive Waste Container Materials: Assessment of Carbon and Low-Alloy Steels	May 1996
CNWRA 97-010	An Analysis of Galvanic Coupling Effects on the Performance of High-Level Nuclear Waste Container Materials	August 1997
CNWRA 98-004	Effect of Galvanic Coupling Between Overpack Materials of High-Level Nuclear Waste Containers—Experimental and Modeling Results	March 1998

PREVIOUS REPORTS IN SERIES (continued)

Number	Name	Date Issued
CNWRA 98-008	Effects of Environmental Factors on Container Life	July 1998
CNWRA 99-003	Assessment of Performance Issues Related to Alternate Engineered Barrier System Materials and Design Options	September 1999
CNWRA 99-004	Effects of Environmental Factors on the Aqueous Corrosion of High-Level Radioactive Waste Containers—Experimental Results and Models	September 1999
CNWRA 2000-06 Revision 1	Assessment of Methodologies to Confirm Container Performance Model Predictions	January 2001
CNWRA 2001-003	Effect of Environment on the Corrosion of Waste Package and Drip Shield Materials	September 2001
CNWRA 2002-01	Effect of In-Package Chemistry on the Degradation of Vitrified High-Level Radioactive Waste and Spent Nuclear Fuel Cladding	October 2001
CNWRA 2002-02	Evaluation of Analogs for the Performance Assessment of High-level Waste Container Materials	March 2002
CNWRA 2002-xx	Passive Dissolution of Container Materials—Modeling and Experiments	August 2002

ABSTRACT

Long lifetimes of the waste package and the drip shield, the two main components of the engineered barrier subsystem, are identified by the U.S. Department of Energy (DOE) as key system attributes for the performance of the proposed high-level waste repository at Yucca Mountain, Nevada. Environmentally assisted cracking of container and drip shield materials, including stress corrosion cracking and hydrogen embrittlement, is considered an important degradation process that may influence the lifetimes of the waste package and the drip shield. In support of the U.S. Nuclear Regulatory Commission (NRC) prelicensing activities on issues important to the postclosure performance of the proposed repository, the Center for Nuclear Waste Regulatory Analyses (CNWRA) is conducting an independent technical assessment of the environmentally assisted cracking susceptibility of engineered barrier materials. This report presents results of the CNWRA experimental work, as well as a review of the DOE model abstractions, in the areas of stress corrosion cracking of Alloy 22, including the effects of minor species in the groundwater, and environmentally assisted cracking of titanium alloys. The CNWRA investigations indicate that Alloy 22 is resistant to stress corrosion cracking in both concentrated chloride solutions and extremely aggressive $PbCl_2$ solutions, whereas Titanium Grade 7 appears to be susceptible to environmentally assisted cracking in the presence of fluoride. Several deficiencies and limitations of the DOE approach are identified for stress corrosion cracking of the Alloy 22 outer container and environmentally assisted cracking of the Titanium Grade 7 drip shield. The effects of waste package environments (including minor environmental species), fabrication and welding, compositional variation, and thermal aging on stress corrosion cracking of Alloy 22, as well as the possible detrimental effect of fluoride on hydrogen-induced cracking of Titanium Grade 7, need to be properly considered. These concerns have been addressed in the DOE and NRC agreements, and DOE has provided a path forward for resolving all the deficiencies and limitations identified in this report at the time of the License Application.

CONTENTS

Section Page

PREVIOUS REPORTS IN SERIES ii
ABSTRACT v
FIGURES ix
TABLES xi
ACKNOWLEDGMENTS xiii
EXECUTIVE SUMMARY xv

1 INTRODUCTION 1-1

1.1 Objective 1-1
1.2 Scope and Organization of the Report 1-2
1.3 Relevant DOE and NRC Agreements 1-3

2 STRESS CORROSION CRACKING OF CONTAINER MATERIALS 2-1

2.1 The DOE Investigations 2-1
2.1.1 Stress Corrosion Cracking 2-2
2.1.2 The DOE Model Abstraction 2-6
2.1.3 Assessment of the DOE Approach 2-11
2.2 The CNWRA Investigations 2-15
2.2.1 Stress Corrosion Cracking Test Methods 2-15
2.2.2 Stress Corrosion Cracking Test Results 2-20
2.3 Summary 2-31

3 EFFECT OF MINOR SPECIES ON STRESS CORROSION CRACKING OF CONTAINER MATERIALS 3-1

3.1 State of Nevada Investigations 3-2
3.2 The DOE Investigations 3-3
3.3 The CNWRA Investigations 3-4
3.3.1 Lead-Speciation Calculations 3-4
3.3.2 Polarization Behavior 3-6
3.3.3 Stress Corrosion Cracking Susceptibility 3-14
3.4 Summary 3-15

4 ENVIRONMENTALLY ASSISTED CRACKING OF DRIP SHIELD MATERIALS . . . 4-1

4.1 The DOE Investigations 4-3
4.1.1 Environmentally Assisted Cracking 4-3
4.1.2 The DOE Model Abstraction 4-5
4.1.3 Assessment of the DOE Approach 4-6
4.2 The CNWRA Investigations 4-8
4.3 Summary 4-13

CONTENTS (continued)

Section Page

5 SUMMARY, CONCLUSIONS, AND RECOMMENDATIONS 5-1

5.1 Stress Corrosion Cracking of Container Materials 5-1
5.2 Effect of Minor Species on Stress Corrosion Cracking of Container Materials 5-2
5.3 Environmentally Assisted Cracking of Drip Shield Materials 5-3
5.4 Future Work 5-4

6 REFERENCES 6-1

FIGURES

Figure		Page
2-1	Dimensions of the Double Cantilever Beam Specimens According to NACE TM0177–96	2-16
2-2	Dimensions of the Compact Tension Specimens	2-17
2-3	Crack Growth Rate for Type 316L SS as a Function of Potential in Concentrated Chloride Solutions Using Double Cantilever Beam	2-20
2-4	Change in Crack Opening Displacement and Compliance Ratio as a Function of Potential for Type 316L SS Compact Tension Specimens	2-21
2-5	Scanning Electron Micrographs at (a) 200× and (b) 2000× Showing the Fracture Surface of Type 316L SS After Testing at −400 mV_{SCE}	2-22
2-6	Change in Crack Opening Displacement and Compliance Ratio as a Function of Initial Stress Intensity for Type 316L SS Compact Tension	2-23
2-7	Scanning Electron Micrographs at (a) 200× and (b) 500× Showing the Fracture Surface of Type 316L SS After Testing at −350 mV_{SCE}	2-23
2-8	Change in Crack Opening Displacement and Compliance Ratio for a Type 316L SS Compact Tension Specimen Tested in 9.1 molal LiCl	2-24
2-9	Scanning Electron Micrographs at (a) 200× and (b) 500× Showing Fracture Surface of Type 316L SS After Testing at −350 mV_{SCE} in 9.1 molal LiCl	2-25
2-10	Change in Crack Opening Displacement and Compliance Ratio for a Type 316L SS Compact Tension Specimen Tested in 9.1 molal LiCl	2-25
2-11	Change in Crack Opening Displacement and Compliance Ratio for a Type 316L SS Compact Tension Specimen Tested in 9.1 molal LiCl	2-26
2-12	Change in Crack Opening Displacement and Compliance Ratio for Alloy 22 Compact Tension Specimens Tested in 9.1 molal LiCl	2-29
2-13	Change in Crack Opening Displacement and Compliance Ratio for Alloy 22 Compact Tension Specimens Tested in 9.1 molal LiCl	2-30
3-1	Molar Percent of Dissolved Lead Species in Lead-Acetate Solutions for a Total Dissolved Lead of 1,600 parts per million at 25 °C [77 °F]	3-5
3-2	Molar Percent of Dissolved Lead Species in $PbCl_2$ Solutions for a Total Dissolved Lead of 1,600 parts per million at 25 °C [77 °F]	3-6
3-3	Effect of Lead on the Anodic Polarization Behavior of Alloy 22 Compared to That in a Lead-Free Solution at 95 °C [203 °F]	3-8
3-4	Effect of Lead on the Anodic Polarization Behavior of Platinum Compared to That in a Lead-Free Solution at 95 °C [203 °F]	3-9
3-5	Effect of Lead Concentration on the Anodic Polarization Behavior of Alloy 22 in $PbCl_2$ Solutions at 95 °C [203 °F]	3-9
3-6	Photograph Comparing Surface Features of Alloy 22 Crevice Specimens After Potentiodynamic Polarization Runs in Supersaturated $PbCl_2$	3-10
3-7	Scanning Electron Micrographs on Alloy 22 Crevice Specimen After Potentiodynamic Polarization Run in a Supersaturated $PbCl_2$ Solution	3-11
3-8	Anodic Current Density and Total Charge as a Function of Time Measured on Alloy 22 at −100 mV_{SCE} in a Supersaturated $PbCl_2$ Solution	3-12
3-9	Scanning Electron Micrographs on Surface Attack of Alloy 22 Tested in a Supersaturated $PbCl_2$ Solution at 95 °C [203 °F]	3-13

FIGURES (continued)

Figure		Page
3-10	Photograph Comparing Surface Features of Alloy 22 Single U-Bend Specimens Tested at −100 mV_{SCE} in a Supersaturated $PbCl_2$ Solution	3-16
3-11	Scanning Electron Micrographs of Alloy 22 Single U-Bend Specimens Tested at −100 mV_{SCE} in a Supersaturated $PbCl_2$ Solution	3-17
4-1	Scanning Electron Micrographs on Fracture Surfaces of Titanium Slow Strain Rate Specimens Tested in Fluoride-Chloride Solution	4-11
4-2	Scanning Electron Micrographs on Fracture Surfaces of Titanium Slow Strain Rate Specimens Showing Brittle Fracture Features	4-12

TABLES

Table		Page
1-1	DOE and NRC Agreements Related to This Report	1-3
2-1	Compositions of Several Aqueous Solutions Used for Corrosion Testing	2-3
2-2	Recipe for Basic Saturated Water	2-4
2-3	Crack Propagation Rates Measured on Alloy 22 Compact Tension Specimens	2-7
2-4	Compositions of Type 316L SS and Alloy 22 Used in Stress Corrosion Cracking Tests	2-16
3-1	Chemical Composition of the Heats of Alloy 22 Used in the State of Nevada Investigation	3-3
3-2	Chemical Composition of the Heats of Alloy 22 Used in This Study	3-7
3-3	Anodic Polarization Test Matrix	3-7
3-4	Chemical Composition from Surface Regions of Alloy 22 Tested in a Supersaturated $PbCl_2$ Solution at 95 °C [203 °F] Applying −100 mV_{SCE}	3-14
3-5	Results of Stress Corrosion Cracking Tests of Alloy 22 U-Bend Specimens in $PbCl_2$ Solutions	3-15
4-1	Nominal Compositions and Mechanical Properties for Titanium Alloys of Possible Use in the Proposed Repository	4-3
4-2	Chemical Composition of the Titanium Alloys Used in This Study	4-8
4-3	Results of Slow Strain Rate Tests of Titanium Alloys in Chloride Solutions	4-9

ACKNOWLEDGMENTS

This report was prepared to document work performed by the Center for Nuclear Waste Regulatory Analyses (CNWRA) for the U.S. Nuclear Regulatory Commission (NRC) under Contract No. NRC–02–97–009. The activities reported here were performed on behalf of the NRC Office of Nuclear Material Safety and Safeguards, Division of Waste Management. The report is an independent product of the CNWRA and does not necessarily reflect the views or regulatory position of the NRC.

The authors gratefully acknowledge V. Jain for technical review, the programmatic review of W. Patrick, and the editorial reviews of C. Cudd, B. Long, and A. Woods. Appreciation is due J. Gonzalez for assistance in preparing this report.

QUALITY OF DATA: Sources of data are referenced in each chapter. CNWRA-generated laboratory data contained in this report meet quality assurance requirements described in the CNWRA Quality Assurance Manual. Data from other sources, however, are freely used. The respective sources of non-CNWRA data should be consulted for determining levels of quality assurance. Experimental data have been recorded in CNWRA scientific notebook numbers 149, 288, 438, and 465.

ANALYSES AND CODES: The OLI Systems Environmental Simulation Program Version 6.5 (OLI Systems, Inc., 2001) was used for the speciation calculations presented in this report. This code is controlled by the requirements of CNWRA Technical Operating Procedure (TOP)–018. Detailed speciation calculations can be found in CNWRA scientific notebook number 430.

REFERENCE:

OLI Systems, Inc. "Environmental Simulation Program." Version 6.5. Morris Plain, New Jersey: OLI Systems, Inc. 2001.

EXECUTIVE SUMMARY

Performance of the engineered barriers after waste emplacement is extremely important to protect the public from any undue long-term risk, as recognized by the U.S. Department of Energy (DOE) in its Repository Safety Strategy for the proposed Yucca Mountain repository. As stated in 10 CFR Part 63, the engineered barrier subsystem must be designed so that, working in combination with natural barriers, radiological exposures to the reasonably maximally exposed individual and release of radionuclides into the accessible environment are limited, as specified in 10 CFR 63.311. For these reasons, performance of both the waste package and the drip shield, the two main components of the engineered barrier subsystem, are noted by DOE among the principal factors for the postclosure safety case. Environmentally assisted cracking of container and drip shield materials, including stress corrosion cracking and hydrogen embrittlement, is considered an important degradation process that may influence the lifetimes of the waste package and the drip shield. These degradation modes of the waste package and the drip shield are considered in Subissues 1 and 6 of the Container Life and Source Term Key Technical Issue. Through the process of prelicensing consultation for issue resolution between DOE and the U.S. Nuclear Regulatory Commission (NRC), these two subissues are considered closed-pending according to the DOE and NRC agreements. DOE agreed to provide additional information pertaining to each agreement for the NRC staff to have all the information needed for regulatory decision making at the time of the License Application.

In support of the NRC prelicensing activities on topics important to the postclosure performance of the proposed repository, the Center for Nuclear Waste Regulatory Analyses (CNWRA) is conducting an independent technical assessment of the environmentally assisted cracking susceptibility of engineered barrier materials. This report provides a review of the DOE model abstractions and laboratory data in the areas of stress corrosion cracking of Alloy 22 (Ni-22Cr-13Mo-4Fe-3W), including evaluation of the effects of minor environmental species, and environmentally assisted cracking of titanium alloys, and presents results of more recent experimental work conducted at CNWRA.

The DOE evaluation of flaw sizes and distributions, residual stresses as a result of fabrication processes, and stress mitigation methods is supported by many assumptions that need to be verified. The present models are not based on the current waste package design or fabrication method. Verification of important assumptions, such as residual stresses after solution annealing and quenching of the disposal container, stress profiles after laser peening, and induction annealing, is necessary to determine the adequacy of the DOE assessment. Tests performed by DOE indicate that Alloy 22 is resistant to chloride stress corrosion cracking. For conditions where stress corrosion cracking has been initiated, the crack propagation rates are low, and crack propagation ceases below the critical stress intensity for stress corrosion cracking. The effects of potential and solution chemistries on stress corrosion cracking susceptibility have been explored mainly using slow strain rate tests, but these variables have not been evaluated for crack propagation rates or critical stress intensities for stress corrosion cracking. The DOE models for stress corrosion crack initiation and propagation do not consider the important effects of environmental composition and potential.

CNWRA conducted experiments to evaluate the stress corrosion cracking susceptibility of Alloy 22 and Type 316L SS (Fe-18Cr-12Ni-2.5Mo) in concentrated chloride solutions. Type 316L SS was found susceptible to stress corrosion cracking when the potential of the

specimen was above the crevice corrosion repassivation potential. In contrast, the initiation of stress corrosion cracking was prevented when the potential was less than the crevice corrosion repassivation potential. When the potential of the specimen was reduced below the repassivation potential after crack initiation and propagation, the crack propagation rate was substantially reduced, as implied by changes in the crack opening displacement and compliance. It is not possible, however, to conclude that stress corrosion cracking is completely arrested when the specimen potential is reduced below the repassivation potential because the sensitivity of the crack growth rate measurements is limited to 3.3×10^{-9} mm/s [1.3×10^{-10} in/s]. In these studies, Alloy 22 was found resistant to stress corrosion cracking in concentrated chloride solutions. No conclusive determination of Alloy 22 stress corrosion cracking susceptibility could be made from the results of the tests conducted in this investigation. Additional tests in progress will help to establish the relationship between the crevice corrosion repassivation potential and the stress corrosion cracking susceptibility of Alloy 22. The effects of variations in the environmental composition and fabrication effects on the stress corrosion cracking susceptibility of Alloy 22 need to be investigated. DOE agreed to provide additional information in agreements CLST 1.12 through 1.16 to address the effects of waste package environments, fabrication and welding, compositional variation, and thermal aging on stress corrosion cracking of Alloy 22. The technical basis for crack plugging and crack arrest that may alter the release of radionuclides arising from stress corrosion cracking will be provided according to agreement TSPAI 3.03.

Studies sponsored by the State of Nevada indicated that the resistance of Alloy 22 to localized corrosion and stress corrosion cracking may be affected by the presence of impurities such as lead, mercury, and arsenic in the water contacting the waste packages. The role of minor species in the groundwater, however, has not been adequately considered by DOE. The DOE analysis thus far has only reported limited data on stress corrosion cracking of Alloy 22 in lead-containing environments. The test solutions used in both the DOE and the State of Nevada investigations were not properly characterized in terms of the lead speciation. Furthermore, the preliminary result from the State of Nevada investigations on stress corrosion cracking testing of Alloy 22 could not be reproduced by the same investigators.

CNWRA performed thermodynamic calculations to evaluate the speciation of lead in lead-containing solutions. Speciation calculations revealed the formation of free Pb^{2+} cations and Pb-Cl complexes in $PbCl_2$ solutions. An experimental investigation was conducted to determine the susceptibility of Alloy 22 to localized corrosion and stress corrosion cracking in a range of lead-containing solutions. The presence of lead promotes a pronounced anodic oxidation peak and simultaneously enhances the dissolution of Alloy 22 characterized by randomly distributed etch pits on a crevice specimen. At an applied potential of -100 mV_{SCE}, which is a potential corresponding to the anodic oxidation peak, Alloy 22 was found resistant to stress corrosion cracking when tested in supersaturated $PbCl_2$ solutions at 95 °C [203 °F]. These results suggest that Alloy 22 is resistant to stress corrosion cracking in supersaturated $PbCl_2$ solutions even at the extremely high lead concentrations and low pH used in the tests. Moreover, no deleterious effect of lead species on localized corrosion was observed in crevice specimens for a wide range of lead concentrations with the exception of the supersaturated $PbCl_2$ solutions. These preliminary results suggest that, provided these high lead concentrations are not attainable in the anticipated repository environments, Alloy 22 is unlikely to be susceptible to stress corrosion cracking or localized corrosion. DOE agreed to provide additional information in agreements CLST 1.01 and CLST 1.10 on the range of concentrations of minor species expected to evolve in Yucca Mountain waters and their effects on the critical

potential for localized corrosion. Although it is not explicitly stated in agreement CLST 1.12, additional information should be provided by DOE if stress corrosion cracking of Alloy 22 in the presence of lead contamination is confirmed for realistic repository conditions.

DOE considered the primary environmentally assisted cracking process for the titanium drip shield is caused by hydrogen absorption leading to hydride embrittlement. DOE evaluated the susceptibility of the drip shield to hydrogen-induced cracking using a critical threshold hydrogen concentration of 1,000 parts per million as a criterion for failure and concluded that hydrogen-induced cracking is not a limiting degradation process affecting function of the drip shield. This analysis was based on the corrosion rate measured from weight loss of coupons to calculate the hydrogen generated by the associated cathodic reaction and on the assumptions involved in the estimation of the fraction of hydrogen absorbed into the metal. The critical hydrogen concentration chosen needs to be evaluated further for Titanium Grade 7 (Ti-0.15Pd) because it is based on the results for a different titanium alloy. Reliance on the corrosion rates measured from weight loss may lead to a nonconservative estimate of the quantity of hydrogen absorbed. Furthermore, the possible detrimental effects of fluoride on hydrogen uptake, and its effects on subsequent hydrogen-induced cracking, have not been evaluated. The susceptibility of Titanium Grade 7 to stress corrosion cracking in basic saturated water should be fully evaluated by DOE.

CNWRA performed limited experiments to evaluate the environmentally assisted cracking susceptibility of Titanium Grade 7 and other titanium alloys in the presence of fluoride using the slow strain rate test method. Preliminary results indicated that the presence of fluoride may lead to an enhanced susceptibility to environmentally assisted cracking. The critical threshold hydrogen concentration and the fraction of hydrogen absorbed considering the catalytic properties of palladium for hydrogen generation need to be experimentally determined or justified by DOE to validate the anticipated performance of the drip shield. DOE agreed to provide additional information on the selection of values of the critical hydrogen concentration and the assumed range of corrosion rates and fraction of hydrogen absorption, as well as the effects of fluoride for environmentally assisted cracking of the drip shield in agreements CLST 6.01 through 6.03 and the effect of rockfall or drift collapse on environmentally assisted cracking of the drip shield in agreement CLST 2.08.

Evaluation of the susceptibility of Alloy 22 and Titanium Grade 7 to stress corrosion cracking and environmentally assisted cracking is necessary to assess the lifetimes of the waste package and the drip shield. This report identifies several deficiencies and limitations in the current DOE approach and technical bases for modeling stress corrosion cracking of the Alloy 22 outer container and environmentally assisted cracking of the titanium drip shield. The effects of waste package environments (including minor environmental species), fabrication and welding, compositional variation, and thermal aging on stress corrosion cracking of Alloy 22, as well as the possible detrimental effects of fluoride on hydrogen-induced cracking of Titanium Grade 7 are being considered by DOE according to the DOE and NRC agreements. DOE provided a path forward for resolving these concerns. Additional confirmatory analyses are planned to further evaluate the information to be provided by DOE and determine the potential associated risk insight. These analyses include stress corrosion cracking and hydrogen-induced cracking experiments and metallurgical stability simulations that consider changes in repository environments, compositional variations, and fabrication processes. Moreover, risk-insight evaluations are planned to demonstrate the consequences of these technical concerns using performance calculations and sensitivity analyses.

1 INTRODUCTION

Performance of the engineered barriers after waste emplacement is extremely important to protect the public from any undue long-term risk, as recognized by the U.S. Department of Energy (DOE) in its Repository Safety Strategy for the proposed Yucca Mountain repository (CRWMS M&O, 2000a). As an independent regulatory agency, the U.S. Nuclear Regulatory Commission (NRC) has published licensing criteria for disposal of high-level wastes in the proposed repository. According to 10 CFR Part 63, the engineered barrier subsystem must be designed so that, working in combination with natural barriers, radiological exposures to the reasonably maximally exposed individual and release of radionuclides into the accessible environment are limited, as specified in 10 CFR 63.311. For these reasons, the performance of both the waste package and the drip shield, the two main components of the engineered barrier subsystem, are noted by DOE among the principal factors for the postclosure safety case (CRWMS M&O, 2000a). The reference waste package design in the DOE site recommendation (CRWMS M&O, 2000b) consists of a 2-cm [0.79-in] thick outer container made of a highly corrosion-resistant Ni-Cr-Mo alloy, Alloy 22 (Ni-22Cr-13Mo-4Fe-3W), and a 5-cm [1.97-in] thick inner container made of Type 316 nuclear grade stainless steel (low C-high N-Fe-18Cr-12Ni-2.5Mo). Additionally, an inverted U-shaped drip shield, fabricated with Titanium Grade 7 (Ti-0.15Pd), will be extended the length of the emplacement drifts to enclose the top and sides of the waste packages. For undisturbed repository conditions, corrosion is expected to be the primary degradation process limiting the life of the waste package and the drip shield. Loss of containment as a result of corrosion will allow the release of radionuclides to the environment surrounding the waste packages.

The corrosion-related processes considered important in the degradation of the waste package and the drip shield include dry-air oxidation, humid-air and uniform aqueous (general) corrosion, localized (pitting, crevice, and intergranular) corrosion, microbially influenced corrosion, stress corrosion cracking, and hydrogen embrittlement. Of these corrosion processes, stress corrosion cracking is one of the most insidious forms of metal failure because it usually occurs in metal and alloys that are extremely resistant to uniform corrosion as a result of the formation of a film on the metal surface that slows down the corrosion rate. Numerous stress corrosion cracking failures have been observed in many industries, including the nuclear power industry. This report focuses on the environmentally assisted cracking of container and drip shield materials, including stress corrosion cracking and hydrogen embrittlement, which is considered by DOE an important degradation process that may strongly influence the lifetimes of the waste package and the drip shield (CRWMS M&O, 2000c,d).

1.1 Objective

In support of the NRC prelicensing activities on topics important to the postclosure performance of the proposed repository, the Center for Nuclear Waste Regulatory Analyses (CNWRA) is conducting an independent technical assessment of the environmentally assisted cracking susceptibility of engineered barrier materials. A summary of the environmental effects and the effect of alloying elements on corrosion and stress corrosion cracking/environmental assisted cracking of nickel- and titanium-based alloys is provided in Cragnolino, et al. (1999). In addition, previous experimental work on the effects of environmental factors and potential on stress corrosion cracking of Alloys 22 and 825 and Type 316L SS in chloride solutions have been reported (Pan, et al., 2000; Dunn, et al., 1999; Cragnolino, et al., 1994). This report

provides a review of the DOE model abstractions of stress corrosion cracking of Alloy 22, including the effects of minor environmental species, and environmentally assisted cracking of titanium alloys, and presents results of more recent experimental work conducted at CNWRA.

1.2 Scope and Organization of the Report

Corrosion processes potentially important in the degradation of the engineered barriers have been reviewed in the Integrated Issue Resolution Status Report (NRC, 2002) and are the subject of Subissues 1 and 6 of the Container Life and Source Term Key Technical Issue (NRC, 2001). Stress corrosion cracking is one failure mode of the Alloy 22 outer container, which could lead to early through-wall penetration of the waste package. Several limitations and deficiencies in the DOE approach and in the technical bases provided for the evaluation of stress corrosion cracking of the waste package have been identified by NRC (2002). The limitations refer to the models adopted by DOE, whereas the main deficiencies are related to the lack of an adequate database supporting these models. The DOE approach to evaluate environmentally assisted cracking of the drip shield considers stress corrosion cracking and hydride-induced cracking as two separate mechanisms. Environmentally assisted cracking of titanium alloys in aqueous environments occurs primarily through a hydrogen embrittlement-type mechanism that is caused by hydrogen absorption and hydride precipitation. Stress corrosion cracking caused by residual stresses, combined with applied stresses as a result of rockfall in the presence of an aqueous environment, could also lead to failure of the drip shield, thus affecting its capability for diverting seepage water away from the waste package surface. Therefore, susceptibilities of the waste package and the drip shield to environmental assisted cracking, regardless of the mechanism involved, need to be evaluated to determine their lifetimes.

This report is organized into five chapters including an introduction in Chapter 1. The issues related to stress corrosion cracking susceptibility of the Alloy 22 waste package outer container are discussed in Chapter 2. An overview of the DOE program to adapt and develop abstracted models for stress corrosion cracking and to evaluate the effects of possible waste package environments and welding residual stresses on stress corrosion cracking of Alloy 22 is provided, as well as an assessment of the model approach and parameters used. Experimental work at CNWRA to evaluate the effects of applied potential and environmental factors on the stress corrosion cracking of Alloy 22 and Type 316L SS using fracture mechanics specimens is also reported in Chapter 2. Chapter 3 addresses possible detrimental effects of impurities present in the groundwater, such as lead, mercury, and arsenic, on corrosion and stress corrosion cracking of Alloy 22. A discussion of the State of Nevada and the DOE investigations to evaluate the effect of such impurities on the stress corrosion cracking susceptibility of Alloy 22 is provided. The CNWRA analyses to evaluate lead solution chemistry and the effect of lead on the anodic polarization behavior and stress corrosion cracking of Alloy 22 are then discussed. Chapter 4 highlights the environmentally assisted cracking of titanium alloys as a drip shield material. A brief description of the DOE models to evaluate hydrogen-induced cracking of the Titanium Grade 7 drip shield and an assessment of the DOE approach are also provided in Chapter 4. The CNWRA experiments to evaluate the environmentally assisted cracking susceptibility of titanium alloys are then discussed. A summary of conclusions and recommendations for future work to provide technical assistance needed to support the resolution of these closed-pending subissues prior to the License Application is included in Chapter 5.

1.3 Relevant DOE and NRC Agreements

As noted, degradation processes of the waste package and the drip shield are considered in Subissues 1 and 6 of the Container Life and Source Term Key Technical Issue (NRC, 2001), and incorporated in the Degradation of Engineering Barriers Integrated Subissue (NRC, 2002). Through the process of prelicensing consultation for issue resolution between DOE and NRC, these two subissues are considered closed-pending according to the DOE and NRC agreements. Agreements pertaining to stress corrosion cracking and environmentally assisted cracking of container and drip shield materials are listed in Table 1-1. According to the agreements for resolving all deficiencies and limitations identified in this report, DOE agreed to provide additional information prior to License Application.

Table 1-1. DOE and NRC Agreements Related to This Report

Agreement	Agreement Statement
CLST 1.01*	Provide the documentation for Alloy 22 and titanium for the path forward items listed on slide 8 [establish credible range of brine water chemistry; evaluate effect of introduced materials on water chemistry; determine likely concentrations and chemical form of minor constituents in YM waters; characterize YM waters with respect to the parameters which define the type of brine which would evolve; evaluate periodic water drip evaporation] DOE will provide the documentation in a revision to AMR "Environment on the Surfaces of the Drip Shield and Waste Package Outer Barrier" by LA.
CLST 1.10*	Provide the documentation for Alloy 22 and titanium for the path forward items listed on slide 21 and 22 [measure corrosion potentials in the LTCTF to determine any shift of potential with time toward the critical potentials for LC; determine critical potentials on welded and welded and aged coupons of Alloy 22 vs those for base metal—particularly important if precipitation or severe segregation of alloying elements occurs in the welds; separate effects of ionic mix of specimens in YM waters on critical potentials—damaging species from potentially beneficial species; determine critical potentials in environments containing heavy metal concentrations] DOE will provide the documentation in a revision to AMRs (ANL–EBS–MD–000003 and ANL–EBS–MD–000004) prior to LA.

Table 1-1. DOE and NRC Agreements Related to This Report (continued)	
Agreement	**Agreement Statement**
CLST 1.12*	Provide the documentation for Alloy 22 and titanium for the path forward items listed on slides 34 and 35. [qualify and optimize mitigation processes; generate SCC data for mitigated material over full range of metallurgical conditions; new vessels for LTCTF will house many of the SCC specimens; continue SSRT in same types of environments as above, specimens in the same range of metallurgical conditions; determine repassivation constants needed for film rupture SCC model to obtain value for the model parameter 'n'; continue reversing direct current potential drop crack propagation rate determinations in same types of environments and same metallurgical conditions as for SSRT and LTCTF tests; evaluate SCC resistance of welded and laser peened material vs non-welded unpeened material; evaluate SCC resistance in induction annealed material; evaluate SCC resistance of full thickness material obtained from the demonstration prototype cylinder of Alloy 22] DOE will provide the documentation in a revision to AMRs (ANL–EBS–MD–000005 and ANL–EBS–MD–000006) prior to LA.
CLST 1.13*	Provide the data that characterizes the distribution of stresses due to laser peening and induction annealing of Alloy 22. DOE will provide the documentation in a revision to AMR (ANL–EBS–MD–000005) prior to LA.
CLST 1.14*	Provide the justification for not including the rockfall effect and deadload from drift collapse on SCC of the waste package and drip shield. DOE will provide the documentation for the rockfall and dead-weight effects in the next revision of the SCC AMR (ANL–EBS–MD–000005) prior to LA.
CLST.1 15*	Provide the documentation for Alloy 22 and titanium for the path forward items listed on slide 39 [install specimens cut from welds of SR design mockup in LTCTF and in other SCC test environments—determine which specimen geometry is most feasible to complement SCC evaluation; evaluate scaling and weld process factors between thin coupons and dimensions in actual welded waste package containers—including thermal/metallurgical structural effects of multi-pass weld processes; provide representative weld test specimens for MIC work, thermal aging and localized corrosion evaluations] DOE will provide documentation for Alloy 22 and Ti path forward items on slide 39 in a revision to the SCC and general and localized corrosion AMRs (ANL–EBS–MD–000003, ANL–EBS–MD–000004, ANL–EBS–MD–000005) by LA.
CLST 1.16*	Provide the documentation on the measured thermal profile of the waste package material due to induction annealing. DOE stated that the thermal profiles will be measured during induction annealing, and the results will be reported in the next SCC AMR (ANL–EBS–MD–000005) prior to LA.

Table 1-1. DOE and NRC Agreements Related to This Report (continued)	
Agreement	**Agreement Statement**
CLST 2.08*	Provide documentation of the path forward items in the "Subissue 2: Effects of Phase Instability of Materials and Initial Defects on the Mechanical Failure and Lifetime of the Containers" presentation, slide 16 [future rockfall evaluations will address (1) effects of potential embrittlement of WP closure material after stress annealing due to aging, (2) effects of drip shield wall thinning due to corrosion; (3) effects of hydrogen embrittlement on titanium drip shield; and (4) effects of multiple rock blocks falling on WP and drip shield; future seismic evaluations will address the effects of static loads from fallen rock on drip shield during seismic events] DOE stated that the rockfall calculations addressing potential embrittlement of the waste package closure weld and rock falls of multiple rock blocks will be included in the next revision of the AMR ANL–UDC–MD–000001, Design Analysis for UCF Waste Packages, to be completed prior to LA. Rock fall calculations addressing drip shield wall thinning due to corrosion, hydrogen embrittlement of titanium, and rock falls of multiple rock blocks will be included in the next revision of the AMR ANL–XCS–ME–000001, Design Analysis for the Ex-Container Components, to be completed prior to LA. Seismic calculations addressing the load of fallen rock on the drip shield will be included in the next revision of the AMR ANL–XCS–ME–000001, Design Analysis for the Ex-Container Components, to be completed prior to LA.
CLST 6.01*	Provide documentation for the path forward items in the "Subissue 6: Alternate EBS Design Features—Effect on Container Lifetime" presentation, slides 7 and 8 [perform more sensitivity measurements of general corrosion rates—same approach as taken for Alloy 22; confirm no deleterious effects of fluoride ion and trace heavy metal ions in water on corrosion behavior of titanium—similar approach to that taken in electrochemically based studies on Alloy 22; establish damaging hydrogen levels in titanium alloys—Grade 2 vs Grades 7 and 16 vs Grade 5 and 24—evaluate hydrogen charged notched tensile speciems and hydrogen pickup of galvanically coupled LTCTF specimens; conduct SCC testing of titanium, similar to approach taken for Alloy 22; confirm intergranular or internal oxidation of titanium is not applicable under YM thermal and environmental conditions] DOE stated that the documentation of the path forward items will be completed and as results become available, they will documented in the revisions of AMRs (ANL–EBS–MD–000005, Stress Corrosion Cracking of the Drip Shield, the Waste Package Outer Barrier and the Stainless Structural Material, and ANL–EBS–MD–000004, General Corrosion and Localized Corrosion of the Drip Shield), to be completed by LA.

Table 1-1. DOE and NRC Agreements Related to This Report (continued)	
Agreement	**Agreement Statement**
CLST 6.02*	Provide additional justification for the use of a 400 ppm hydrogen criterion or perform a sensitivity analysis using a lower value. DOE stated that additional justification will be found in the report "Review of Expected Behaviour of Alpha Titanium Alloys under Yucca Mountain Condition" TDR–EBS–MD–000015, which is in preparation and will be available in January 2001.
CLST 6.03*	Provide the technical basis for the assumed fraction of hydrogen absorbed into titanium as a result of corrosion. DOE stated that additional justification will be found in the report "Review of Expected Behaviour of Alpha Titanium Alloys under Yucca Mountain Condition" TDR–EBS–MD–000015, which is in preparation and will be available in January 2001.
TSPAI 3.03†	Provide the technical basis for crack arrest and plugging of crack openings (including the impact of oxide wedging and stress redistribution) in assessing the impact of SCC of the drip shield and waste package in revised documentation (ENG1.1.2 and ENG1.4.1). DOE will provide the technical basis for crack arrest and plugging of crack openings (including the impact of oxide wedging and stress redistribution) in assessing the stress corrosion cracking of the drip shield and waste package in an update to the Stress Corrosion Cracking of the Drip Shield, Waste Package Outer Barrier, and the Stainless Steel Structural Material AMR (ANL–EBS–MD–000005) in accordance with the scope and schedule for existing agreement item CLST 1.12.

*Schlueter, J.R "U S. Nuclear Regulatory Commission/U S Department of Energy Technical Exchange and Management on Container Life and Source Term (September 12–13, 2000)." Letter (October 4) to S Brocoum, DOE. Washington, DC. NRC. 2000.

†Reamer, C.W. "U S Nuclear Regulatory Commission/U.S. Department of Energy Technical Exchange and Management on Total System Performance Assessment and Integration (August 6–10, 2001)" Letter (August 23) to S Brocoum, DOE. Washington, DC: NRC. 2001.

2 STRESS CORROSION CRACKING OF CONTAINER MATERIALS

Stress corrosion cracking is recognized as a possible failure mechanism for waste packages after emplacement in the proposed Yucca Mountain repository (CRWMS M&O, 2000c,d). Stress corrosion cracking requires a combination of an applied or residual tensile stress, a susceptible material or microstructure, and an aggressive environment that promotes stress corrosion cracking. There are several plausible mechanisms for the application of tensile stresses. Applied tensile stresses may exist in emplaced waste packages owing to the weight of the waste package and the geometry of the waste package and emplacement pallet contact (CRWMS M&O, 2000e). Applied and residual stresses may develop as a consequence of rockfall and drift collapse (NRC, 2002). Fabrication and closure welds of the waste packages may also impart significant residual stresses (NRC, 2002; CRWMS M&O, 2001a, 2000c,d). Mitigation processes such as laser peening and solution annealing may reduce the residual stresses imparted during the disposal container fabrication and closure welding. Although nickel base alloys are resistant to stress corrosion cracking (Speidel, 1981; Copson, 1959; Cragnolino, et al., 1999), fabrication processes may alter the microstructure of the alloy and decrease the stress corrosion cracking resistance.

The susceptibility of stainless steel and nickel base alloys to stress corrosion cracking has been presented previously in several reviews (Cragnolino and Sridhar, 1992; Sridhar and Cragnolino, 1992; Cragnolino, et al., 1999; Jones and Bruemmer, 1990; Staehle, et al., 1970). Chlorides and reduced sulfur species can promote localized corrosion and stress corrosion cracking of stainless steel and nickel base alloys. In addition, groundwater contaminants such as lead have been implicated in the stress corrosion cracking of nickel base alloys at high temperatures and may be potentially aggressive species (Agrawal and Paine, 1990). The effect of minor species should be considered in the evaluation of waste package stress corrosion cracking susceptibility (NRC, 2002; Payer, et al., 2002). This chapter provides an overview of the U.S. Department of Energy (DOE) stress corrosion cracking testing and modeling program and an assessment of the model approach and parameters used, as well as the experimental work conducted at the Center for Nuclear Waste Regulatory Analyses (CNWRA) to evaluate stress corrosion cracking of the Alloy 22 outer container. The possible detrimental effects of minor species are addressed in Chapter 3.

2.1 The DOE Investigations

The current DOE waste package design incorporates features, materials, and special processing methods intended to promote a long life for anticipated repository conditions. The proposed design and fabrication of the waste package have been documented in DOE reports (CRWMS M&O, 2001a,b, 2000f,g), and the design has been reviewed and discussed by the U.S. Nuclear Regulatory Commission (NRC) (2002) as well as by the DOE Waste Package Materials Performance Peer Review Panel (Payer, et al., 2002). The DOE approach to evaluate stress corrosion cracking of the waste packages has been previously reviewed and discussed (Payer, et al., 2002; NRC, 2002; Cragnolino, et al., 1999). The proposed waste package design incorporated an outer Alloy 22 container with a dual closure lid that houses an inner container manufactured from Type 316L nuclear grade stainless steel. The inner container is proposed to provide mechanical integrity for container handling and emplacement operations. DOE does not take credit for the Type 316L nuclear grade stainless steel inner container in the evaluation of waste package stress corrosion cracking (CRWMS M&O, 2000d).

Resistance to corrosion, including uniform corrosion, localized corrosion, and stress corrosion cracking, is the basis for the selection of Alloy 22 as the outer container (CRWMS M&O, 2000h).

After fabrication of the outer Alloy 22 disposal container, solution annealing is proposed to mitigate residual stresses as a result of the container fabrication process (CRWMS M&O, 2000i). Solution annealing at temperatures in the range of 1,125 to 1,150 °C [2,057 to 2,102 °F] may redissolve second-phase precipitates formed in the interdendritic regions of the welds and in the heat-affected zones adjacent to the welds known to be detrimental to both localized corrosion resistance and mechanical properties (Heubner, et al., 1989). Nondestructive examination in accordance with the requirements of the American Society of Mechanical Engineers Boiler and Pressure Vessel Code (1995) will be used to identify fabrication defects. After the disposal containers are loaded, the inner Type 316L nuclear grade stainless steel container will be sealed using a lid with shear rings welded in place. A dual closure lid is proposed for the Alloy 22 outer disposal container. In the current design, the inner lid will be welded and laser peened to provide compressive stresses in the vicinity of the closure weld. The outer lid will be welded and then induction annealed at a temperature of 1,125 °C [2,057 °F] to mitigate residual tensile stresses.

The DOE assessment of stress corrosion cracking of the waste containers only considers residual stresses in the vicinity of the closure weld. All other fabrication welds are assumed to be fully annealed and not subject to stress corrosion cracking (CRWMS M&O, 2000i). Applied stresses from dead-weight loads, such as those arising from the emplacement and contact of the waste package with the emplacement pallet, seismic events, rockfall, and drift collapse, and residual stresses as a result of waste package handling and emplacement are not considered in the DOE abstraction of stress corrosion cracking (CRWMS M&O, 2000b,i). The DOE assessment of the stress corrosion cracking of Alloy 22 consists of both testing and modeling described in the following sections.

2.1.1 Stress Corrosion Cracking

The DOE investigations of the stress corrosion cracking susceptibility of candidate container materials used a variety of materials, specimen configurations, and testing conditions. Stress corrosion cracking investigations have focused on the determination of stress corrosion cracking susceptibility and measurement of crack propagation rates. A review of the initial work on Alloy 22 and other nickel-chromium-molybdenum alloys conducted at Lawrence Livermore National Laboratory was reported by Cragnolino, et al. (1999). The initial investigations on Alloy 22 in dilute acidified chloride solutions (5 percent NaCl, pH = 2.7) reported crack propagation rates of 1.8×10^{-7} mm/s [7.1×10^{-9} in/s] and a threshold stress intensity for stress corrosion cracking (K_{Iscc}) of approximately 30 MPa·m$^{1/2}$ [27 ksi·in$^{1/2}$] (McCright, 1998; Roy, et al., 1998). It was noted that the initial results of the stress corrosion tests with double cantilever beam fracture mechanic specimens were in contrast to the previous results of Speidel (1981), who reported no stress corrosion cracking in concentrated sodium chloride solutions (22 percent) for alloys with a minimum of 35 percent nickel (Cragnolino, et al., 1999).

Subsequent DOE studies of Alloy 22 stress corrosion cracking susceptibility have been conducted using annealed and as-welded U-bend specimens in environments based on variations of J–13 Well water under open circuit conditions (McCright, et al., 2002;

Estill, et al., 2002). Compositions of the test solutions used in the DOE investigations are listed in Tables 2-1 and 2-2. Specimens were positioned in three locations within the large test cells in the long-term corrosion test facility at Lawrence Livermore National Laboratory to have specimens exposed to completely immersed, partially immersed (i.e., waterline), and vapor-phase conditions. The Alloy 22 single U-bend specimens exposed for periods of up to 2 years showed no signs of stress corrosion cracking when tested in simulated acidified water and simulated concentrated water at 60 and 90 °C [140 and 194 °F]. The Alloy 22 double U-bend specimens showed no signs of cracking after testing in basic saturated water at 105 °C [221°F] (Estill, et al., 2002).

Table 2-1. Compositions of Several Aqueous Solutions Used for Corrosion Testing (CRWMS M&O, 2000)

Ion	Concentration							
	Simulated Dilute Water		Simulated Concentrated Water		Simulated Acidified Water		Simulated Saturated Water	
	60 and 90 °C [140 and 194 °F]		60 and 90 °C [140 and 194 °F]		60 and 90 °C [140 and 194 °F]		100 °C [212 °F]	
	mg/L	mM	mg/L	mM	mg/L	mM	mg/L	mM
K^+	34	0 87	3,400	87	3,400	87	142,000	3,632
Na^+	40	17.8	40,900	1,780	40,900	1,780	487,000	21,182
Mg^{2+}	1	0.04	<1	20.04	1,000	41	0	0.00
Ca^{2+}	0.5	0.01	<1	20.01	1,000	25	0	0.00
F^-	14	0.74	1,400	74	0.00	0.00	0	0.00
Cl^-	67	1.89	6,700	189	24,250	684	128,000	3,610
NO_3^-	64	1.03	6,400	103	23,000	371	1,313,000	21,175
SO_4^{2-}	167	1.74	16,400	174	38,000	396	0	0.00
HCO_3^-	947	15.52	70,000	1,148	0.00	0.00	0	0.00
Si	27 60 °C [140 °F] 49 90 °C [194 °F]	—	27 60 °C [140 °F] 49 90 °C [194 °F]	—	27 60 °C [140 °F] 49 90 °C [194 °F]	—	—	—

Reference CRWMS M&O. "Environment on the Surfaces of the Drip Shield and Waste Package Outer Barrier." ANL–EBS–MD–000001. Rev. 00 ICN 01 Las Vegas, Nevada: CRWMS M&O 2000.

Table 2-2. Recipe for Basic Saturated Water (CRWMS M&O, 2000)		
Chemicals	**Grams**	**M**
KCl	9.7	2.32
NaCl	8.8	2.69
NaF	0.2	0.085
$NaNO_3$	13.6	2.86
Na_2SO_4	1.4	0.176
H_2O	56.0	—
Na_2CO_3	10.6	1.786
$Na_2SiO_3 \cdot 9H_2O$	4.0	0.251
Reference: CRWMS M&O. "Environment on the Surfaces of the Drip Shield and Waste Package Outer Barrier." ANL–EBS–MD–000001. Rev 00 ICN 01 Las Vegas, Nevada CRWMS M&O. 2000		

In addition to the constant deflection U-bend tests, slow strain rate tests and uniaxial tension tests have been reported recently by Estill, et al. (2002) and Gordon.[1] Transgranular stress corrosion cracking of Alloy 22 slow strain rate specimens at high anodic potentials (400 mV versus Ag/AgCl) was recently reported by Estill, et al. (2002) in simulated concentrated water at 73 °C [163 °F]. Even with transgranular cracking, the specimen was quite ductile with an elongation to failure of approximately 47 percent and a reduction in area of at least 64 percent. For comparison, specimens with completely ductile failure had elongation to failure in the range of 61 to 65 percent and a reduction in area of at least 71 to 85 percent. When the temperature was reduced to 22 °C [72 °F], no stress corrosion cracking was observed. In addition, no stress corrosion cracking was observed when specimens were tested in basic saturated water at lower potentials (200 mV versus Ag/AgCl) even when nitrate and sulfate were removed.

The initiation of stress corrosion cracking on smooth specimens has been studied using constant load specimens.[2] The tests were conducted in concentrated (7,500×) J–13 Well water with a pH 12.4. Specimens were loaded to applied stresses between 0.75 to 2.5 times the yield strength of the materials and immersed in solution at 105 °C [221 °F]. Alloy 22 specimens were tested in a variety of conditions including as-received, thermally aged to produce topologically close-packed phases, thermally aged to produce long-range ordering, cold worked, and welded. The welded specimens exposed weld metal and the heat-affected zone.

---

[1]Gordon, G "Stress Corrosion Cracking." *Presentation to the Waste Package Materials Performance Peer Panel Review September 25, 2001* Las Vegas, Nevada. 2001

[2]Ibid

No stress corrosion cracking was observed on Alloy 22 specimens after 4,000 hours of testing. Other materials including Titanium Grade 7 and sensitized Type 304 SS were found susceptible to stress corrosion cracking in tests where the applied stresses were between 1.0 and 1.4 times the yield strength of the material. Failure times were very short for sensitized Type 304 SS when a crevice condition was used and up to 800 hours for Titanium Grade 7.

Stress corrosion crack propagation rates have been measured using fatigue precracked compact tension fracture mechanics-type specimens of Alloy 22 and Titanium Grade 7 in the as-received and 20-percent cold-worked condition. Testing was performed in autoclaves at 110 °C [230 °F] in solutions similar in composition to basic saturated water[3] (Andresen, et al., 2001; CRWMS M&O, 2000d). Tests were conducted at stress intensities of 30 and 45 $MPa{\cdot}m^{1/2}$ [27 and 41 $ksi{\cdot}in^{1/2}$]. Cyclic loading at a frequency between 0.01 and 0.001 Hz was used to initiate crack growth of the fatigue precracked specimens (Andresen, et al., 2001). After crack growth was assured, the specimens were gently transitioned to static loading conditions by gradually increasing minimum load. Crack propagation rates were determined using reversing current potential drop measurements with an estimated crack length resolution of 1 µm [2.5×10^{-4} in]. Specimens were tested at the corrosion potential in solutions saturated with oxygen by the slow flow of laboratory air into the autoclave. For the conditions used, the dissolved oxygen concentration was estimated to be 0.91 parts per million considering the temperature and the salting out effect (Andresen, et al., 2001).

Crack propagation rates for Alloy 22 tested with an initial stress intensity of 30 $MPa{\cdot}m^{1/2}$ [27 $ksi{\cdot}in^{1/2}$] under cyclic loading conditions using a frequency of 0.001–0.003 Hz and a load ratio (minimum load to maximum load) of 0.6 were in the range of 2.1×10^{-8} to 3.3×10^{-8} mm/s [8.3×10^{-10} to 1.3×10^{-9} in/s]. When the load ratio was changed to 0.7 after more than 3,700 hours of testing, the crack propagation rate was similar to that measured with a load ratio of 0.6. After testing for more than 4,400 hours, a static hold was introduced, and the crack propagation appeared to cease. Nevertheless, it was estimated that the crack propagation rate for Alloy 22 under static conditions would be in the range of 1×10^{-9} to 2×10^{-9} mm/s [4×10^{-11} to 8×10^{-11} in/s]. The addition of 20-percent cold work did not significantly alter the crack propagation rates measured under cyclic loading conditions. Crack propagation rates for the cold-worked specimen for static conditions were in the range of 5×10^{-10} to 2.6×10^{-9} mm/s [2×10^{-11} to 1.0×10^{-10} in/s]. Faster crack propagation rates were measured on a specimen tested at a stress intensity of 45 $MPa{\cdot}m^{1/2}$ [41 $ksi{\cdot}in^{1/2}$]. At a load ratio of 0.7, the measured crack propagation rate was 2.3×10^{-7} mm/s [8.3×10^{-9} in/s] at a loading frequency of 0.01 Hz, 2.3×10^{-8} mm/s [8.3×10^{-10} in/s] at a loading frequency of 0.001 Hz, and in the range of 1.3×10^{-9} to 2.1×10^{-9} mm/s [5.1×10^{-11} to 8.3×10^{-11} in/s] under static conditions.

Similar crack propagation rates were reported by Estill, et al. (2002) for fatigue precracked compact tension specimens tested in simulated acidified water and simulated concentrated water at 95 °C [203 °F]. For cyclic loading at 0.001 Hz with a load ratio of 0.7 and a maximum stress intensity of 45 $MPa{\cdot}m^{1/2}$ [41 $ksi{\cdot}in^{1/2}$], the crack propagation rates were 2×10^{-8} to 3×10^{-8} mm/s [8×10^{-10} to 1×10^{-9} in/s] in simulated acidified water. The crack propagation rate slowed to 2×10^{-10} mm/s [8×10^{-12} in/s] under static conditions. Similarly, in simulated concentrated water, the crack propagation rates were 3×10^{-8} mm/s [1×10^{-9} in/s] under cyclic conditions and 5×10^{-10} mm/s [2×10^{-11} in/s] under static conditions. A summary of crack

[3]Ibid

propagation rates using fatigue precracked compact tension specimens is provided in Table 2-3.

2.1.2 The DOE Model Abstraction

As previously indicated, DOE modeling of waste package stress corrosion cracking only considered the performance of the Alloy 22 waste package outer container. In addition, the only stress considered was the residual hoop stress from the container closure welds. Applied or residual stresses from rockfall, drift collapse, and seismic events were not considered in the stress corrosion cracking models (CRWMS M&O, 2000i). Residual stresses from the disposal container fabrication sequence also were not considered because these stresses were assumed to be removed in the container solution annealing process (CRWMS M&O, 2000d). The DOE stress corrosion crack model abstraction included a waste package manufacturing defects abstraction model, residual weld stress finite element model, determination of the minimum stress and stress intensity for crack initiation and crack growth, and crack growth rate based on the slip dissolution model.

The DOE model abstraction for stress corrosion cracking of the waste packages considered manufacturing defects and both stress and stress intensity profiles in the closure welds. The number of waste package that have a stress intensity above the critical stress intensity for stress corrosion cracking is based on estimations of the number of flaws per unit length of weld, fraction of surface breaking flaws, orientation of the flaws, and residual stress profile of the closure welds. Stress corrosion cracking is assumed to propagate at a rate determined using the slip dissolution model when either the stress intensity calculated for a surface breaking flaw exceeds the critical stress intensity for stress corrosion cracking or when the residual stress exceeds the critical stress for the initiation of stress corrosion cracking in the absence of a flaw. Details of the DOE models used in the assessment of stress corrosion cracking are described next.

Manufacturing Defects Abstraction Model

The manufacturing defects abstraction model was developed to calculate the probability or frequency and the size of manufacturing defects in the Alloy 22 waste package outer barrier closure lids welds. The abstracted model calculates the flaw depth distribution using a log normal probability density function. The flaw size distribution is derived considering the probability of nondetection as a function of flaw size that, in turn, is dependent on numerous variables including the type of material, operator skill, access to the weld, and type of defect (CRWMS M&O, 2000i,j). Estimation of the number of outer surface breaking flaws of 6.839×10^{-4} flaws/mm [0.017 flaws/in] was based on a simulation using the RR-PRODIGAL code assuming a manual metal arc weld on 20.32-cm [8-in] diameter, 2.54-cm [1-in] thick stainless steel pipe (Khaleel, et al., 1999). This estimation, based on a weld simulation, contradicts the statement included in the DOE Analysis Model Reports (CRWMS M&O, 2000i,j), in which evaluation of an actual stainless steel weld is reported. The simulated weld was assumed to be subjected to volumetric inspection using radiographic testing and surface inspection using penetrant testing (Khaleel, et al., 1999). The flaw density of the uninspected weld can be calculated considering the fraction of flaws that penetrate the outer surface and the flaw reduction factors for radiographic and penetrant testing. The flaw density of the uninspected weld was also adjusted for geometrical consideration of thickness and

Table 2-3. Crack Propagation Rates Measured on Alloy 22 Compact Tension Specimens				
Material Condition	**Stress Intensity**	**Cyclic Loading Frequency**	**Crack Propagation Rate/ Solution/Temperature**	**Reference**
As-received	30 MPa·m$^{1/2}$ [27 ksi·in$^{1/2}$]	0.001–0.003 Hz at R = 0.6	2.1×10^{-8} to 3.3×10^{-8} mm/s [8.3×10^{-10} to 1.3×10^{-9} in/s] Basic Saturated Water 110 °C [230 °F]	Andresen, et al. 2001
As-received	30 MPa·m$^{1/2}$ [27 ksi·in$^{1/2}$]	Static	1×10^{-9} to 2×10^{-9} mm/s [4×10^{-11} to 8×10^{-11} in/s] (estimated values) Basic Saturated Water 110 °C [230 °F]	Andresen, et al., 2001
20-percent cold-worked	30 MPa·m$^{1/2}$ [27 ksi·in$^{1/2}$]	Static	5×10^{-10} to 2.6×10^{-9} mm/s [2×10^{-11} to 1.0×10^{-10} in/s] Basic Saturated Water 110 °C [230 °F]	Andresen, et al., 2001
As-received	45 MPa·m$^{1/2}$ [41 ksi·in$^{1/2}$]	0.01 Hz at R = 0.7	2.3×10^{-7} mm/s [8.3×10^{-9} in/s] Basic Saturated Water 110 °C [230 °F]	Andresen, et al., 2001
As-received	45 MPa m$^{1/2}$ [41 ksi·in$^{1/2}$]	0.001 Hz at R = 0.7	2.3×10^{-8} mm/s [8.3×10^{-10} in/s] Basic Saturated Water 110 °C [230 °F]	Andresen, et al., 2001
As-received	45 MPa·m$^{1/2}$ [41 ksi·in$^{1/2}$]	Static	1.3×10^{-9} to 2.1×10^{-9} mm/s [5.1×10^{-11} to 8.3×10^{-11} in/s] Basic Saturated Water 110 °C [230 °F]	Andresen, et al., 2001
As-received	45 MPa·m$^{1/2}$ [41 ksi·in$^{1/2}$]	0.001 Hz at R = 0.7	2×10^{-8} to 3×10^{-8} mm/s [8×10^{-10} to 1×10^{-9} in/s] Basic Saturated Water 95 °C [203 °F]	Estill, et al., 2002
As-received	45 MPa·m$^{1/2}$ [41 ksi·in$^{1/2}$]	Static	2×10^{-10} mm/s [8×10^{-12} in/s] Simulated Acidified Water 95 °C [203 °F]	Estill, et al., 2002
As-received	45 MPa·m$^{1/2}$ [41 ksi·in$^{1/2}$]	0.001 Hz at R = 0.7	3×10^{-8} mm/s [1×10^{-9} in/s] Simulated Acidified Water 95 °C [203 °F]	Estill, et al., 2002

Table 2-3. Crack Propagation Rates Measured on Alloy 22 Compact Tension Specimens (continued)				
Material Condition	**Stress Intensity**	**Cyclic Loading Frequency**	**Crack Propagation Rate/ Solution/Temperature**	**Reference**
As-received	45 MPa·m$^{1/2}$ [41 ksi·in$^{1/2}$]	Static	5×10^{-10} mm/s [2×10^{-11} in/s] Simulated Acidified Water 95 °C [203 °F]	Estill, et al., 2002

References:
Andresen, P L , P.W. Emigh, L M. Young, and G M. Gordon. "Stress Corrosion Cracking of Annealed and Cold-Worked Titanium Grade 7 and Alloy 22 in 110 °C Concentrated Salt Environments " Proceedings of the CORROSION 2001 Conference. Paper No 01130 Houston, Texas· NACE International 2001

Estill, J C , K J King, D.V. Fix, D.G. Spurlock, G.A Hurst, S R. Gordon, R.D Mccright, and R B Rebak. "Susceptibility of Alloy 22 to Environmentally Assisted Cracking in Yucca Mountain Relevant Environments." Proceedings of the CORROSION 2002 Conference. Paper No. 535 Houston, Texas: NACE International. 2002.

circumference of the waste package closure weld (CRWMS M&O, 2000i). The total expected flaws in the uninspected waste package closure weld was then adjusted for the probability for flaws detected using ultrasonic testing to give a final distribution of flaws in the waste package closure weld. A Poisson distribution is used to determine the expected flaws that occur in the closure weld of a given waste package. The probability that one or more flaws will occur in a closure weld is given by Eq. (2-1)

$$P(X \geq 1) = 1 - P(X = 0) = 1 - \exp(-\lambda) \tag{2-1}$$

where

X — probability distribution for the number of flaws
λ — the mean flaw density of the closure weld

Residual Closure Weld Stresses

The residual stresses from the closure weld operation were modeled using an asymmetric two-dimensional finite element model (CRWMS M&O, 2000d). However, the analysis was performed on an outdated waste package design using a single Alloy 22 closure lid. Residual stresses from the closure incorporated a thermal analysis of the weld that considered the temperature history caused by each pass of the multipass welding operation. The additional metal deposited in each pass was included in the thermal analyses as well as the residual stresses from previous passes and the location of the heat input from welding. The effect of the welding passes was simulated through heat generated in the finite elements that represent the weld pass. The heat input is then transferred to adjoining parts of the waste package. The net heat input, H_{net}, was calculated using Eq. (2-2)

$$H_{net} = \frac{f_1 E I}{v} \tag{2-2}$$

where

f_1	—	the heat transfer coefficient
E	—	the welding voltage
I	—	the current
v	—	the travel velocity

For the hot wire gas tungsten arc welding process, the parameters selected were 12.1 to 13 V, 330 to 335 amps, 20.3 cm/min [8.0 in/min], and a heat transfer efficiency of 21–48 percent. Using the average values and adding 15 percent to account for the heat input from the filler wire, the net heat input was calculated to be 4,882 J/cm [2,964 cal/in]. The heat input is modeled as a triangular shaped pulse with a 2-second time interval. The cooling time is assumed equal to the time to complete one weld pass.

Residual stress calculations for the as-welded condition were performed considering the radial, longitudinal, and hoop stresses. For a 2.54-cm [1-in] thick lid, the maximum radial stresses were tensile {103 MPa [15 ksi]} on the inner surface, compressive {−158 MPa [−23 ksi]} near the middle of the lid thickness, and tensile {207 MPa [30 ksi]} on the outer surface. Maximum longitudinal stresses were tensile {193 MPa [28ksi]} on the inner surface and decreased to less than 27.5 MPa [4.0 ksi] on the outer surface. Maximum hoop stresses were tensile and varied from 248 MPa [36 ksi] on the inner surface to more than 345 MPa [50 ksi] on the outer surface. For comparison, the minimum tensile strength for Alloy 22 is 310 MPa [45 ksi] (ASTM International, 2001a).

Two types of flaws were considered in the stress intensity factor calculations: circumferential flaws and radial flaws. Radial flaws are oriented perpendicular to the weld. Circumferential flaws are oriented parallel to the weld. Hoop stresses are the driving forces for radial cracks. Correspondingly, radial stresses are the driving forces for circumferential cracks. The true stress intensity at the crack tip was adjusted using a geometry correction factor. For circumferential flaws, the geometry correction factor decreased with increased crack depth-to-thickness ratio. As a consequence of the geometry correction factor, the stress intensity factor for circumferential flaws was less than 22 $MPa \cdot m^{1/2}$ [20 $ksi \cdot in^{1/2}$]. For radial cracks, the geometry correction factor was assumed to be 1. As a result, the stress intensity of radial flaws increased with the increasing crack depth-to-thickness ratio from approximately 11 $MPa \cdot m^{1/2}$ [10 $ksi \cdot in^{1/2}$] for a crack depth-to-thickness ratio of 0.01 to nearly 88 $MPa \cdot m^{1/2}$ [80 $ksi \cdot in^{1/2}$] for a crack depth-to-thickness ratio of 0.8.

Mitigation of weld residual stresses using laser peening was modeled using, as a basis, measured compressive stress in the range 138–414 MPa [20–60 ksi] for a thickness of 1.5 mm [0.060 in] with increased depths for multiple peening operations (CRWMS M&O, 2000d). The calculated hoop stress profile was compressive from the outside surface to a depth of approximately 2 mm [0.078 in] (CRWMS M&O, 2000i). The maximum mean tensile hoop stress of 170 MPa [25 ksi] occurred at a distance 5 mm [0.196 in] from the outside surface. Stress intensity profiles for hoop stresses were compressive for a distance 5 mm [0.196 in] from the outside surface (CRWMS M&O, 2000i).

Calculation of the residual stresses in the outer waste package lid after thermal annealing was based on a thermal cycle that increased the temperature of the weld region to 1,120 °C [2,048 °F] in 35 seconds. The temperature profile was held for 10 seconds and then lowered to

room temperature in 30 seconds (CRWMS M&O, 2000d). Calculated hoop stress profiles after induction annealing reached a maximum of -300 MPa [-43 ksi] at the outside surface and were compressive to a depth of 8 mm [0.31 in]. At 20 mm [0.78 in] from the outside surface, the hoop stress was calculated to be 430 MPa [62.3 ksi]. Calculated stress intensities from hoop stresses were negative up to a depth of 11 mm [0.43 in] (CRWMS M&O, 2000d,i).

Threshold Stress Intensity Model

The threshold stress intensity model assumes there is a minimum stress intensity necessary to initiate stress corrosion cracking. The initial threshold stress intensity was based on the experimental results of Roy, et al. (1998) who reported final stress intensity values for wedge-loaded, precracked, double cantilever beam specimens exposed to deaerated brine adjusted to a pH of 2.7 and tested at 90 °C [194 °F]. An average final stress intensity of 33 MPa·m$^{1/2}$ [30 ksi·in$^{1/2}$] (measured after exposure) was assumed to be the threshold stress intensity for stress corrosion cracking and to have a normal distribution with a standard deviation of 1.77 MPa·m$^{1/2}$ [1.61 ksi·in$^{1/2}$] (CRWMS M&O, 2000d). In the absence of a preexisting flaw, a minimum stress is used to determine the initiation of stress corrosion cracking, which was assumed to be 20–30 percent of the yield strength for Alloy 22, or approximately 64–95 MPa [9–14 ksi]. This range was later expanded to 10–40 percent of the yield strength, or 32–129 MPa [5–19 ksi] (CRWMS M&O, 2000i).

Slip Dissolution/Film Rupture Model

A review of the slip dissolution model as well as other models for stress corrosion cracking of engineering alloys was reported by Cragnolino, et al. (2001a). In addition, the application of the slip dissolution/film rupture model to predict stress corrosion crack propagation rates of Alloy 22 waste packages has been previously reviewed and discussed (NRC, 2002). The slip dissolution/film rupture model for stress corrosion crack propagation assumes that crack advance is faradaically related to the metal oxidation that occurs when the protective film at the crack tip is ruptured. The slip dissolution/film rupture model has been used to predict stress corrosion cracking of Type 304 SS and Alloy 600 in boiling water reactor environments (Andresen and Ford, 1994; Ford and Andresen, 1988). The average crack growth rate, V_t, is related to the strain rate at the crack tip, ε_{ct}. Stress corrosion crack propagation in the Alloy 22 outer barrier is modeled using Eq. (2-3)

$$V_t = \overline{A}\left(K_I\right)^{\overline{n}} \tag{2-3}$$

where

V_t — crack growth rate in mm/s
K_I — stress intensity factor in MPa·m$^{1/2}$

The parameters $\overline{A}$ and $\overline{n}$ are related to the repassivation slope n and calculated as shown in Eqs. (2-4) and (2-5)

$$\overline{A} = A\, n^{36} \left(4.1 \times 10^{-14}\right)^{n} \tag{2-4}$$

$$\overline{n} = 4n \tag{2-5}$$

where the values of A and n are dependent on both environmental parameters and material parameters. Because of the lack of sufficient data, the preexponential parameter A of 7.8×10^{-2}, a value reported for austenitic stainless steels in boiling water reactor environments, was used for Alloy 22 (CRWMS M&O, 2000i).

Based on initial work conducted with Alloy 22 stress corrosion crack specimens, the value of n was determined to be in the range 0.75–0.84. More recent crack growth rates, ranging from 2.1×10^{-8} to 7.6×10^{-9} mm/s [8.3×10^{-10} to 3.0×10^{-10} in/s], were measured using a compact tension specimen with an initial stress intensity of 30 MPa·m$^{1/2}$ [27 ksi·in$^{1/2}$] in an air-saturated alkaline solution (pH 13.4) and a composition similar to basic saturated water at 110 °C [230 °F] after a 3,585-hour exposure. These crack growth rates were then used to estimate the value of the repassivation parameter n (CRWMS M&O, 2000d). Assuming a value for A of 7.8×10^{-2}, values of n ranging from 0.843 to 0.92 were then calculated from the measured crack growth rates listed previously and selected to represent the lower and upper bounds of n using a uniform distribution (CRWMS M&O, 2000d).

2.1.3 Assessment of the DOE Approach

Stress Corrosion Cracking Testing

DOE used similar specimens and testing parameters to evaluate crack growth rates in all the modified J–13 Well environments, including basic saturated water, simulated acidified water, and simulated concentrated water. The crack growth rates in all solutions were similar. Although there were wide variations in pH among the solutions, it should be noted that all solutions had similar nitrate-to-chloride concentration ratios. Thus, it appears that pH has little effect on the stress corrosion crack propagation rate. Simulated concentrated water and basic saturated water have fluoride, whereas simulated acidified water does not. Although conclusive assessment of crack growth rates using limited testing is not advisable, it would appear that faster crack propagation rates may be attributed to the presence of fluoride.

Solution composition and potential appear to be the dominant factors that determine stress corrosion crack susceptibility in slow strain rate tests reported by Estill, et al (2002). Stress corrosion cracking only occurred at high anodic potentials where the transpassive dissolution of molybdenum had been reported (Ilevbare, et al., 2002). Although simulated concentrated water and basic saturated water have fluoride and similar nitrate to chloride ratios (Tables 2-1 and 2-2), no stress corrosion cracking was observed in any slow strain rate tests conducted in basic saturated water at potentials of 200 mV versus Ag/AgCl, even when the potentially inhibiting nitrate and sulfate anions were removed. Additional results from King, et al. (2002) clearly demonstrate the stress corrosion cracking susceptibility of Alloy 22 in simulated concentrated water is strongly dependent on potential. It appears the absence of stress corrosion cracking in the DOE slow strain rate tests conducted in basic saturated water, with or

without inhibiting nitrate and sulfate species, may be a result of potentials selected rather than a difference in solution chemistry. At higher potentials, such as those used in slow strain rate tests conducted in simulated concentrated water, stress corrosion cracking of Alloy 22 may occur in other environments such as basic saturated water. These results indicate that potential is an important factor in assessing stress corrosion cracking susceptibility.

The stress corrosion crack initiation tests reported by Gordon[4] suggest the initiation of stress corrosion cracking on Alloy 22 is unlikely in solutions containing mixed anions, including inhibiting anions such as nitrate. The rapid failure time for sensitized Type 304 SS may suggest the environment used did not have a sufficient concentration of inhibiting species to prevent stress corrosion cracking on this susceptible alloy microstructure. The effect of the environment was revealed by the shorter failure time for sensitized Type 304 SS with a crevice. The addition of a crevice would be expected to result in a low pH, high-chloride concentration environment that may promote localized corrosion (Sridhar and Dunn, 1994). In the presence of stress, this aggressive environment may also facilitate the initiation of stress corrosion cracking (Cragnolino, et al., 1994). Compared to sensitized Type 304 SS, Alloy 22 and even welded Alloy 22, are far more resistant to localized corrosion and stress corrosion cracking. Variations in solution chemistry such as a decrease in the concentration of inhibitive anions relative to an aggressive anion, such as chloride, may promote stress corrosion cracking of Alloy 22, particularly for microstructures altered by welding or thermal aging.

From the DOE analysis, it is apparent that Alloy 22 is quite resistant to stress corrosion cracking in the simulated Yucca Mountain groundwater solutions. One key concern is the effect of more severe environments on the stress corrosion cracking susceptibility of Alloy 22. As discussed in Brossia, et al. (2001), it is not clear the environments used in the DOE-sponsored work adequately bound the range of expected environments that may be encountered in disposal conditions.

Stress Corrosion Cracking Models

The DOE assessment of the flaw density relevant to stress corrosion cracking is based on a limited assessment of a simulated manual gas metal arc weld on 25.4-mm [1-in] thick stainless steel. Although expected, the flaw density may not be markedly different between gas metal arc welding and a gas tungsten arc weld; the effect of the welding method was not considered in the DOE assessment of expected flaws. Several factors that may affect the number of flaws in the closure welds are briefly mentioned by DOE but not actually assessed or considered in the calculation of expected flaws, based on the examination of the welded stainless steel material. The effect of material type on the expected number of flaws as a result of welding is mentioned in the DOE assessment; however, no factor is introduced in the DOE analyses to account for the difference in the number of welding flaws expected for stainless steels compared with Alloy 22. High concentrations of molybdenum and the addition of tungsten in Alloy 22 tend to increase the viscosity of the weld pool. This, in turn, may increase the number of expected defects in the waste package closure welds. Similarly, the type of defect and access to the weld are also briefly mentioned but not considered in the DOE assessment. An assessment of ultrasonic detection of welding flaws has been reported for a closure weld mockup, however, the effect of flaw orientation was not reported (CRWMS M&O, 2001a).

---

[4]Ibid.

Because of their orientation, circumferential flaws may be much easier to detect using ultrasonic inspection with a straight beam ultrasonic transducer positioned on the outside diameter surface of the waste package. The DOE assessment indicates that radial flaws are a greater concern for the initiation of stress corrosion cracking. The detection of radial flaws may not be possible using a transducer positioned on the outside diameter of the waste package because the orientation of radial flaws would be parallel to the ultrasonic beam path. Detection of surface or near-surface breaking radial flaws may be difficult also using an angle beam ultrasonic transducer described in the Waste Package Project FY-01 Closure Methods Report (CRWMS M&O, 2001a). Detection of surface or near-surface flaws using ultrasonic inspection is known to be difficult (American Society for Metals, 1976).

The DOE assessment of stress corrosion cracking assumes the only source of applied or residual stresses required for stress corrosion cracking will be in the final closure weld (CRWMS M&O, 2000c,d). Residual stresses from the fabrication of the disposal container were assumed to be completely eliminated as a result of solution annealing and quenching. Verification of this assumption has not been demonstrated. Recently, the DOE Waste Package Materials Performance Peer Review Panel (Payer, et al., 2002) raised the concern that rapid cooling as a consequence of quenching for the solution annealing temperature may produce unacceptably high tensile residual stresses, although slow cooling may lead to the initiation and growth of deleterious phases at grain boundaries. The panel recommended the thorough evaluation of stress mitigation processes and the consideration of alloy thermal stability. Specific suggestions of the DOE Waste Package Materials Performance Peer Review Panel (Payer, et al., 2002) were to examine slow cooling after annealing, which would require using an alloy not susceptible to sensitization, or other deleterious grain boundaries and second-phase precipitation processes and careful design and control of the quenching processes to minimize development of tensile stresses.

The residual stresses in the final closure weld will be dependent on the design of the waste package closure weld and the welding processes. The calculation of heat input for the evaluation of residual stress in the as-welded condition uses parameters for hot wire gas tungsten arc welding that likely are different from standard gas tungsten arc welding (CRWMS M&O, 2000d). The hot wire variation of gas tungsten arc welding typically uses faster travel speeds and can have higher metal deposition rates that, in turn, requires fewer welding passes. Slower travel speeds, along with an increased number of passes, can be expected for the narrow groove gas tungsten arc welding processes (CRWMS M&O, 2001a) and can significantly alter the heat input. The heat input calculation used by DOE also used a heat transfer coefficient given a value of 21–48 percent; however, justification for the range of selected values was not provided.

In addition to the welding parameters used to calculate the residual stresses, the DOE analysis did not consider the significant variability of thermal conductivity, coefficient for thermal expansion, Young's modulus, and yield strength of Alloy 22 with respect to temperature. The boundary conditions used for both the thermal and stress analyses were not provided but are required to assess the validity of the model. For example, it is not clear if the spent nuclear fuel decay heat was considered or if the possible variation in the waste package thermal output was accounted for in the models. Values for the temperature or heat flux conditions that were applied at the boundaries of the model were not provided.

To characterize the uncertainty of the weld residual stress calculated by the finite element analysis, it is assumed the calculated residual stress is the mean stress, and the uncertainty in the residual stress is represented with the upper and lower bounds around the calculated mean stress (CRWMS M&O, 2000d). For the optimum case, the uncertainty range is assumed to be ±5 percent of the mean yield strength. The realistic case assumes the uncertainty range is ±10 percent of the mean yield strength, and the most conservative case assumes ±30 percent of the mean yield strength. It is not clear that the calculated mean stress is valid. A large uncertainty range may not adequately bound the effect of a higher mean stress.

The DOE stress corrosion cracking models considered weld residual stress the only source of stress significant to stress corrosion cracking (CRWMS M&O, 2000d). Other sources of stress are assumed either insignificant, such as dead-weight loaded stress, or temporary, like seismic stress. Accordingly, the effects of other possible types of applied stresses in the repository have not been assessed. In particular, stresses generated at the line of contact of the waste package with the emplacement pallet should be evaluated. DOE has not provided analyses demonstrating the drip shield will respond to all credible seismic loads with a probability of greater than 10^{-8} per year in a purely elastic manner (i.e., plastic deformations imply the existence of residual stresses). In addition, DOE has not provided analyses demonstrating the drip shield will protect the waste package from credible static and dynamic rockfall loads. Residual stresses from waste package fabrication or applied stresses resulting from seismic events combined with the necessary environmental conditions may be sufficient to cause stress corrosion cracking of the outer container. As a result, the waste package may experience localized plastic deformations in locations where it interacts with the drip shield and pallet. Existing stress corrosion cracks in the closure lid weld area may propagate at an increased rate.

The analyses of residual stresses and the threshold stress intensity for stress corrosion cracking performed by DOE has been previously reviewed and discussed (NRC, 2002). Using a finite element method, residual stress analyses performed by DOE indicate that, given the calculated maximum stress intensity factors from weld residual stress and a threshold stress intensity for stress corrosion cracking, K_{ISCC}, determined by Lawrence Livermore National Laboratory, a radially oriented flaw perpendicular to the weld may initiate stress corrosion cracking of the Alloy 22 outer container. In contrast, no stress corrosion cracking initiation at a circumferentially oriented flaw parallel to the weld is expected because the maximum stress intensity for this type of flaw is expected to be less than 20 $MPa \cdot m^{1/2}$ [18 $ksi \cdot in^{1/2}$] and below the threshold value. These arguments are based on the threshold or minimum stress intensity criterion. The threshold stress intensity, however, could be lower in a different environment than that tested (Speidel, 1981). In addition, it is not clear that the DOE assessment of the effects of residual stresses considers the complex simultaneous contributions of tensile, radial, and circumferential stresses in the assessment of the threshold stress intensity. In general, a biaxial tensile stress state may cause ductile materials to behave in a more brittle fashion. The validity of measurements of the threshold stress intensity as a bounding parameter for performance should be assessed through an appropriate combination of experimental and modeling work. It is also recognized that the threshold stress intensity values are affected by the electrode potential (Silcock, 1982; Russell and Tromans, 1979). On the basis of these observations, it is apparent that the composition of the environment is another constraint that must be considered when using the threshold stress intensity as a bounding parameter for the initiation of stress corrosion cracks.

In the application of the slip dissolution/film rupture model to Alloy 22, DOE adopted values ranging from 0.843 to 0.92 for the repassivation slope, *n* (CRWMS M&O, 2000d). This range of values for *n* was calculated from a single experiment conducted for 3,385 hours during cyclic loading conditions $R = 0.5–0.7$, with frequency 0.001–0.003 Hz, at a maximum $K_I = 30$ MPa·m$^{1/2}$ [27 ksi·in$^{1/2}$]. Input for the model includes average crack growth rates ranging from 2.1×10^{-11} to 7.6×10^{-12} m/s [8.3×10^{-10} to 3.0×10^{-10} in/s] and the empirical relationship adopted from the work of Ford and Andresen (1988) on the stress corrosion cracking of austenitic stainless steels in boiling water reactor environments as previously reviewed by Sridhar, et al. (1993). In the empirical relationships developed by Ford and Andresen (1988), the two interdependent model parameters (*n* and *A*) used to define the crack propagation rate/crack tip strain rate relationship in the slip dissolution/film rupture model are dependent on material properties and the environment at the crack tip. From analysis of the extensive work conducted by Ford and Andresen (1988), it can be concluded that most final expressions for calculating crack propagation rates and crack tip strain rates require the input of field data to adjust several of the parameters included in the model. Obtaining the field data is particularly necessary in the case of the parameter *n*, but also applies to the preexponential coefficient *A*. The model parameters in the slip dissolution/film rupture model are largely empirical correlations on the basis of a combination of laboratory experimental results and field observations. Therefore, application of these empirical relationships to Alloy 22 requires a more complete database to limit propagation of the uncertainty characterizing currently available data into the modeling of stress corrosion cracking of Alloy 22.

2.2 The CNWRA Investigations

Stress corrosion cracking tests were conducted to evaluate the stress corrosion cracking susceptibility of a variety of candidate container materials. Previous investigations showed the stress corrosion cracking susceptibility of Type 316L SS and Alloy 825 were dependent on chloride concentration, temperature, and potential. Short-term susceptibility tests showed that no stress corrosion cracking was initiated in aggressive solutions characterized by high chloride concentrations and elevated temperatures when the potential of the specimen is maintained below the repassivation potential for localized corrosion (Dunn, et al., 2002; Cragnolino, et al., 1994; Sridhar, et al., 1995). Because these preliminary tests were conducted using U-bend and slow stain rate tensile specimens, an assessment of the crack propagation rate could not be conducted. More recently, stress corrosion cracking tests have been conducted using fatigue precracked fracture mechanics-type specimens to determine crack propagation rate as a function of environmental conditions (Dunn, et al., 2002, 2000, Pan, et al., 2000). Tests reported here were conducted to assess the effect of the environment on the stress corrosion crack propagation rates.

2.2.1 Stress Corrosion Cracking Test Methods

Stress corrosion cracking tests were conducted using both compact tension and double cantilever beam specimens. The chemical compositions of the Alloy 22 and Type 316L SS heats used in this investigation are shown in Table 2-4. Stress corrosion cracking tests were conducted using the wedge-opening-loaded, double cantilever beam specimens (NACE International, 1996) shown in Figure 2-1 and the compact tension specimens shown in Figure 2-2. Specimens were machined from hot-rolled and annealed plates. Specimens were machined from a 12.7-mm [0.5-in] plate with a long transverse-longitudinal orientation

Table 2-4. Compositions of the Heats of Type 316L SS and Alloy 22 Used in Stress Corrosion Cracking Tests (wt%)														
Heat	Ni	Cr	Mo	W	Fe	Co	Si	Mn	Cu	N	V	P	S	C
Type 316L SS P80746	10.04	16.35	2.07	—	68.91	—	0.490	1.56	0.27	0.06	—	0.026	0.018	0 014
Alloy 22 2277-8-3175	57.8	21.40	13.6	3.00	3.80	0.09	0.030	0.12	—	—	0.15	0.008	0.002	0.004
Alloy 22 2277-8-3193	55 9	21.79	13.42	2.97	3.94	1.62	0.024	0.20	—	—	0.13	0.008	0.001	0.003
Alloy 22 2277-7-3101	56.1	21.57	13.39	2.90	5.17	0.37	0.023	0 26	—	—	0.16	0.011	0.001	0.003

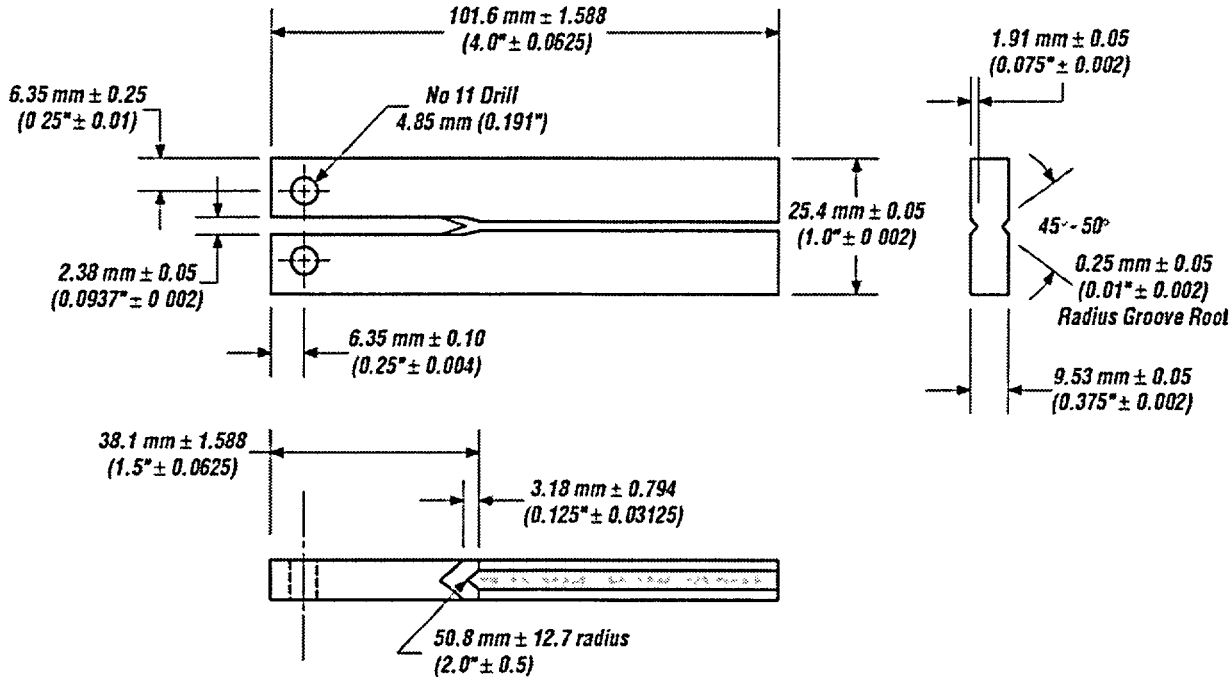

Figure 2-1. Dimensions of the Double Cantilever Beam Specimens According to NACE TM0177–96 (NACE International, 1996)

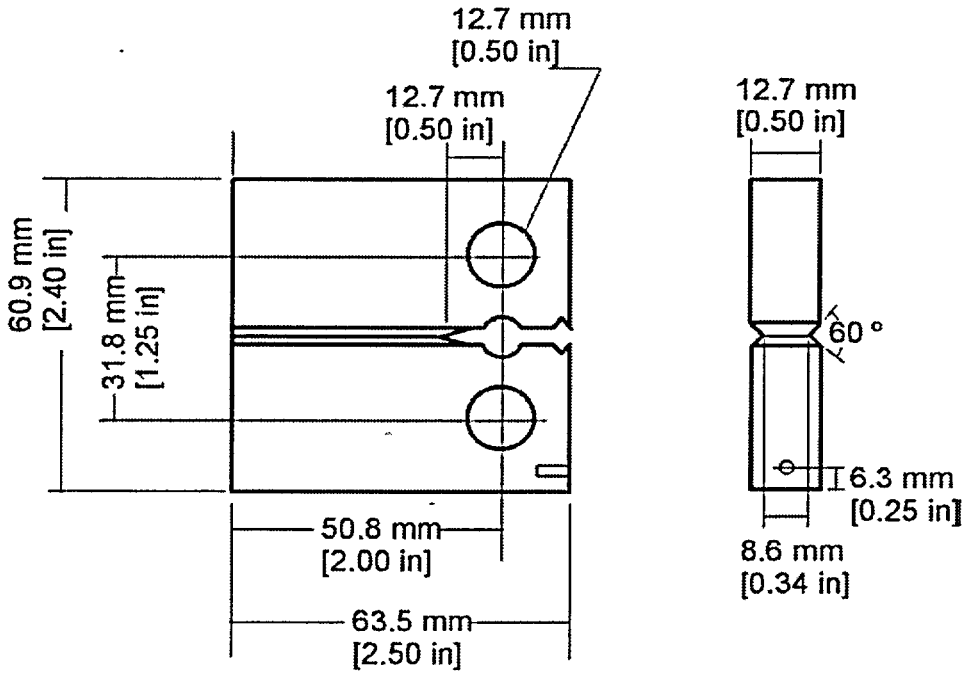

Figure 2-2. Dimensions of the Compact Tension Specimens

(T-L orientation) where the crack plane is perpendicular to the width direction (T direction), and the crack propagation is in the longitudinal rolling direction (L direction). Double cantilever beam specimens were also machined from a 25.4-mm [1.0-in] plate with a short-longitudinal orientation (S-L orientation) where the fracture plane is perpendicular to the short transverse direction (S direction) and the crack propagation is in the L direction (ASTM International, 1999). Test specimens were fatigue precracked using a servo hydraulic test machine following the guidelines for fatigue precracking specified in ASTM E399–90 Annex A2 (ASTM International, 1999).

All stress corrosion cracking tests were conducted in 2-L [0.44-gal] test cells equipped with a fritted gas bubbler, platinum counter electrode, temperature probe, and a water-cooled Luggin probe with a saturated calomel electrode used as a reference and maintained at room temperature. Stress corrosion cracking susceptibility was evaluated in concentrated $MgCl_2$ solutions (9.1 and 14.0 molal chloride) at 110 °C [230 °F] and concentrated LiCl solutions (9.1 molal chloride) at 95 °C [203 °F]. The potential of the specimens was controlled with a potentiostat. Tests were conducted using applied potentials both above and below the repassivation potential for crevice corrosion (E_{rcrev}) measured in cyclic potentiodynamic polarization tests (ASTM International, 2001b) using crevice corrosion test specimens described by Dunn, et al. (2000).

The double cantilever beam and compact tension specimens were periodically removed from the test cells and inspected with an optical microscope at low magnification. Scanning electron microscope photographs were used to document the starting condition of the specimens, changes in surface features, and signs of cracking. For the wedge-opening-loaded double cantilever beam specimens, the wedge was removed by loading the specimen in a servo-hydraulic load frame at the end of each test. A clip gage, installed to measure crack opening displacement, was used for the final compliance measurement. The final wedge load

was also determined. The stress at which the crack is arrested, expressed as threshold stress intensity, K_{ISCC}, can then be calculated. At the completion of each test, the specimens were rinsed in deionized water and dried. Most specimens were cleaned ultrasonically in an HCl solution that contained 2-butyne-1,4-diol as an inhibitor. Posttest examination was performed with an optical microscope and a scanning electron microscope.

Double Cantilever Beam Specimens

For the double cantilever beam specimens, the fatigue precracking was used to provide an initiation crack that extended past the specimen chevron notch. Stress calculations were performed assuming the double cantilever beam specimen was a straight beam subjected to pure bending. The initial stress intensity, K_I, for the side grooved double cantilever specimen was calculated (NACE International, 1996) according to Eq. (2-6)

$$K_I = \frac{Pa(2\sqrt{3} + 2.3\, h/a)(B/B_n)^{1/\sqrt{3}}}{Bh^{3/2}} \tag{2-6}$$

where

B	—	thickness of the specimen
B_n	—	net thickness of the specimen at the side grooves
P	—	load
a	—	crack length
h	—	height of the specimen arms

As reported previously by Pan, et al. (2000), the double cantilever beam specimens were fatigue-precracked under load control at 20 Hz, with a load ratio of 0.10 and a maximum stress intensity of 19.6 MPa·m$^{1/2}$ [17.8 ksi·in$^{1/2}$]. Compliance curves were measured prior to wedge opening loading. The initial crack length for all specimens was approximately 32.8 mm [1.29 in]. Alloy 22 double-tapered wedges were used to load the specimens to an initial stress intensity of 32.7 MPa·m$^{1/2}$ [29.7 ksi·in$^{1/2}$]. For a crack length of 32.8 mm [1.29 in], an initial loading of 2,482 N [558 lb] is required to achieve a K_I value of 34.8 MPa·m$^{1/2}$ [29.7 ksi·in$^{1/2}$].

Compact Tension Specimens

Stress corrosion cracking tests with compact tension specimens were conducted using both wedge opening loading and sustained loading conditions. The tests with wedge-opening-loaded specimens are constant crack opening displacement tests in which the stress intensity decreases with crack growth, whereas in the constant load tests, the stress intensity increases as the crack propagates. Tests were also conducted using cyclic loading with a frequency of 0.001 Hz and a load ratio of 0.7.

For all compact tension specimens, a crack length/specimen width ratio, or a/W ratio, of 0.45 to 0.55, consistent with the ASTM E399 (ASTM International, 1999), was used to determine the length of the initial fatigue precrack. In some cases, following the completion of fatigue precracking, specimens were wedge-opening-loaded using stress intensities below that used in the tests to allow the fatigue precrack to be examined with a microscope. After the fatigue

precrack had been examined, the loading wedge was removed and the specimen was prepared for testing. For the wedge-opening-loaded specimens, tapered wedges were used to apply stress intensities at the specimen crack tip ranging from 21.8 to 54.5 MPa m$^{1/2}$ [19.8 to 49.5 ksi·in$^{1/2}$]. The stress intensity for the compact tension specimens was calculated according to Eq. (2-7) (Anderson, 1991)

$$K = \frac{f(a/W)P}{(BB_nW)^{1/2}} \tag{2-7}$$

where the function *f(a/W)* was calculated according to Eq. (2-8)

$$f(a/W) = \frac{\left(2+\frac{a}{W}\right)\left(0.866+4.64\frac{a}{W}-13.32\frac{a^2}{W^2}+14.72\frac{a^3}{W^3}-5.64\frac{a^4}{W^4}\right)}{\left(1-\frac{a}{W}\right)^{3/2}} \tag{2-8}$$

Testing of the statically loaded compact tension specimens was conducted in mechanical load frames (dead-weight loaded) using stress intensities from 20 to 47 MPa m$^{1/2}$ [18 to 43 ksi·in$^{1/2}$]. Applied loads and specimen crack opening displacements were measured throughout the test. Specimen compliance was periodically measured by recording the crack opening displacement while slowly reducing the load and reapplying the load. The change in crack opening displacement (ΔCOD) was determined by subtracting the initial crack opening displacement from the final crack opening displacement at each time interval using Eq. (2-9)

$$\Delta\text{COD} = \text{COD}_{t=t} - \text{COD}_{t=0} \tag{2-9}$$

where

$\text{COD}_{t=t}$— crack opening displacement at any time
$\text{COD}_{t=0}$— crack opening displacement immediately after the load was applied (time = 0)

Tamaki, et al. (1990) showed that propagation of a crack through a Type 316 SS tapered double cantilever beam specimen resulted in measurable changes in compliance. Because the value of the compliance measurement obtained in this study was dependent on both the crack length and slight changes in the geometry of the load frame, a compliance ratio was used to compare time dependent changes in compliance measured in different tests. The compliance ratio was determined using Eq. (2-10)

$$\text{Compliance ratio} = \frac{\text{Compliance}_{t=t}}{\text{Compliance}_{t=0}} \tag{2-10}$$

where

$\text{Compliance}_{t=t}$— compliance at any time during the test
$\text{Compliance}_{t=0}$— initial compliance measurement after the load was applied (time = 0)

If stress corrosion cracking is initiated from the fatigue precrack and propagates through the specimen, the delta crack opening displacement should increase from the initial value of 0, the Compliance$_{t=t}$ should be greater than the Compliance$_{t=0}$, and the compliance ratio will be greater than 1. In the case where no stress corrosion cracking is initiated, the delta crack opening displacement should remain at or near 0, and the compliance ratio should remain at or near 1 for the duration of the test. Finally, for the case where stress corrosion cracking is initiated and then stops, both the delta crack opening displacement and the compliance ratio should increase while the crack is propagating and then remain constant after the crack is arrested.

2.2.2 Stress Corrosion Cracking Test Results

Type 316L SS Test Results

The effect of potential on the stress corrosion crack propagation rate for Type 316L SS double cantilever beam and wedge-opening-loaded compact specimens tested with initial applied stress intensities of 22 to 33 MPa m$^{1/2}$ [20 to 30 ksi·in$^{1/2}$] is shown in Figure 2-3. All tests were conducted using an initial stress intensity above the critical stress intensity for stress corrosion cracking for Type 316L SS that was determined to be 13.1 MPa m$^{1/2}$ [11.9 ksi·in$^{1/2}$] from wedge load measurements on double cantilever beam specimens exposed to 9.1 molal chloride as $MgCl_2$ (Pan, et al., 2000). The crack propagation rates were determined by measuring the length of the crack divided by the total test time (Cragnolino, et al., 2001b; Pan, et al., 2000).

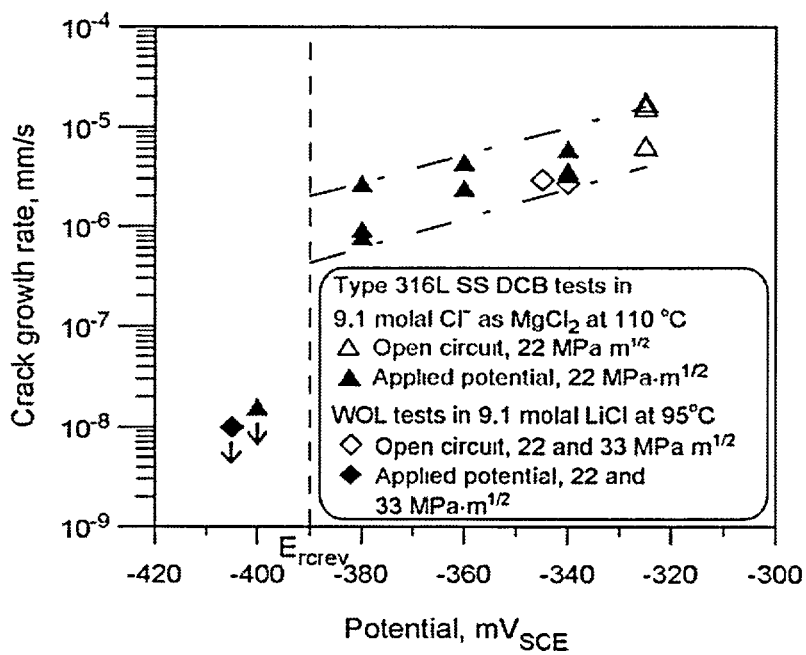

Figure 2-3. Crack Growth Rate for Type 316L SS as a Function of Potential in Concentrated Chloride Solutions Using Double Cantilever Beam (DCB) and Wedge Opening Loaded (WOL) Specimens. DCB Tests in 9.1 molal Cl^- (30 Percent $MgCl_2$) at 110 °C [230 °F] and 22 MPa·m$^{1/2}$ [20 ksi ·in$^{1/2}$] and WOL Tests in 9.1 molal LiCl at 95 °C [203 °F] and 22 and 33 MPa·m$^{1/2}$ [20 and 30 ksi ·in$^{1/2}$].

At potentials below the crevice corrosion repassivation potential, measured to be −395 mV_{SCE}, stress corrosion cracking was not observed even after 116 days of continuous exposure to concentrated chloride solutions. In contrast, stress corrosion cracking was quickly initiated when the potential of the specimen was maintained above the crevice corrosion repassivation potential. The crack propagation rate was observed to be dependent on potential. At −380 mV_{SCE}, the crack propagation rate was in the range 7.3×10^{-7} to 2.5×10^{-6} mm/s [2.9×10^{-8} to 9.8×10^{-8} in/s] and increased to 1.8×10^{-5} mm/s [7.1×10^{-7} in/s] under open circuit conditions where the corrosion potential was −330 to −320 mV_{SCE}.

Figure 2-4 shows results obtained with compact tension specimens tested under static loading conditions, using an initial stress intensity of 47 MPa $m^{1/2}$ [43 ksi·$in^{1/2}$]. It is apparent from Figure 2-4 that significant crack opening displacement and changes in compliance were observed for the specimen maintained at −350 mV_{SCE}. At the completion of the test, significant crack propagation was observed, and more than one crack was initiated. Examination of the fracture surface revealed transgranular crack growth that propagated a minimum of 4.32 mm [0.17 in] from the end of the fatigue precrack. Assuming that cracking was initiated immediately after the load was applied, the minimum crack growth rate was 6.5×10^{-6} mm/s [2.5×10^{-7} in/s]. No significant change in crack opening displacement or compliance ratio was observed for specimens maintained at −375 and −400 mV_{SCE}. Both specimens showed some increase in the crack opening displacement that is not attributable to crack initiation and growth but is attributable to mechanical deformation of the test specimen. The test at −375 mV_{SCE} was conducted in two test segments. The first test segment lasted approximately 300 hours and the

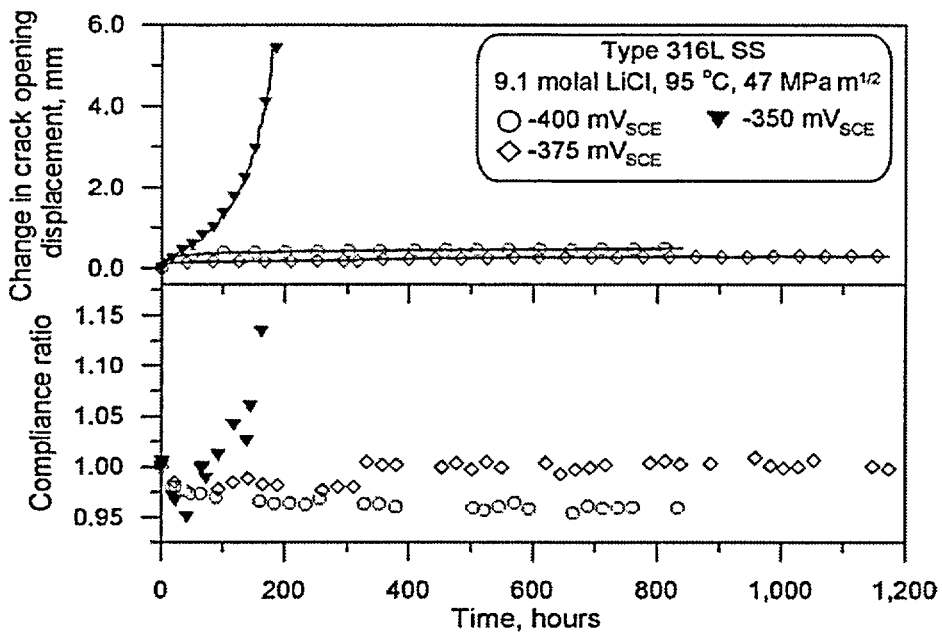

Figure 2-4. Change in Crack Opening Displacement and Compliance Ratio as a Function of Potential for Type 316L SS Compact Tension Specimens Tested in 9.1 molal LiCl at 95 °C [203 °F] and 47 MPa·$in^{1/2}$ [43 ksi·$in^{1/2}$]

second slightly less than 900 hours. Because the compliance ratio was determined using the initial compliance at the start of the test, the compliance ratio at the start of the second test segment was 1.0. Although the compliance ratio appeared to increase from the end of the first test segment to the start of the second test segment, this increase was a consequence of the method to determine the parameter plotted in Figure 2-4 rather than an indication of stress corrosion cracking. For the specimen tested at −375 mV_{SCE}, it is apparent the compliance ratio did not increase with time during the second test segment. For both specimens, the posttest examinations revealed no indication of stress corrosion cracking.

The specimen tested at −400 mV_{SCE}, which is below the repassivation potential, was fractured by additional fatigue cycling in a servo-hydraulic test machine. Scanning electron micrographs of the fracture surface are shown in Figure 2-5. The fracture surface has two distinct regions, one associated with the initial fatigue precrack and the second associated with the fatigue after testing. Plastic deformation is visible in the fatigue region. Detailed inspection of this region did not reveal any evidence of either intergranular or transgranular stress corrosion cracking. Uncertainty in the stress corrosion crack propagation is based on the resolution of the scanning electron microscope examination and the length of the test. Assuming a resolution of 10 μm [3.9×10^{-4} in] and a test time of 839 hours, the uncertainty in the stress corrosion crack propagation rate can be calculated as 3.3×10^{-9} mm/s [1.3×10^{-10} in/s].

The effect of stress intensity is shown in Figure 2-6. When the initial stress intensity was reduced from 47 to 20 MPa $m^{1/2}$ [43 to 18 ksi·$in^{1/2}$], significant changes in crack opening displacement and compliance ratio did not occur until after 700 hours of exposure at −350 mV_{SCE}. Posttest examination of the specimen tested at 20 MPa $m^{1/2}$ [18 ksi·$in^{1/2}$] revealed transgranular stress corrosion cracking (Figure 2-7). The fracture surfaces of the two specimens were similar. It was not possible to determine when stress corrosion cracking was initiated in the test conducted at the lower stress intensity. Assuming stress corrosion cracking initiated immediately after the load was applied, reducing the stress intensity reduced the average crack propagation rate from 6.5×10^{-6} to 2.3×10^{-6} mm/s [2.6×10^{-7} to

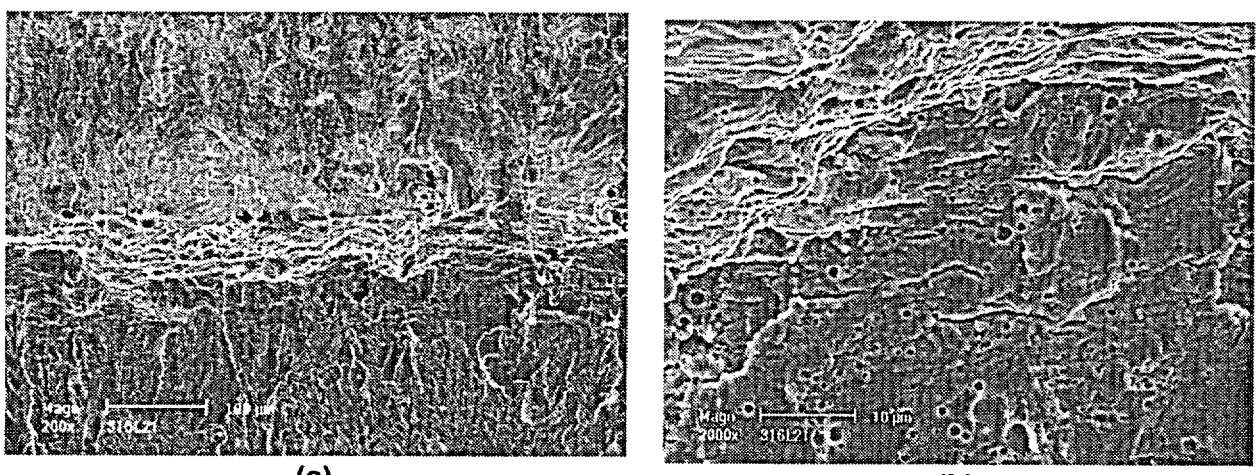

(a) (b)

Figure 2-5. Scanning Electron Micrographs at (a) 200× and (b) 2000× Showing the Fracture Surface of Type 316L SS After Testing at −400 mV_{SCE} in 9.1 molal LiCl. The Initial Stress Intensity Was 47 MPa $m^{1/2}$ [42.8 ksi·$in^{1/2}$].

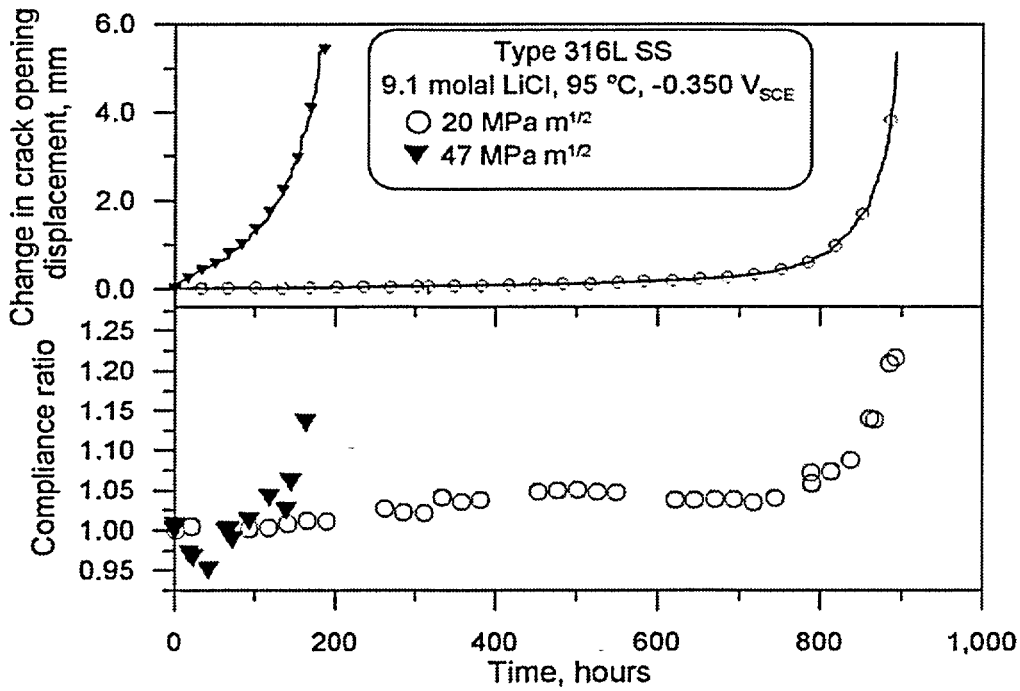

Figure 2-6. Change in Crack Opening Displacement and Compliance Ratio as a Function of Initial Stress Intensity for Type 316L SS Compact Tension Specimens Tested in 9.1 molal LiCl at a Potential of −350 mV_{SCE}, a Temperature of 95 °C [203 °F] and Initial Stress Intensity Values of 20 and 47 MPa·in$^{1/2}$ [18 and 43 ksi·in$^{1/2}$].

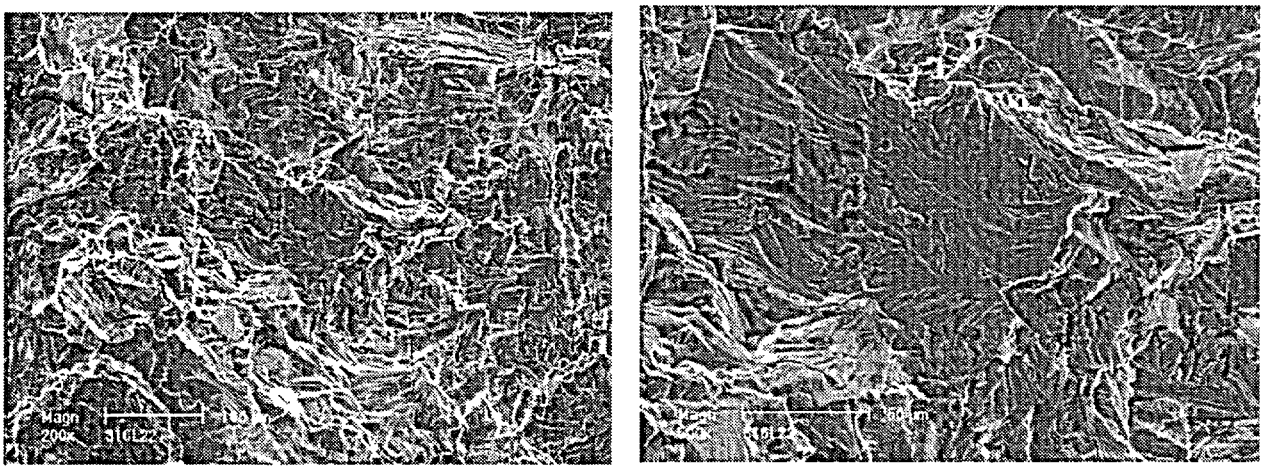

(a) (b)

Figure 2-7. Scanning Electron Micrographs at (a) 200× and (b) 500× Showing the Fracture Surface of Type 316L SS After Testing at −350 mV_{SCE} in 9.1 molal LiCl. The Initial Stress Intensity Was 20 MPa·m$^{1/2}$ [18 ksi·in$^{1/2}$].

9.1×10^{-8} in/s]. Alternatively, assuming the crack did not initiate until 700 hours, the calculated crack propagation rate would increase to 7.6×10^{-6} mm/s [3.0×10^{-7} in/s], which is similar to the crack propagation rate calculated for the specimen tested at 47 MPa·m$^{1/2}$ [43 ksi·in$^{1/2}$].

The effect of potential was also investigated using cyclic loading tests. Figure 2-8 shows the results obtained for a Type 316L SS specimen tested in 9.1 molal LiCl at -350 mV_{SCE} using cyclic loading for the first 30 hours of testing. After the first 30 hours, a constant load was applied. The crack opening displacement and the compliance ratio gradually increased for the first 100 hours of testing. A sharp increase in the compliance ratio was observed after 120 hours of testing, indicating crack propagation. Examination of the specimen fracture surface revealed transgranular stress corrosion cracking (Figure 2-9). An additional test was conducted in which the applied potential of the specimen was gradually decreased from -350 to -400 mV_{SCE} at a rate of 10 mV/hr after crack initiation and propagation (Figure 2-10). Cyclic loading at a frequency of 0.001 Hz and a load ratio of 0.7 was continued as the potential was decreased. It is apparent from Figure 2-10 that the crack opening displacement increased during the first 250 hours of testing, although the potential of the specimen was maintained at -350 mV_{SCE}. Once the potential was decreased, the crack opening displacement change slowed gradually. After changing from cyclic to static loading, the delta crack opening displacement increased abruptly several times before reaching a constant value after 500 hours. The lack of crack propagation was also indicated by the constant compliance ratio. The potential of the specimen was allowed to reach to open circuit condition by disconnecting the potentiostat. The corrosion potential in the air-saturated solution was in the range of -340 to -350 mV_{SCE}. At open circuit, both the crack opening displacement and the compliance ratio increased sharply indicating the reinitiation and propagation of cracks. Examination of the fracture surfaces following the test confirmed the transgranular path. Figure 2-11 shows the results for a similar test where the initial conditions are selected to promote stress corrosion

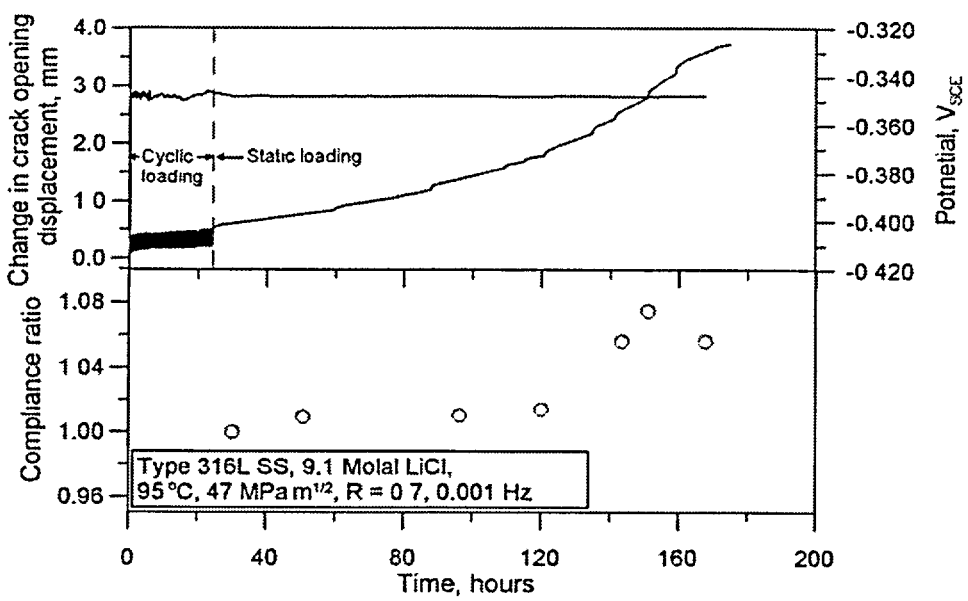

Figure 2-8. Change in Crack Opening Displacement and Compliance Ratio for a Type 316L SS Compact Tension Specimen Tested in 9.1 molal LiCl at a Potential of -350 mV_{SCE}. Cyclic Loading Was Used To Initiate Stress Corrosion Cracking.

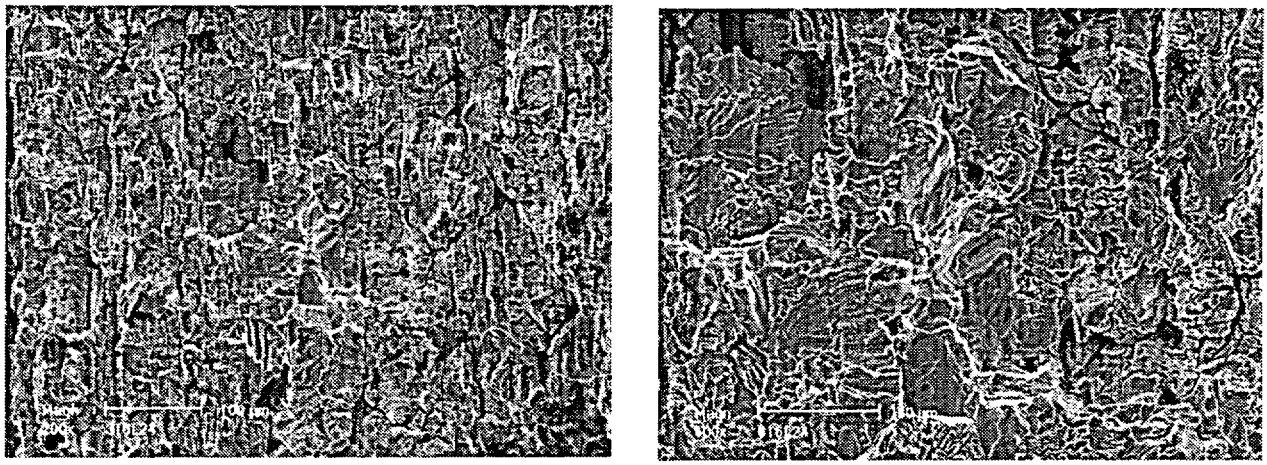

(a) (b)

Figure 2-9. Scanning Electron Micrographs at (a) 200× and (b) 500× Showing Fracture Surface of Type 316L SS After Testing at −350 mV_{SCE} in 9.1 molal LiCl at 95 °C [203 °F] and 47 $MPa{\cdot}m^{1/2}$ [43 $ksi{\cdot}in^{1/2}$]. Cyclic Loading at 0.001 Hz with R = 0.7 Was Used To Initiate Stress Corrosion Cracking.

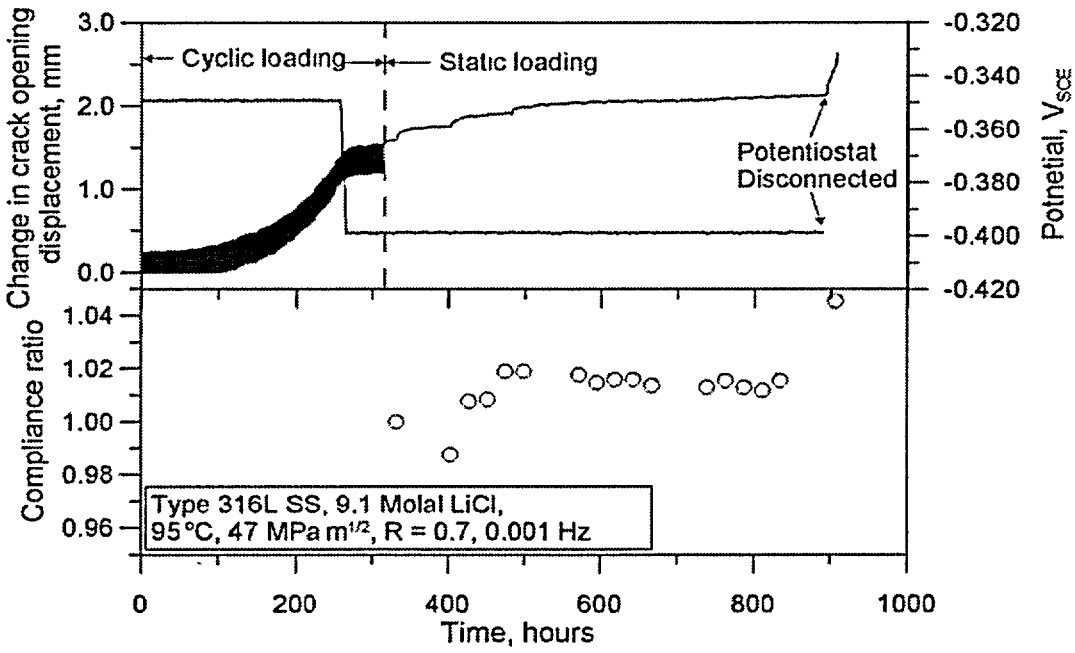

Figure 2-10. Change in Crack Opening Displacement and Compliance Ratio for a Type 316L SS Compact Tension Specimen Tested in 9.1 molal LiCl at 95 °C [203 °F] and 47 $MPa{\cdot}m^{1/2}$ [43 $ksi{\cdot}in^{1/2}$]. Cyclic Loading at a Potential of −350 mV_{SCE} Was Used To Initiate Stress Corrosion Cracking.

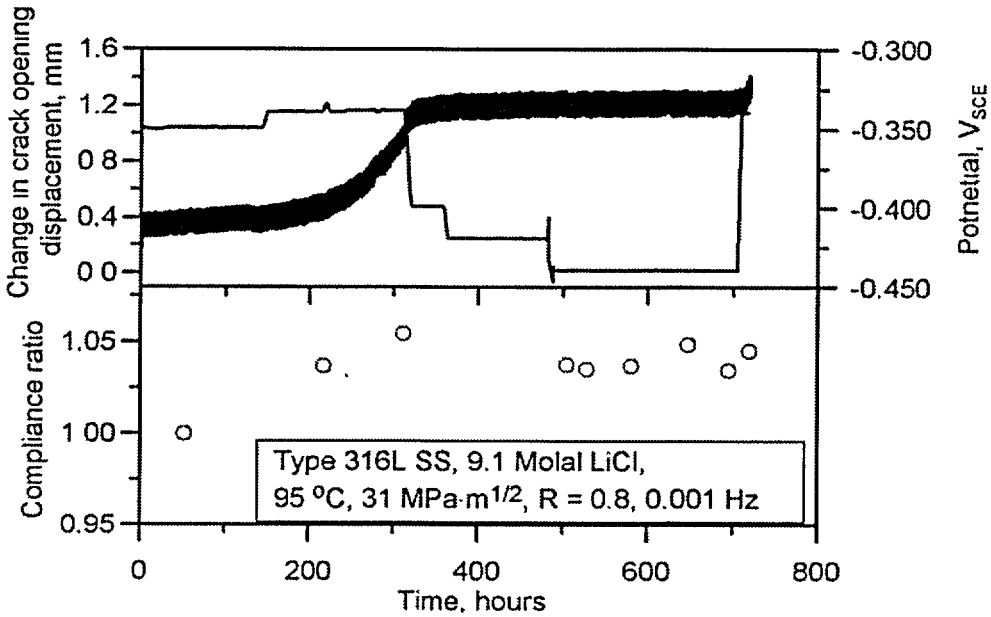

Figure 2-11. Change in Crack Opening Displacement and Compliance Ratio for a Type 316L SS Compact Tension Specimen Tested in 9.1 molal LiCl at 95 °C [203 °F] and 31 MPa·m$^{1/2}$ [28 ksi·in$^{1/2}$]. Cyclic Loading at a Potential of −350 to −340 mV$_{SCE}$ Was Used To Initiate Stress Corrosion Cracking.

cracking. After stress corrosion crack growth was assured, the potential of the specimen was again decreased at a rate of 10 mV/hr. Cyclic loading at a frequency of 0.001 Hz and a load ratio of 0.7 was continued throughout the test. A rapid increase in the change in crack opening displacement was observed during crack propagation, although the potential of the specimen was maintained above the repassivation potential. When the potential of the specimen was reduced below the repassivation potential for crevice corrosion, the change in crack opening displacement was relatively constant. Slow changes in the crack opening displacement may be attributed to slow crack growth as a consequence of the continued cyclic loading.

Analysis of Type 316L SS Tests

Results obtained for Type 316L SS in concentrated chloride solutions show that stress corrosion cracking was rapidly initiated, and crack propagation rates in the range 10^{-6} to 10^{-5} mm/s [4×10^{-8} to 4×10^{-7} in/s] were measured (Cragnolino, et al., 2001b; Pan, et al., 2000) when the potential of the test specimen was maintained above the crevice corrosion repassivation potential. No stress corrosion cracking was initiated when the applied potential was maintained below the crevice corrosion repassivation potential. Increasing the applied stress intensity at the crack tip from 22 to 55 MPa m$^{1/2}$ [20 to 50 ksi·in$^{1/2}$] did not increase the susceptibility of the material to stress corrosion cracking when the applied potential was less than the crevice corrosion repassivation potential. The effect of potential on the stress corrosion cracking susceptibility is in agreement with Eremias and Marichev (1980) who

reported that, in 10.8 molal LiCl solutions, the critical stress intensity for stress corrosion cracking for an austenitic stainless steel increased when the specimen potential was decreased.

Posttest examination of the compact tension specimen maintained below the crevice corrosion repassivation potential revealed the fracture surface was dominated by ductile failure (Figure 2-5). Linear features observed in Figure 2-5 appear similar to cracks perpendicular to the fatigue precrack. Several investigations reported crack branching in annealed stainless steel (Speidel, 1977, 1976; Staehle, 1971). The features in Figure 2-5 are not consistent with stress corrosion cracking. Dimples created by microvoid coalescence are visible for most of the area. These crack-like features may be attributed to local ductile tearing as a consequence of the high stress intensity used in the test.

Although the potentiostatic tests showed stress corrosion cracking was not initiated so long as the potential of the test specimen was below the crevice corrosion repassivation potential, it was desirable to determine the effect of potential on crack propagation. This was accomplished by conducting tests where stress corrosion cracking was initiated and allowed to propagate with the potential of the specimen above the crevice corrosion repassivation potential prior to reducing the potential to just below the repassivation potential. The results shown in Figures 2-10 and 2-11 suggest that the propagation rate was substantially reduced when the potential of the specimen was lowered to a value a few millivolts less than the crevice corrosion repassivation potential. The test was performed so the potential of the specimen could be gradually reduced to prevent sudden changes to the chemistry of the actively growing crack. Cyclic loading was continued for more than 30 hours after the potential of the specimen was reduced to promote crack initiation and growth. After a static load was applied, the crack opening displacement increased, albeit slowly, throughout the remainder of the test. The compliance ratio increased slightly for approximately 180 hours after the potential was reduced before eventually reaching a constant value. The plateau in the compliance ratio suggests that either the crack ceased to propagate or the rate of crack propagation was slow and could not be detected by changes in compliance. It is not possible, however, to conclude that crack growth was arrested when the potential of the specimen was reduced below the crevice corrosion repassivation potential because there was a measurable increase in the crack opening displacement as a function of time.

It should be noted the increase in crack opening displacement may not be an indication of crack propagation. Because of the combination of a constant load and an increase in the length of the crack as a consequence of stress corrosion cracking in the initial part of the test, the stress intensity at the crack tip also increased. Assuming that 80 percent of the crack propagation occurred in the initial 500 hours of the test (based on the observation that 80 percent of the change in the crack opening displacement occurred in the initial 500 hours of testing), the value of the crack length to specimen width ratio (a/W) would increase from 0.45 to 0.55. Correspondingly, the stress intensity at the crack tip would increase from 47 to 64 MPa $m^{1/2}$ [43 to 58 ksi·$in^{1/2}$]. The increased stress intensity was in excess of the maximum stress intensity for plane stress conditions. Ductile yielding and ductile tearing, which are possible under these conditions, may be responsible for the slight increase in the crack opening displacement while the potential was maintained at -400 mV_{SCE}.

Results obtained for Type 316L SS in this study are partially in agreement with the results of Russell and Tromans (1979), who reported the arrest of stress corrosion cracking for

Type 316L SS in 44.7 percent $MgCl_2$ (15.6 molal chloride) when the potential was reduced from -250 to -350 mV_{SCE}. Crack arrest was not instantaneous, however, and was reported to decrease gradually during 1.5 hours. In addition, the minimum crack propagation rate reported by after stress corrosion cracking arrest was 10^{-6} mm/s [3.9×10^{-8} in/s], which was substantially lower than the crack propagation rate of 4×10^{-4} mm/s [1.5×10^{-7} in/s] at higher potentials. The differences in crack propagation rates measured by Russell and Tromans (1979) and those measured in this study can be attributed to differences in the types of test specimens and testing conditions. Both testing time and the resolution of the crack growth rate were not reported in Russell and Tromans (1979). As a result, it is not possible to determine if stress corrosion cracking arrest was achieved by reducing the potential, or if crack propagation continued at a rate less than 10^{-6} mm/s [3.9×10^{-8} in/s]. The results of tests performed in this study suggest the stress corrosion crack propagation rate was reduced when the potential was reduced below the crevice corrosion repassivation potential. However, a conclusive determination of crack arrest may be possible only using lower stress intensities where ductile failure is not a concern or a more sensitive method for detection of crack growth.

Alloy 22 Test Results

Tests were conducted in 14.0 molal chloride as $MgCl_2$ using double cantilever beam specimens at a stress intensity of 32.7 MPa $m^{1/2}$ [29.7 ksi·$in^{1/2}$] (Pan, et al., 2000). After 21 weeks of exposure under open circuit conditions where the corrosion potential was in the range of -280 to -250 mV_{SCE}, grain boundary attack was observed on the side groove of a specimen with a transverse-longitudinal orientation, however, no stress corrosion cracking was identified from either an initial inspection of the specimen side groove or a detailed examination of the fracture surface after the specimen was fractured by fatigue. Some minor cracking was observed on the side groove of a specimen with a short-longitudinal orientation after 10 weeks of testing. Continued exposure for a cumulative 52 weeks did not result in any crack propagation. At the end of the tests, the specimens were heat-tinted at 371 °C [700 °F] and then mechanically overloaded to failure. Examination of the fracture surfaces after testing clearly revealed both tinted and untinted regions on the fracture surface. No features of stress corrosion cracking were observed; however, the appearance of the untinted region of the fracture surface, created as a consequence of mechanical overloading after exposure, tended to be flat and slightly faceted, indicating a less ductile failure.

Results obtained with statically loaded Alloy 22 compact tension specimens using an initial stress intensity of 47 MPa $m^{1/2}$ [43 ksi·$in^{1/2}$] are shown in Figure 2-12. The crevice corrosion repassivation potential for Alloy 22 in 9.1 molal LiCl at 95 °C [203 °F] was measured as -247 mV_{SCE} using cyclic polarization. Based on this measurement, the potential of the specimens was maintained close to the repassivation potential (-250 mV_{SCE}) and 5–30 mV above the crevice corrosion repassivation potential (-245 to -220 mV_{SCE}). The specimens were exposed in 800-hour test segments, at which time the specimens were removed from the test cell and examined for signs of stress corrosion cracking. At the start of the test, the crack opening displacement increased to just greater than 0.1 mm for the specimen maintained above the crevice corrosion repassivation potential. A smaller increase in the crack opening displacement was observed for the specimen maintained close to the crevice corrosion repassivation potential. After initially increasing, the crack opening displacement remained constant for both specimens. A slight increase in the crack opening displacement was

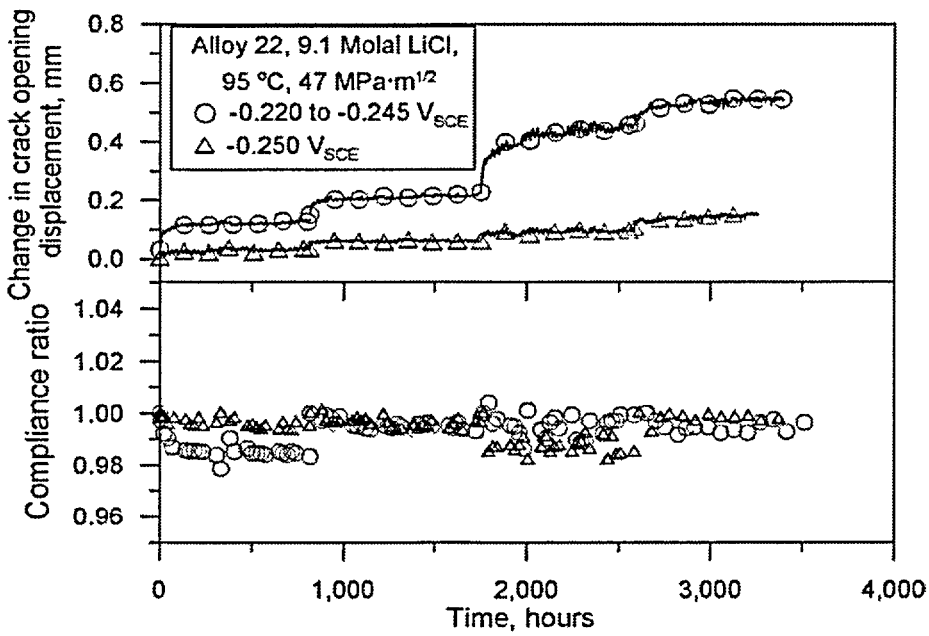

Figure 2-12. Change in Crack Opening Displacement and Compliance Ratio for Alloy 22 Compact Tension Specimens Tested in 9.1 molal LiCl at 95 °C [203 °F] and 47 MPa·m$^{1/2}$ [43 ksi·in$^{1/2}$]

observed at the start of each test segment. The compliance ratio was determined separately for each test segment. For both specimens, the compliance ratio was at or less than 1. The discontinuous increase in the compliance ratio from 0.98 to 1.00 for the specimen maintained anodic to the crevice corrosion repassivation potential was a result of the reinitialization of the compliance ratio calculation rather than an indication of crack propagation. Visual examination of the specimen side groove after exposure for 800 and 1,600 hours revealed some plastic deformation that opened the crack and perhaps blunted the tip of the fatigue precrack. Some secondary cracking was observed on the specimens maintained anodic to the crevice corrosion repassivation potential. The secondary cracks appeared to initiate at grain boundaries that were visible after fatigue precracking and prior to testing. This observation suggests that extensive mechanical damage and perhaps some intergranular fracture occurred during fatigue precracking. Testing of the specimens continues to assess the stress corrosion cracking resistance of Alloy 22.

A cyclic loading test of a fatigue precracked Alloy 22 compact tension specimen was also conducted in 9.1 molal LiCl (Figure 2-13). The potential of the specimens was continuously maintained above the crevice corrosion repassivation potential. An anodic current density of approximately 2×10^{-8} A/cm^2 [1.8×10^{-5} A/ft^2] was recorded when the applied potential was −230 mV$_{SCE}$ or less. When the potential was increased to −225 mV$_{SCE}$, a significant increase in the passive current was observed, and the potential of the specimen was promptly reduced to avoid the initiation of localized corrosion. The crack opening displacement and the compliance ratio were virtually constant during the entire test and were not influenced by variations in the

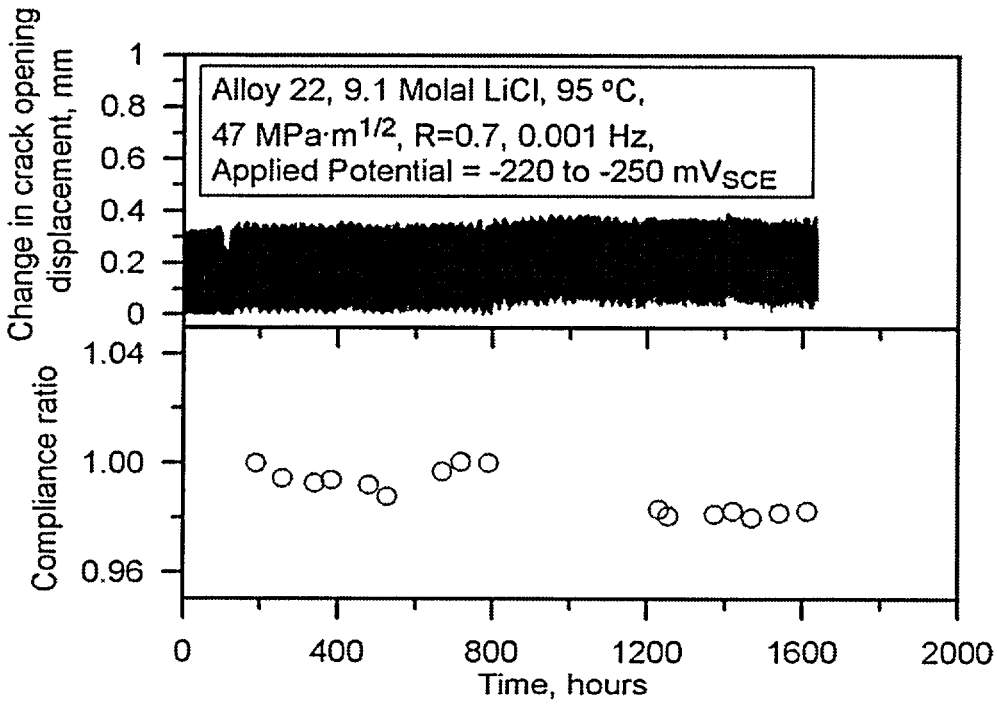

Figure 2-13. Change in Crack Opening Displacement and Compliance Ratio for Alloy 22 Compact Tension Specimens Tested in 9.1 molal LiCl at 95 °C [203 °F] and 47 MPa·m$^{1/2}$ [43 ksi·in$^{1/2}$] Under Cyclic Loading Conditions

applied potential. Examination of the sides of the specimens after testing revealed no indication of stress corrosion cracking. Additional exposures under similar conditions are planned.

Analysis of Alloy 22 Tests

Tests conducted with Alloy 22 did not conclusively indicate susceptibility to stress corrosion cracking in concentrated chloride solutions. The absence of stress corrosion cracking under conditions investigated are in agreement with the original results reported by Copson (1959) that alloys with more than 40 percent nickel are resistant to chloride stress corrosion cracking. In later work by Speidel (1981), using fracture mechanics specimens with an initial stress intensity of 60 MPa m$^{1/2}$ [56 ksi·in$^{1/2}$], no stress corrosion cracking was initiated on alloys containing more than 40 percent nickel in boiling concentrated NaCl solutions. In this investigation, limited secondary cracking and increased crack opening displacement obtained under constant loading conditions when the potential was maintained above the crevice corrosion repassivation potential, suggest that chloride stress corrosion cracking may be possible in aggressive conditions; however, the stress corrosion crack propagation rate may be very slow. In addition, the potential range for stress corrosion cracking decreases as the chloride concentration increases. Tamaki, et al. (1990) suggest that in concentrated chloride solutions, the potential range for stress corrosion cracking may be limited to a few millivolts above crevice corrosion repassivation potential. At higher potentials, localized corrosion in the form of crevice corrosion may occur preferentially to stress corrosion cracking. The visual

observation of crevice corrosion and the significant increase in current observed when the potential of the Alloy 22 specimen was increased to −225 mV_{SCE} are consistent with the observations of Tamaki, et al. (1990). An attempt to use cyclic loading to initiate stress corrosion cracking was based on the recently reported results of Andresen, et al. (2001). Using cyclic loading at a frequency 0.001–0.003 Hz, Andresen, et al. (2001) reported the initiation of stress corrosion cracking on Alloy 22 in concentrated high pH salt solutions at 110 °C [230 °F]. The crack growth rates reported by Andresen, et al. (2001) are 5×10^{-10} mm/s [2×10^{-11} in/s]. At this low crack propagation rate, test times of more than 200 days are needed to have a crack extension of 0.01 mm [3.9×10^{-4} in]. It should be noted the tests performed at the CNWRA and the test results reported by Andresen, et al. (2001) are limited to temperatures of 110 °C [230 °F]. Stress corrosion cracking in concentrated chloride solutions at higher temperatures has been reported for highly alloyed nickel-chromium-molybdenum alloys (Sridhar and Cragnolino, 1992). Consequently, it may be possible to have crack propagation for highly alloyed nickel base alloys at temperatures in excess of 200 °C [392 °F].

2.3 Summary

Results of the DOE testing, in agreement with data reported in the literature, suggest that Alloy 22 is resistant to chloride stress corrosion cracking. It must be noted, however, that the DOE tests have been conducted using a limited range of solution chemistries and temperatures, which have not been demonstrated to bound the environmental conditions expected within the drifts of the proposed repository. Stress corrosion crack propagation tests demonstrated the importance of a minimum critical stress intensity in the presence of an existing flaw. Environmental, potential, and fabrication effects on the crack propagation rates or threshold stress intensity for stress corrosion cracking have not been reported.

Independent investigations conducted at CNWRA demonstrated that both potential and stress intensity have pronounced effects on crack initiation and propagation for chloride stress corrosion cracking of Type 316L SS. The resistance of Alloy 22 to chloride stress corrosion cracking has also been demonstrated in these studies; however, as in the DOE investigations, tests were limited to temperatures not likely to bound those temperatures expected in the proposed repository.

The present DOE model abstraction for stress corrosion cracking of waste packages considers the important contributions of flaw frequency, size distribution, and orientation, as well as the residual stress, stress profiles, and stress intensity factors. The model abstraction has many of the necessary components to assess susceptibility to stress corrosion cracking and predict crack propagation rates. The model abstraction, however, is supported by many assumptions, parameters, and calculations that need to be verified, such as flaw frequency and distribution parameters, residual stresses after solution annealing and quenching of the disposal container, and both magnitude and variation in the residual stress profiles after laser peening and induction annealing. Effects of waste package fabrication, material composition and material property variations, and environmental variations are not yet accounted for in the DOE model abstraction. DOE agreed to provide the information necessary to assess the stress corrosion cracking susceptibility of the waste packages for conditions that may exist in the proposed repository as well as the effects of stress corrosion cracking on the release of radionuclides. Agreements pertaining to stress corrosion cracking of candidate container materials were documented during technical exchanges between DOE and NRC. DOE is

scheduled to provide the information outlined in stress corrosion cracking related agreements for the Container Life and Source Term and the Total System Performance Assessment and Integration Key Technical Issues in December of 2003.

Although the effects of waste package fabrication and stress mitigation processes on the stress corrosion cracking susceptibility of Alloy 22 have not been provided, DOE agreed to provide stress corrosion cracking data for Alloy 22 for a full range of metallurgical conditions in agreement CLST 1.12. The data that DOE agreed to provide in agreement CLST 1.12 should assess the possible detrimental effects of fabrication processes on both the critical stress intensity for stress corrosion cracking and on crack propagation rates. DOE also agreed to determine the effects of geometry and thermal and metallurgical effects of multipass welding processes by conducting stress corrosion crack susceptibility tests using specimens from a waste package mockup in agreement CLST 1.15.

Stress mitigation methods, such as laser peening and induction annealing, are important for reducing the susceptibility of the waste packages to stress corrosion cracking. At present, the stress and stress intensity profiles used in the DOE model abstraction are based on calculations with many inherent assumptions such as the uncertainty in the stress distribution. In agreement CLST 1.13, DOE agreed to provide the data that characterize the distribution of stresses owing to laser peening and induction annealing. Although reduction of residual stresses may be possible using the proposed induction annealing processes, detrimental effects of the thermal process must be considered together with thermal stability of the container material. DOE will provide documentation of the measured thermal profile of the waste package material in the induction annealing process in agreement CLST 1.16. The information that will be provided is necessary to evaluate possible changes to the material microstructure that may alter both the stress corrosion cracking and localized corrosion susceptibility.

The DOE model abstraction is limited to the residual stresses associated with waste package closure. Applied and residual stresses from rockfall and dead-weight loads that may occur in the event of drift collapse are not considered in the abstraction. Applied and residual stresses on the waste packages will depend on the characteristics of the rockfall or drift collapse events including rock size, rock shape, impact velocity, volume of material, and design of the engineered barrier subsystem. DOE agreed to provide the justification for not including the effects of rockfall and drift collapse on the stress corrosion cracking of the waste package in agreement CLST 1.14. In addition, release of radionuclides from waste packages that fail from stress corrosion cracking may be determined by the geometry of the crack openings and the deposition of corrosion products and mineral deposits. DOE agreed to provide the technical basis for crack plugging and crack arrest that may alter the release of radionuclides according to agreement TSPAI 3.03.

3 EFFECT OF MINOR SPECIES ON STRESS CORROSION CRACKING OF CONTAINER MATERIALS

Small concentrations of lead ranging from 2.5 to 6 parts per million are known to cause stress corrosion cracking of Alloy 600 (Ni-18Cr-5Fe) in deionized water adjusted to pH 10 with the addition of ammonia (Copson and Dean, 1965). The presence of lead in pressurized water reactor environments was also reported to cause stress corrosion cracking of Alloy 600 steam generator tubes in the 1990s (Agrawal and Paine, 1990; Helie, et al., 1995). The lead concentration measured in the sludge deposits of most steam generators was in a range of 100 to 500 parts per million; however, higher concentrations of lead to 10,000 parts per million were detected on the surface scale of the Alloy 600 tubes (Agrawal and Paine, 1990). Helie, et al. (1995), attributed the lead-assisted stress corrosion cracking of nickel base alloys (Alloys 600, 690, and 800) to enhanced dissolution and/or oxidation of the alloys. An activation energy of 125 kJ/mol [30 kcal/mol] has been measured (Helie, et al., 1995), indicating that stress corrosion cracking susceptibility decreases substantially with decreasing temperature.

Rock-water interactions during extended periods can leach specific detrimental species that may become concentrated in the water dripping on the drip shield and waste packages. Carlos, et al. (1995) observed the presence of Mn-oxide minerals, in which lead was found as a minor component, in the vicinity of the proposed repository at Yucca Mountain. These lead-containing minerals (i.e., oxides and carbonates), however, are known to have very limited solubilities in water. Groundwater and the host rock in the Yucca Mountain region were reported to have measurable concentrations of trace elements, such as lead and mercury, at or below the parts per million level (Perfect, et al., 1995). There are no good estimates of the concentration that these species can reach by multiple evaporation cycles of the groundwater.

Studies sponsored by the State of Nevada indicated that the resistance of the Alloy 22 outer container to localized corrosion and stress corrosion cracking may be affected by the presence of impurities (i.e., lead, mercury, and arsenic) in the water contacting the waste packages. Even though the test conditions used in the State of Nevada investigations were extremely severe for lead concentrations, temperature, and stress, the possible detrimental effects of impurities, such as lead, mercury, or arsenic, require further evaluation. The U.S. Department of Energy (DOE) agreed to provide additional information about the range of concentrations of minor species expected to evolve in Yucca Mountain waters and their effects on the critical potential for localized corrosion and about the stress corrosion cracking susceptibility of Alloy 22, according to agreements CLST 1.01 and CLST 1.10. If greater concentrations of minor species are found in Yucca Mountain waters, the current model abstraction for stress corrosion cracking needs reevaluation to account for the effects of these species. A review of the State of Nevada and the DOE investigations, as well as the work conducted at the Center for Nuclear Waste Regulatory Analyses (CNWRA) about the effects of minor species on stress corrosion cracking of Alloy 22 are provided in this chapter.

3.1 State of Nevada Investigations

Barkatt, et al.[1] reported the stress corrosion cracking of Alloy 22 in concentrated J–13 Well water containing 5,000 parts per million of lead (as lead acetate) at 250 °C [482 °F] as a part of the experimental program for the State of Nevada on engineered barrier subsystem materials. The test solution was simulated J–13 Well water with a 1,000× concentration factor and acidified to a pH of 0.5 with the addition of HCl. Only one stress corrosion cracking test was conducted under such environmental conditions using a single U-bend specimen. In a recent presentation to the DOE Waste Package Materials Performance Peer Review Panel, Gorman[2] reported additional test results for the effects of lead and mercury on corrosion and stress corrosion cracking of Alloy C-22. Stress corrosion cracking susceptibility was evaluated in various solution environments using single U-bend specimens. The test solutions were also based on 1,000× J–13 Well water with the addition of 18,000 parts per million of silica and 5,000 parts per million of lead in the form of lead acetate and the addition of HCl or NaOH for pH adjustment. Contrary to the previously reported results, no stress corrosion cracking was observed in a series of tests in which the temperature ranged from 210 to 250 °C [410 to 482 °F] and the initial pH ranged from acidic to basic (pH 0.5, 1, 3, 5, and 14) with a duration of 4 to 6 weeks in most of the cases. Localized corrosion in the form of crevice corrosion and pitting, however, was observed in several of the test specimens. From these test results, it is clearly evident that Alloy C-22 was found to be resistant to stress corrosion cracking, contrary to previous observations of severe cracking with 5,000 parts per million of lead at 250 °C [482 °F] and pH 0.5. The lack of reproducibility in the stress corrosion cracking data was attributed to heat-to-heat variations or to minor changes in test conditions.

Pulvirenti, et al. (2002a) summarized the results of stress corrosion cracking tests of Alloy 22 in lead-containing solutions described in the above two presentations. Two different heats of Alloy 22 were used; their chemical compositions are listed in Table 3-1. Note the significant difference in cobalt content among the major alloying elements (1.96 versus 0.72 wt% for Heats 1 and 2) in Table 3-1; however, the cobalt content in these heats was within the chemical composition range specified in ASTM B575 in Table 3-1 (ASTM International, 2001a) and is not expected to affect cracking behavior of Alloy 22. Four U-bend specimens of dimensions 63.5 × 19 × 3.2 mm [2.50 × 0.75 × 0.12 in] were tested at 250 °C [482 °F] in 1,000× J–13 Well water with 0.5 percent (5,000 parts per million) of lead (as lead acetate) acidified to pH 0.5. Of these tests, only 1 specimen from Heat 1 exhibited a crack at the apex of the U-bend after 8 days, and then it extended to a through crack after 15 days. In contrast, the other 3 specimens from Heat 2 experienced pitting in the apex and the legs, but no evidence of cracking, after testing was extended to 64 days. Additional tests were conducted to evaluate the effects of pH and temperature using U-bend specimens of dimensions 44.45 × 12.5 × 3.2 mm [1.75 × 0.49 × 0.12 in] from Heat 2. No stress corrosion cracking was observed in any cases in acidified 0.5 percent (5,000 parts per million) of lead solutions having pH ranging from 1 to 6.5 at temperatures ranging from 210 to 250 °C [410 to 482 °F].

---

[1]Barkatt, A , A.L Pulvirenti, J.A. Gorman, and C.R. Marks. "Tests to Explore Specific Aspects of the Corrosion Resistance of C-22." *Presentation to the Nuclear Waste Technical Review Board August 1, 2000* Carson City, Nevada. 2000

[2]Gorman, J A "Preliminary Tests Regarding Effects of Lead and Mercury on C-22 and Extrapolation to Service Conditions." *Presentation to the DOE Waste Package Materials Performance Peer Review Panel July 24, 2001* Cleveland, Ohio 2001

Table 3-1. Chemical Composition of the Heats of Alloy 22 Used in the State of Nevada Investigation (wt%) (Pulvirenti, et al., 2002)												
Heat	Ni	Cr	Mo	W	Fe	Co	Mn	V	Si	P	S	C
Heat 1	Balance	21.2	13.3	3 0	4.5	1.96	0.25	0.14	0.038	0.006	0.003	0.003
Heat 2	56.89	21.5	13.37	2.91	3.97	0.72	0.23	0.14	0 02	0.006	0.002	0.004
Alloy N06022*	Balance	20.0–22.5	12.5–14.5	2.5–3.5	2.0–6.0	2.5 max	0.50 max	0.35 max	0.08 max	0.02 max	0.02 max	0.015 max

Reference:
Pulvirenti, A.L , K M Needham, M A Adel-Hadadi, C R Marks, J A Gorman, and A. Barkatt. "Effects of Lead, Mercury, and Reduced Sulfur Species on the Corrosion of Alloy 22 in Concentrated Groundwaters as a Function of pH and Temperature " Proceedings of the Materials Research Society Conference Symposium Proceedings 713 Paper No. JJ11 6 Warrendale, Pennsylvania: Materials Research Society 2002.

*Composition requirements specified in ASTM B575

In addition to the minor compositional differences between the heats of Alloy 22, the surface finishes of the test specimens were also different. Specimens from Heat 1 were polished to a 120-grit surface finish, whereas Heat 2 specimens were a 600-grit surface finish. More importantly, the 5,000 parts per million of lead concentrations used in the State of Nevada investigations were simply based on the amount of lead acetate added into the solutions. It is not clear from the description of their experimental procedures if the initial lead concentrations in solution have been experimentally confirmed in these investigations. The lead concentration from a posttest solution analysis, however, was only 1,311 parts per million.[3] Surface analysis showed the presence of a significant amount of metallic lead on the surface of the Alloy 22 specimens (Pulvirenti, et al., 2002a). The presence of metallic lead seems to be due to the reduction of Pb^{2+} species. These observations and the lack of reproducibility in the stress corrosion cracking data suggest that the reported testing of Alloy 22 in the presence of lead species is open to question. Additional investigations with specimens exposed to well-characterized solution environments are needed to assess the occurrence of stress corrosion cracking of Alloy 22, as reported in the State of Nevada investigations.

3.2 The DOE Investigations

Stress corrosion cracking resulting from minor constituents in the repository environment, such as lead, has been recognized as a factor that may affect the performance of waste package materials (Payer, et al., 2002). At present, the only DOE data about stress corrosion cracking of Alloy 22 in lead-containing environments were reported by Estill, et al. (2002). The effect of lead was evaluated using mill-annealed Alloy 22 round tensile specimens, 11 mm [0.438 in] in diameter and 184 mm [7.25 in] long, tested in water containing 1-percent $PbCl_2$ addition (7,450 parts per million of lead) (pH ~4) at 95 °C [203 °F] and in simulated acidified water

[3]Barkatt, A , A L Pulvirenti, J.A Gorman, and C.R. Marks. "Tests to Explore Specific Aspects of the Corrosion Resistance of C-22 " *Presentation to the Nuclear Waste Technical Review Board August 1, 2000* Carson City, Nevada 2000.

containing 0.005 percent $Pb(NO_3)_2$ addition (30 parts per million of lead) (pH ~3) at 95 °C [203 °F]. Slow-strain rate tests were conducted under open-circuit conditions using a strain rate of 1.6×10^{-6} s^{-1}. No stress corrosion cracking was observed in any tests. As was the case for the State of Nevada investigations, the lead concentration in the test solution used by DOE was not experimentally determined.

DOE asserted that even though stress corrosion cracking in Alloy 22 is possible under extreme conditions, evaporation and concentration of the water to realistic and conservative limits will result in much lower levels of lead than used in the State of Nevada investigations. Furthermore, the waste package and drip shield designs account for the potential degradation modes that may occur in Alloy 22 under extreme conditions. The Titanium Grade 7 drip shield that is not susceptible to the effects of lead will protect the Alloy 22 waste package from dripping water that could contain high levels of harmful impurities on the surface of the waste package. For the waste package, the fabrication process also includes stress mitigation to preclude stress corrosion cracking.

3.3 The CNWRA Investigations

CNWRA conducted a limited analysis to evaluate lead-solution chemistry and its effect on the anodic polarization behavior and stress corrosion cracking of Alloy 22, which is discussed in the following sections.

3.3.1 Lead-Speciation Calculations

Lead-solution chemistry was calculated for several lead compounds to determine speciation of lead in various lead-containing solutions. Thermodynamic calculations for the speciation of lead were conducted using the Environmental Simulation Program Version 6.5, which is a steady-state process simulator developed by OLI Systems, Inc. for evaluating aqueous chemical processes in industrial and environmental applications. The Environmental Simulation Program Version 6.5 represents standard-state thermodynamic properties using the Helgeson-Kirkham-Flowers equation-of-state (Helgeson, et al., 1981) and excess properties using the aqueous activity coefficient expressions developed by Bromley (1972) and Pitzer (1991, 1973). These models enable simulation of aqueous chemical systems for temperatures to 300 °C [572 °F], pressures to 150 MPa [22 ksi], and ionic strengths to 30 molal.

In the State of Nevada investigations (Pulvirenti, et al., 2002a), lead in the form of lead acetate was used to evaluate its effect on corrosion and stress corrosion cracking of Alloy 22. Lead-speciation calculations in lead-acetate solutions were carried out using the Environmental Simulation Program Version 6.5. In these calculations, lead was introduced as lead acetate at a fixed concentration of 0.008 molal (1,600 parts per million of lead), and chloride was introduced as NaCl at various concentrations to give the desired concentration of free chloride. The pH was not constrained during the simulations. The calculated pH values varied from 6.5 at a chloride concentration of 0.014 molal to 8.2 at chloride concentration of 5.98 molal. Figure 3-1 shows the calculated results for the dissolved lead species in the lead-acetate solution as a function of free chloride concentration. It is clear from Figure 3-1 that, of all the nonacetate-containing species, free Pb^{2+} is the predominant species when the chloride concentration is below 0.1 molal. For chloride concentrations above 0.1 molal, however, the

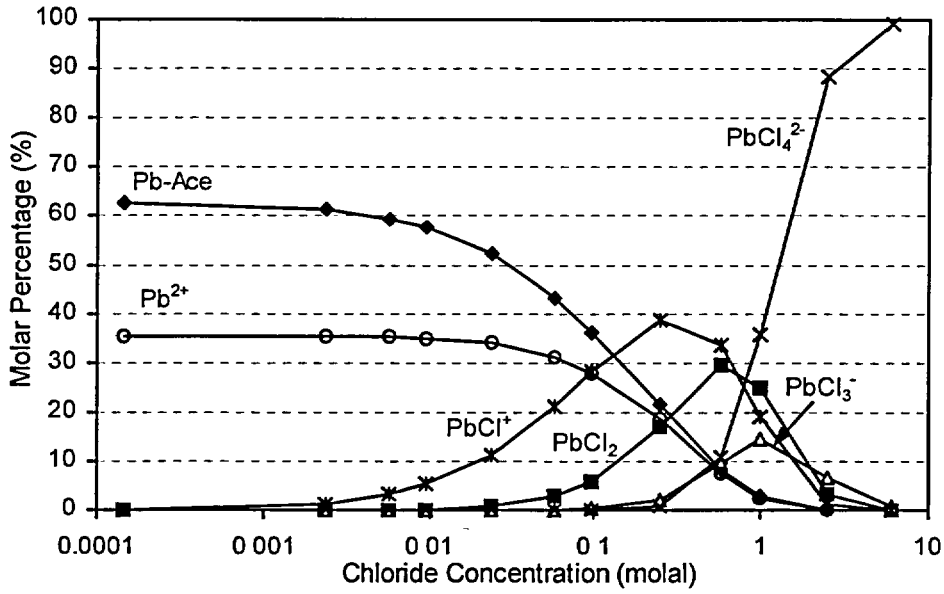

Figure 3-1. Molar Percent of Dissolved Lead Species in Lead-Acetate Solutions for a Total Dissolved Lead of 1,600 parts per million at 25 °C [77 °F]. The Pb-Ace Term Represents the Total Dissolved Lead Acetate Species.

free Pb^{2+} concentration decreases as the chloride concentration increases. The free Pb^{2+} molar percent is reduced to less than 3 percent at approximately 1 molal of chloride. The main nonacetate-containing species is $PbCl^+$ at intermediate chloride concentrations (0.1 to 1.0 molal), and in the form of $PbCl_4^{2-}$ at chloride concentrations above 1.0 molal. It is important to note that the degree of dissociation of lead acetate in term of free Pb^{2+} concentration is only approximately 35 percent. In this case, lead-acetate species (Pb-Ace) accounts for approximately 50 to 60 percent of the total dissolved lead.

Similar lead speciation calculations were also conducted for $PbCl_2$, a soluble lead compound used in the DOE investigations. Although $Pb(NO_3)_2$ is also very soluble, it was excluded from the calculations because of the possible effect of nitrate as a corrosion inhibitor. The calculated results for the dissolved lead species in $PbCl_2$ solution as a function of free chloride concentration are shown in Figure 3-2. Conditions were kept the same except lead acetate was replaced with $PbCl_2$. The calculated pH values vary from 5.0 at a chloride concentration of 0.014 molal to 6.94 at chloride concentration of 5.98 molal. As shown in Figure 3-2, the speciation behavior of $PbCl_2$ is similar to that of lead acetate in Figure 3-1 with the exception of the high free Pb^{2+} ion concentrations observed at low-chloride concentrations. The degree of dissociation of $PbCl_2$ can be up to 80 percent, as evidenced by the free Pb^{2+} ion concentrations. Only a small amount of the total dissolved lead is in the form of $PbCl_2$ when the chloride concentration is below 0.1 molal. As a result of these speciation calculations, $PbCl_2$ was selected for use in all the following corrosion tests because of its high free Pb^{2+} content.

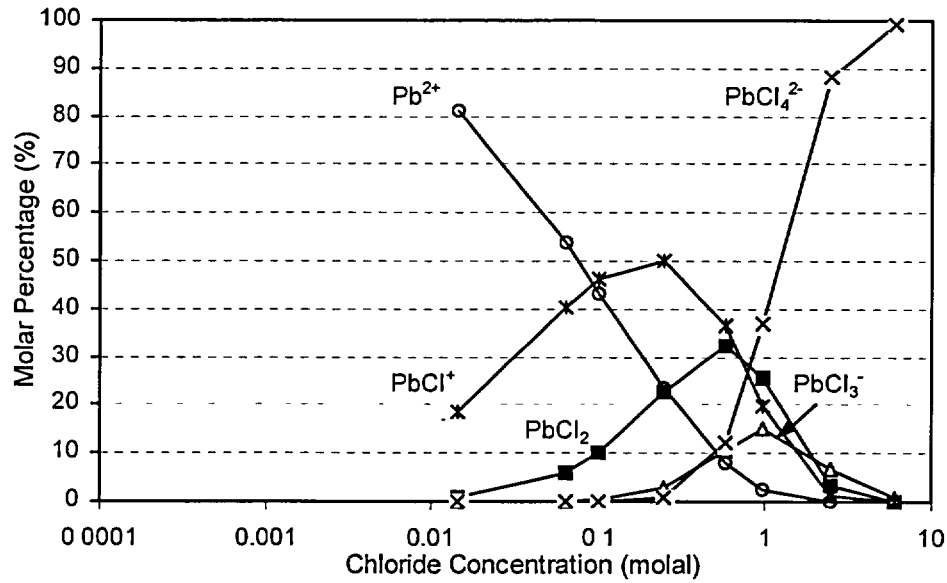

Figure 3-2. Molar Percent of Dissolved Lead Species in $PbCl_2$ Solutions for a Total Dissolved Lead of 1,600 parts per million at 25 °C [77 °F]

3.3.2 Polarization Behavior

The chemical compositions of the mill-annealed Alloy 22 heats used in this investigation are listed in Table 3-2. Crevice corrosion specimens machined with flat surfaces from a 12.7-mm [0.50-in] thick heat 2277-8-3175 plate were fitted with two polytetrafluoroethylene crevice-forming washers held with insulated Alloy C-276 hardware. Cylindrical specimens 6.2 mm [0.24 in] in diameter and 48.6 mm [1.91 in] long were also machined from the same heat. As noted previous, $PbCl_2$ was selected among several lead compounds for its high solubility and dissociation rate. Solution composition as total dissolved lead species and chloride ion concentrations were measured by inductively coupled plasma-atomic emission spectroscopy and ion chromatography. Comparative anodic polarization tests were conducted in a range of deaerated $PbCl_2$ solutions by adjusting the solution pH using HCl. The test matrix is shown in Table 3-3. All cyclic potentiodynamic polarization tests were conducted in electrochemical cells made of glass and polytetrafluoroethylene at 95 °C [203 °F] at a scan rate of 0.167 mV/s using the procedures provided in ASTM Standard G–61 (ASTM International, 2001b).

Figure 3-3 compares the potentiodynamic polarization curves of creviced Alloy 22 specimens in $PbCl_2$-containing (1,800 parts per million of lead, 700 parts per million of chloride, and pH 4.9) and lead-free NaCl (700 parts per million of chloride and pH 4.7) solutions. Figure 3-3 clearly shows that the presence of lead promoted the occurrence of an anodic peak in the range of −400 to −300 mV_{SCE} with a significant increase in current densities to 5×10^{-4} A/cm^2 [0.46 A/ft^2], compared to the passive current density of ~10^{-6} A/cm^2 [~9.3×10^{-4} A/ft^2]

Table 3-2. Chemical Composition of the Heats of Alloy 22 Used in This Study (wt%)												
Heat	Ni	Cr	Mo	W	Fe	Co	Mn	V	Si	P	S	C
Alloy 22 2277-8-3175	57.80	21.40	13.60	3.00	3.80	0.09	0.12	0.15	0.030	0.008	0.002	0.004
Alloy 22 2277-1-3133	55.53	21.44	13.27	2.85	4.76	0.65	0.22	0.15	0.030	0.012	0.002	0.005

Table 3-3. Anodic Polarization Test Matrix				
	Test Solution			
Specimen	Pb (ppm)*	Cl (ppm)	pH	Remarks
22–t1	1,800	700	4.9	Unsaturated $PbCl_2$ solution at room temperature
22–t2	—	700	4.7	NaCl solution
22–t3	3,100	1,100	4.5	Saturated $PbCl_2$ solution at room temperature
22–t7	1,500	8,600	0.5	Saturated $PbCl_2$ solution at room temperature and pH adjusted with HCl to 0.5
22–t8	3,600	1,400	3.0	Saturated $PbCl_2$ solution at room temperature and pH adjusted with HCl to 3.0
22–t10	16,300	16,000	0.5	Supersaturated $PbCl_2$ solution at 95 °C and pH adjusted with HCl to 0.5
22–t11	5,400	1,900	3.0	Supersaturated $PbCl_2$ solution at 95 °C and pH adjusted with HCl to 3.0
22–t30	—	16,000	0.5	NaCl solution
Pt–t5	2,800	1,000	4.9	Unsaturated $PbCl_2$ solution at room temperature
Pt–t6	—	1,000	4.9	NaCl solution

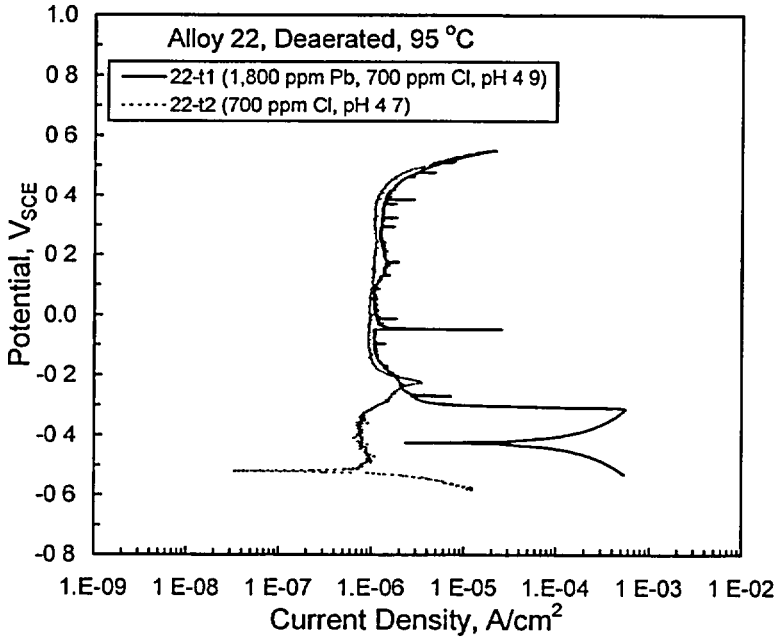

Figure 3-3. Effect of Lead on the Anodic Polarization Behavior of Alloy 22 Compared to That in a Lead-Free Solution at 95 °C [203 °F] and a Scan Rate of 0.167 mV/s (ppm—parts per million)

exhibited in the lead-free solution. The $PbCl_2$-containing solution also resulted in numerous high current spikes when the potential was scanned in the passive region. The anodic peak and high current spikes were not observed in the lead-free NaCl solution.

Similar potentiodynamic polarization tests were conducted using a platinum electrode in $PbCl_2$-containing (2,800 parts per million of lead, 1,000 parts per million of chloride, and pH 4.9) and lead-free NaCl (1,000 parts per million of chloride and pH 4.9) solutions, as shown in Figure 3-4. An anodic peak in the range of −400 to −100 mV_{SCE} and many current spikes were also observed in the solution containing lead. This anodic peak with high current densities is related to the anodic oxidation of Pb^{2+} species and simultaneously enhances dissolution in Alloy 22. The effect of lead concentration on the polarization behavior of Alloy 22 is shown in Figure 3-5. Figure 3-5 shows three polarization curves for creviced specimens comparing the anodic behavior observed in 3,100 parts per million of lead (pH 4.5), 5,400 parts per million of lead (pH 3.0), and 16,300 parts per million of lead (pH 0.5) solutions. In all cases, Alloy 22 exhibited an anodic peak with a nose at potentials ranging from −370 to −120 mV_{SCE}. Also shown in Figure 3-5 is an increase in the passive current of approximately 5×10^{-5} A/cm^2 [4.6×10^{-2} A/ft^2] and high current spikes in the passive region in a supersaturated $PbCl_2$ solution (16,300 parts per million lead and pH 0.5) test. The passive current density for this test was approximately seven times greater than those of the tests in lower lead concentrations.

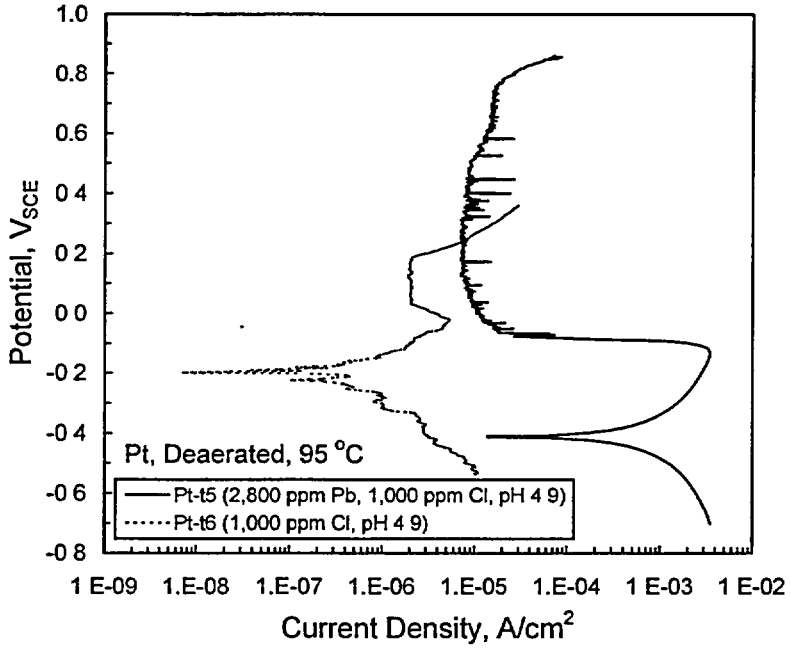

Figure 3-4. Effect of Lead on the Anodic Polarization Behavior of Platinum Compared to That in a Lead-Free Solution at 95 °C [203 °F] and a Scan Rate of 0.167 mV/s (ppm—parts per million)

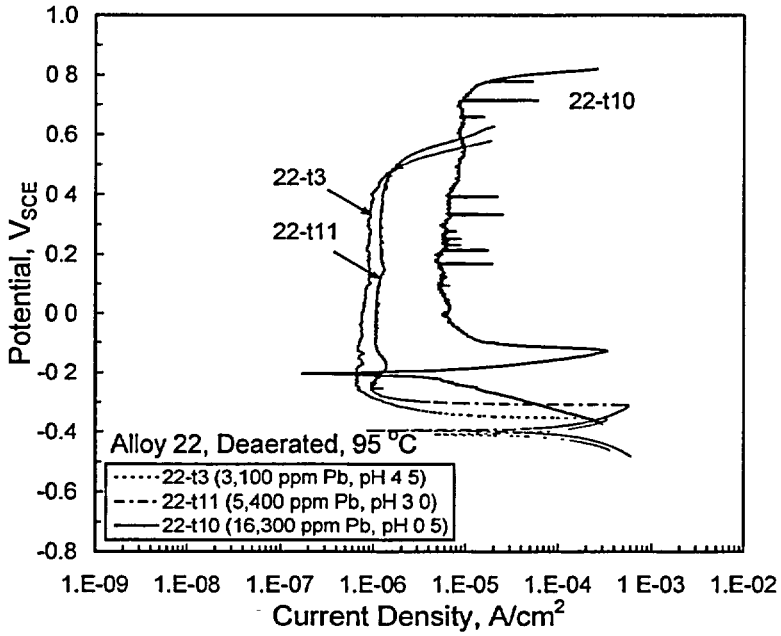

Figure 3-5. Effect of Lead Concentration on the Anodic Polarization Behavior of Alloy 22 in $PbCl_2$ Solutions at 95 °C [203 °F] and a Scan Rate of 0.167 mV/s (ppm—parts per million)

Optical microscopic examination of the crevice specimens after testing revealed that while the surface of the specimen was clean after testing in the lead-free NaCl (16,000 parts per million of chloride and pH 0.5) solution, preferential localized attack occurred at the crevice sites in the specimen tested in the supersaturated $PbCl_2$ (16,300 parts per million of lead, 16,000 parts per million of chloride, and pH 0.5) solution, as shown in Figure 3-6. Scanning electron micrographs, obtained from one of the corroded crevice sites show areas of enhanced dissolution inside the crevice site and etch pits outside the crevice site in Figure 3-7. Etch pitting has been observed on metal under active dissolution conditions in strongly acidic solutions (Ives, 1974). No localized corrosion was observed in crevice specimens tested in solutions with lead concentrations ranging from 1,500 to 5,400 parts per million.

The enhanced dissolution of Alloy 22 in lead-containing solutions resulting from a pronounced anodic oxidation peak was evaluated in supersaturated, deaerated $PbCl_2$ solution (pH 0.5) at 95 °C [203 °F] using cylindrical specimens under potentiostatic conditions applying potentials ranging from −100 to 200 mV_{SCE}. Examination of the tested specimens did not reveal significant attack on the surfaces of the specimens except for that tested at −100 mV_{SCE}. The current density and total charge as a function of time from this potentiostatic test is shown in Figure 3-8. The lead concentration after the posttest solution analysis was 7,500 parts per million. As seen in the plotted current density changes with time, the current density increased initially with time and reached a stable high value of ~1 × 10^{-4} A/cm^2 [~9.3 × 10^{-2} A/ft^2] for a

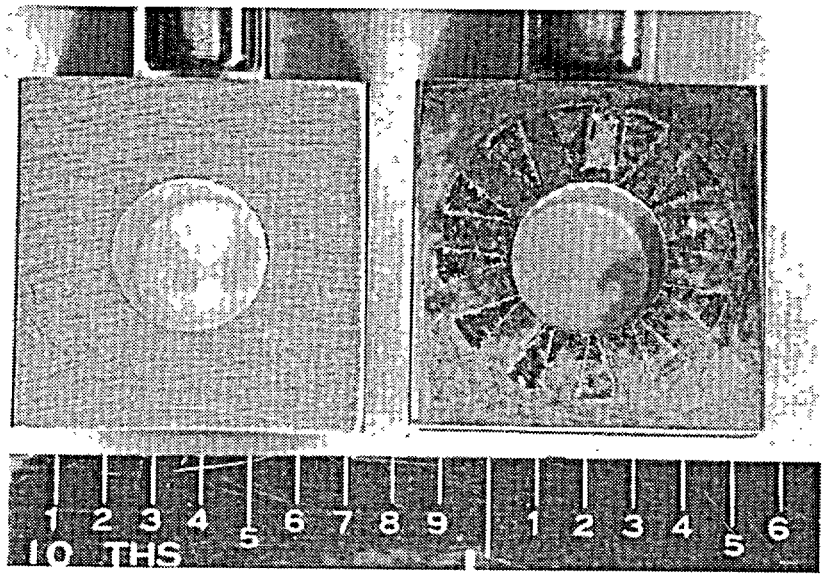

22-t30
NaCl solution

22-t10
$PbCl_2$ solution

Figure 3-6. Photograph Comparing Surface Features of Alloy 22 Crevice Specimens After Potentiodynamic Polarization Runs in Supersaturated $PbCl_2$ and Lead-Free NaCl Solutions (pH 0.5) at 95 °C [203 °F] {Each Small Division on the Ruler is 2.54 mm [0.1 in].}

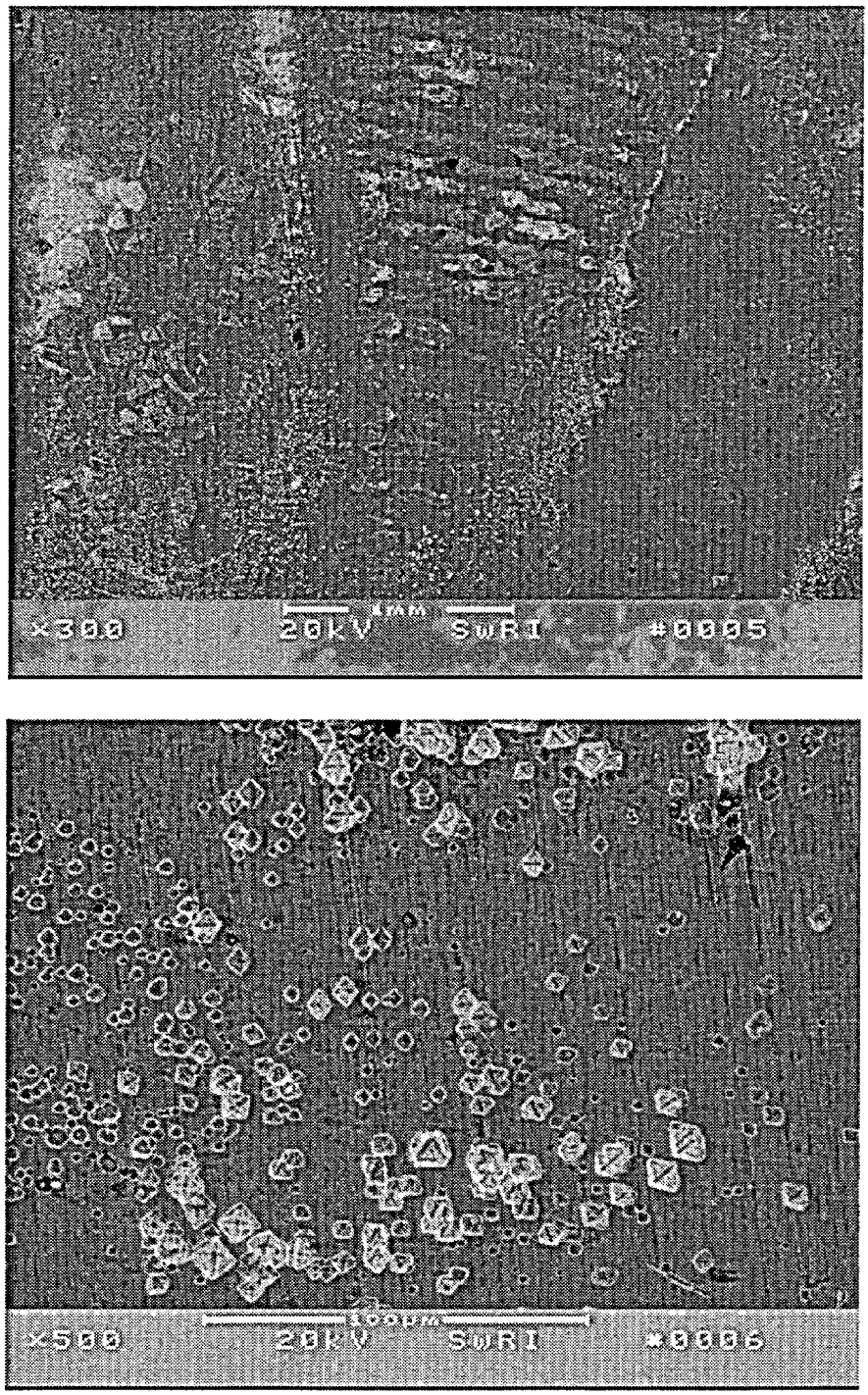

Figure 3-7. Scanning Electron Micrographs on Alloy 22 Crevice Specimen After Potentiodynamic Polarization Run in a Supersaturated $PbCl_2$ Solution at 95 °C [203 °F] Showing Areas of Enhanced Dissolution Inside the Crevice Site (Top) and Etch Pits Outside the Crevice Site (Bottom)

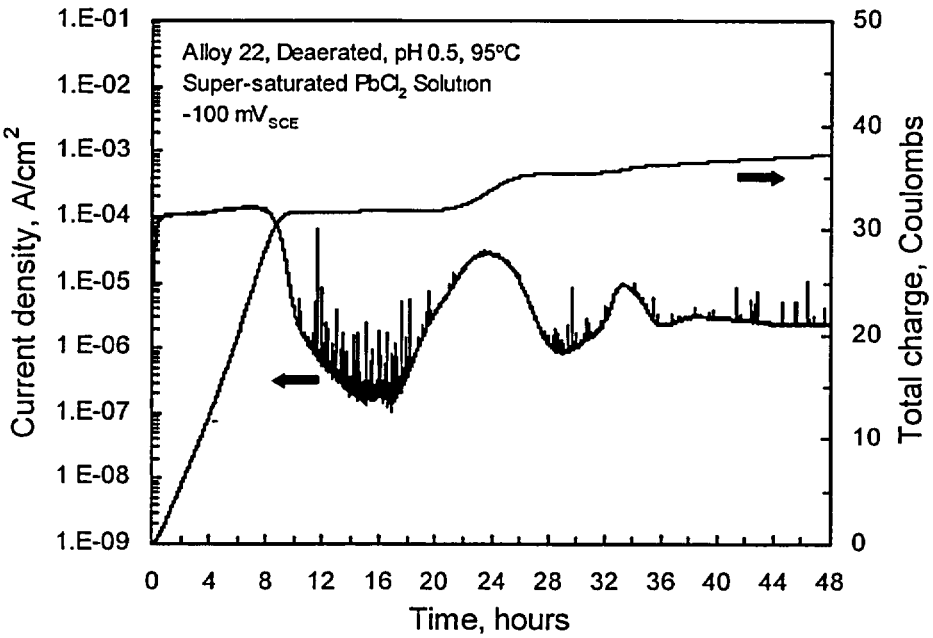

Figure 3-8. Anodic Current Density and Total Charge as a Function of Time Measured on Alloy 22 at −100 mV_{SCE} in a Supersaturated $PbCl_2$ Solution (pH 0.5) at 95 °C [203 °F]

period of 8 hours. This high anodic current period resulted in a high total charge at the end of the test where a total charge of 37.15 coulombs was recorded. Furthermore, many large current spikes were observed throughout the test, suggesting periodic events of passivity breakdown and repassivation. The typical morphology of the attack observed on the test specimen is shown in Figure 3-9. Note that many corrosion troughs formed along the axial axis of the cylinder specimen. The formation of corrosion troughs may be attributed to enhanced anodic dissolution in supersaturated $PbCl_2$ solution. The chemical compositions using the energy-dispersive x-ray spectroscopy analysis from inside and outside the corrosion troughs are provided in Table 3-4. It is clearly seen in Table 3-4 that preferential dissolution of Alloy 22 was observed for such conditions. The measured concentrations of molybdenum and tungsten were much lower than the bulk content of these elements in Alloy 22. In addition, the nickel content is slightly lower, but the chromium is slightly higher, inside the corrosion trough.

Many experiments have shown an enhanced dissolution of Alloy 600 in the presence of lead (Sakai, et al., 1992; Costa, et al., 1995). Sakai, et al. (1992) analyzed the surface film on Alloy 600 after testing in various $PbCl_2$ solutions at 280 °C [536 °F]. They found that nickel is depleted and chromium is enriched in the outer region of the surface film, particularly in more acidic conditions with higher soluble lead concentrations. Enhanced nickel dissolution was attributed to an active electrochemical reaction between soluble lead and nickel/iron on the alloy surface. Formation of a Ni-Pb-anion complex on the metallic surface was observed to enhance the dissolution of Alloy 600 when it was tested in a perchloric acid solution containing 0.01 M PbO (2,070 parts per million of lead) at room temperature (Costa, et al., 1995). The deleterious

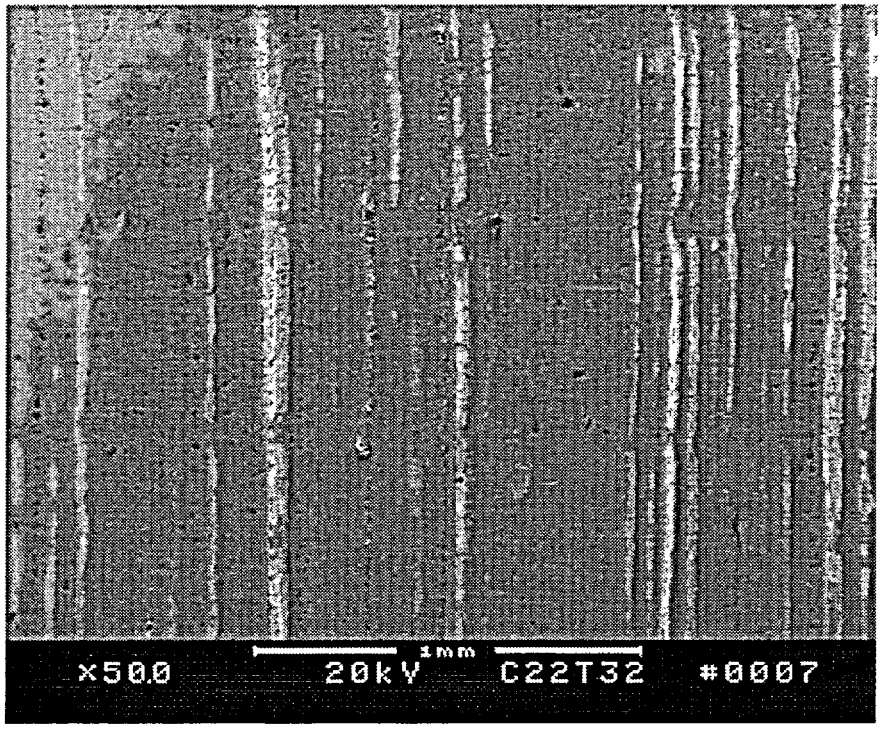

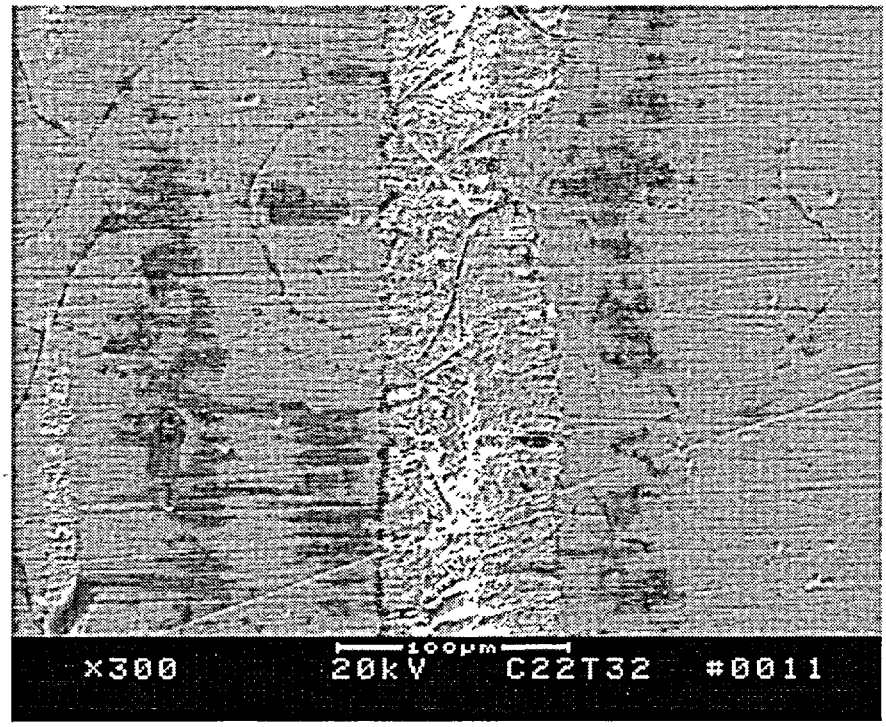

Figure 3-9. Scanning Electron Micrographs on Surface Attack of Alloy 22 Tested in a Supersaturated $PbCl_2$ Solution at 95 °C [203 °F] Applying −100 mV_{SCE} for 2 Days

Table 3-4. Chemical Composition from Surface Regions of Alloy 22 Tested in a Supersaturated $PbCl_2$ Solution at 95 °C [203 °F] Applying −100 mV_{SCE} for 2 Days (wt%)							
Probe Location	**Ni**	**Cr**	**Mo**	**W**	**Fe**	**Co**	**V**
Outside Trough	57.6	21.7	12.2	3.14	3.93	0.87	0.16
Inside Trough	55.1	22.1	5.90	1.50	3.91	0.95	0.19

effect of lead on corrosion was not detected in Alloy 690 because the growth of a continuous chromium oxide film is expected to be faster as a result of its high chromium content (Costa, et al., 1995). The exact interaction of lead with Alloy 22 and the mechanism of the observed enhanced dissolution are not clear. Nevertheless, if such a high lead concentration is possible in Yucca Mountain waters, the importance of the effect of lead as a water impurity on the long-term corrosion of Alloy 22 cannot be underestimated.

3.3.3 Stress Corrosion Cracking Susceptibility

Both single and double U-bend specimens were used to evaluate the stress corrosion cracking susceptibility of Alloy 22. The U-bend specimens were machined from a 12.7-mm [0.50-in] thick heat 2277-1-3133 plate and stressed into U-bends with a radius of bend curvature of 6.35 mm [0.250 in], according to ASTM G–30 (ASTM International, 2001c). Bolts and nuts made of Alloy C-276, electrically isolated from the specimens by zirconia spacers, were used for the single-stage stressing operation. The resulting tensile stress was perpendicular to the rolling direction, and the total strain on the outside of the bend was approximately 25 percent. All stress corrosion cracking tests were conducted in supersaturated deaerated $PbCl_2$ solution at 95 °C [203 °F], acidified to approximately pH 0.5 by the addition of HCl, under an applied potential of −100 mV_{SCE}. The applied potential value was selected based on the anodic peak observed in the polarization behavior experiments, as shown in Figure 3-5. Two U-bend specimens were tested simultaneously in glass cells. The specimens were partially immersed in the solutions with either the apexes or the legs of the U-bends submerged in the liquid phase.

Test conditions and results of the stress corrosion cracking testing of Alloy 22 U-bend specimens are provided in Table 3-5. No evidence of cracking was observed in any of the U-bend specimens for the duration of the tests, as illustrated in Figure 3-10. Localized corrosion in the form of grain boundary attack, however, can be seen on the legs of the U-bend specimens (22–t40) above the solution level, as shown in Figure 3-11. To evaluate the combined effect of stress and the localized attack above the vapor/solution interface, subsequent tests were conducted by inverting the specimens to locate the stressed apex in the vapor phase. No stress corrosion cracking was detected after 1,008 hours of testing in the 22–t41 specimens. Additionally, the effect of thermal aging on stress corrosion cracking of Alloy 22 was also evaluated using U-bend specimens aged at 870 °C [1,598 °F] for 5 minutes. As observed in the mill-annealed alloy, no stress corrosion cracking was detected after 1,008 hours of testing in the 22–t45 specimens. These U-bend test results suggest that Alloy 22 is resistant to stress corrosion cracking in extremely aggressive, supersaturated $PbCl_2$ solutions, as characterized by high lead concentrations and low solution pH.

Table 3-5. Results of Stress Corrosion Cracking Tests of Alloy 22 U-Bend Specimens in $PbCl_2$ Solutions						
		Test Solution				
Specimen	Specimen Position	Pb (ppm)*	Cl (ppm)	pH	Test Duration	Test Results
22–t40–SU1	Apex in solution	11,600	16,500	0.507	40 days (945 hours)	No stress corrosion cracking, shallow pits at the legs
22–t40–DU1 (Inner U-Bend)	Apex in solution	11,600	16,500	0.507	40 days (945 hours)	No stress corrosion cracking, shallow pits at the legs
22–t40–DU1 (Outer U-Bend)	Apex in solution	11,600	16,500	0.507	40 days (945 hours)	No stress corrosion cracking, shallow pits at the legs
22–t41–SU2	Legs in solution	9,500	14,700	0.502	42 days (1,008 hours)	No stress corrosion cracking, shallow pits near the apex
22–t41–DU2 (Inner U-Bend)	Legs in solution	9,500	14,700	0.502	42 days (1,008 hours)	No stress corrosion cracking, shallow pits near the apex
22–t41–DU2 (Outer U-Bend)	Legs in solution	9,500	14,700	0.502	42 days (1,008 hours)	No stress corrosion cracking, shallow pits near the apex
22–t45–DU3 (Inner U-Bend)	Apex in solution	11,900	15,900	0 509	42 days (1,008 hours)	No stress corrosion cracking, shallow pits at the legs
22–t45–DU3 (Outer U-Bend)	Apex in solution	11,900	15,900	0.509	42 days (1,008 hours)	No stress corrosion cracking, shallow pits at the legs
*ppm—parts per million						

3.4 Summary

Studies sponsored by the State of Nevada indicated the resistance of the Alloy 22 outer container to localized corrosion and stress corrosion cracking may be affected by the presence of impurities, such as lead, mercury, and arsenic, in the water contacting the waste packages. Stress corrosion cracking of Alloy 22 was reported to occur at 250 °C [482 °F] in a 1,000× J–13 Well water containing 5,000 parts per million of lead (as lead acetate) and acidified by the addition of HCl to pH 0.5. The State of Nevada investigators could not reproduce this preliminary result, however. Limited data on stress corrosion cracking of Alloy 22 in lead-containing environments have been reported by DOE. No stress corrosion cracking was observed in slow strain rate tests in water containing 1 percent $PbCl_2$ (7,450 parts per million of lead) at 95 °C [203 °F]. It should be noted that the test solutions used in both the DOE and the State of Nevada investigations were not properly characterized in terms of the lead speciation.

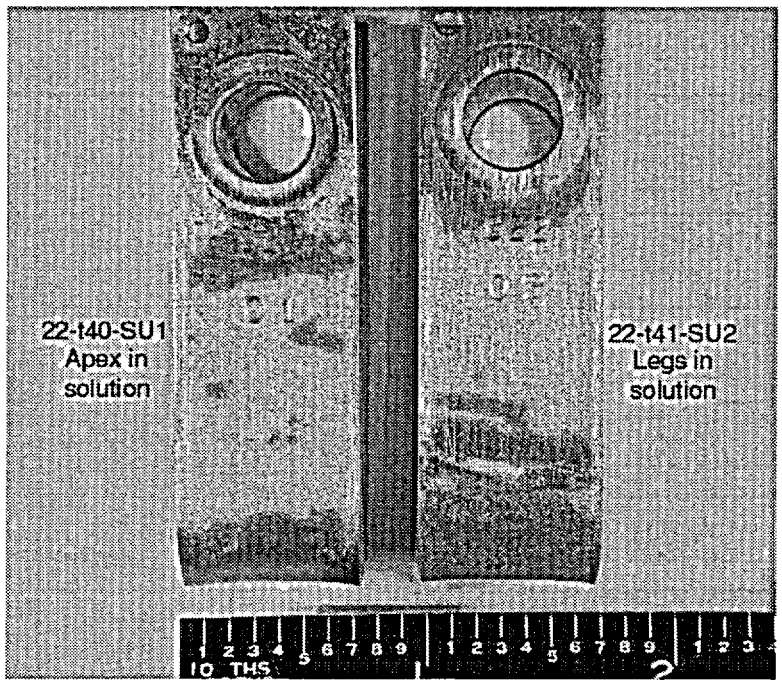

Figure 3-10. Photograph Comparing Surface Features of Alloy 22 Single U-Bend Specimens Tested at −100 mV_{SCE} in a Supersaturated $PbCl_2$ Solution (pH 0.5) at 95 °C [203 °F]. {Each Small Division on the Ruler is 2.54 mm [0.1 in].}

CNWRA conducted a limited analysis to evaluate lead-solution chemistry and its effect on the anodic polarization behavior and stress corrosion cracking of Alloy 22. Speciation calculations revealed the formation of Pb^{2+} ions and Pb-Cl complexes in $PbCl_2$ solution. The presence of lead species in a supersaturated $PbCl_2$ solution (16,300 parts per million of lead) with pH 0.5 by the addition of HCl promotes the occurrence of a pronounced anodic oxidation peak (also observed on platinum) and simultaneously enhances the dissolution of Alloy 22. This enhanced dissolution in a crevice specimen was characterized by the presence of randomly distributed etch pits. No localized corrosion was observed in crevice specimens tested in solutions with lead concentrations ranging from 1,500 to 5,400 parts per million. In addition, no stress corrosion cracking was observed at an applied potential of −100 mV_{SCE}, which is a potential corresponding to the anodic oxidation peak, when both single and double U-bend specimens were tested in supersaturated $PbCl_2$ solutions (9,500–11,900 parts per million of lead) with pH 0.5 at 95 °C [203 °F].

These results suggest that Alloy 22 is resistant to stress corrosion cracking in supersaturated $PbCl_2$ solutions even at the extremely high lead concentrations and low pH used in the tests. Moreover, no deleterious effect of lead species on localized corrosion was observed in crevice specimens for a wide range of lead concentrations with the exception of supersaturated $PbCl_2$ solutions. Based on these preliminary results and provided these high lead concentrations are not attainable in the anticipated repository environments, Alloy 22 is unlikely to be susceptible to stress corrosion cracking or localized corrosion. DOE agreed to provide additional information in agreements CLST 1.01 and CLST 1.10 for the range of concentrations of minor species

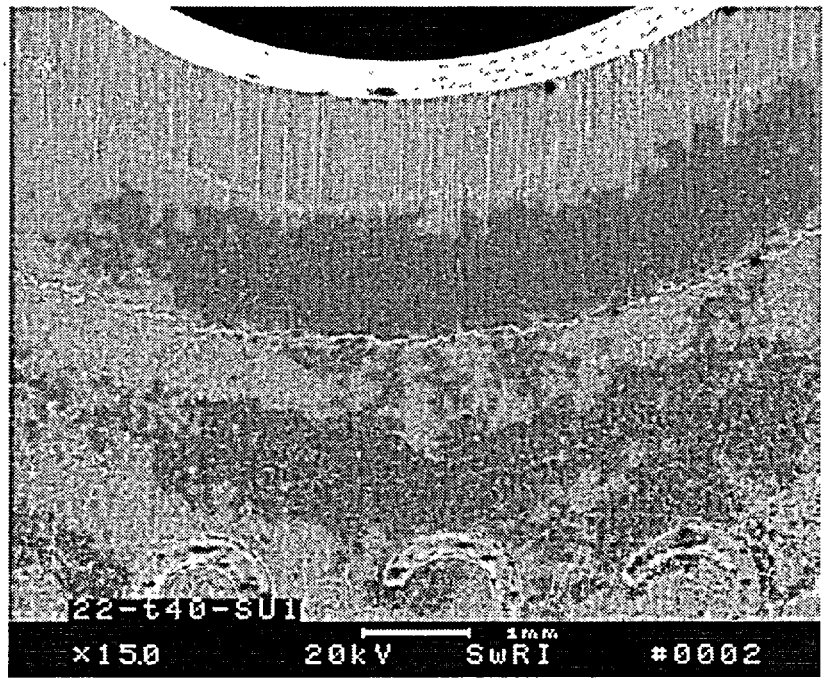

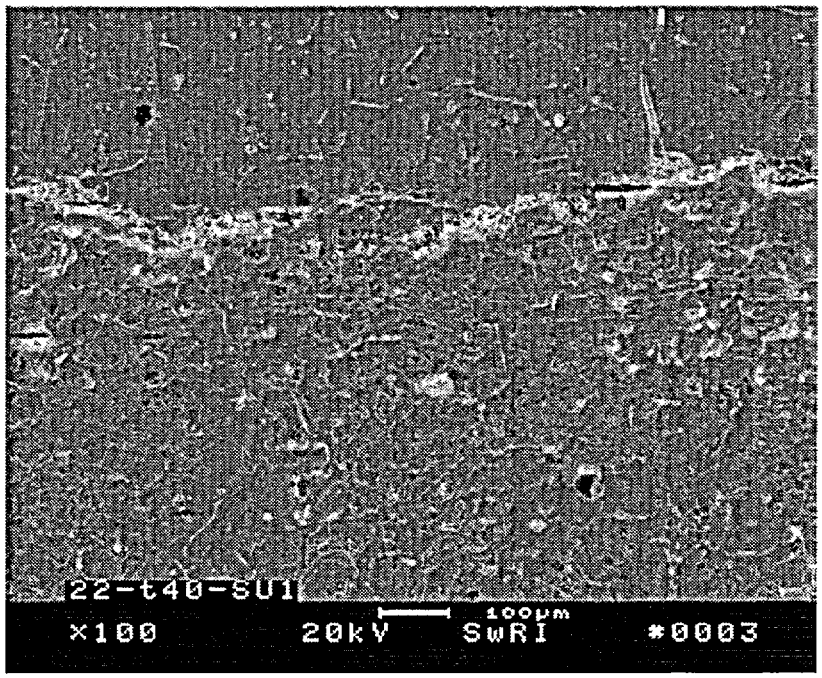

Figure 3-11. Scanning Electron Micrographs of Alloy 22 Single U-Bend Specimens Tested at −100 mV_{SCE} in a Supersaturated $PbCl_2$ Solution (pH 0.5) at 95 °C [203 °F] Showing Surface Attack (Top) and Details of the Grain Boundary Attack (Bottom) on the Leg Above the Vapor/Solution Interface

expected to evolve in Yucca Mountain waters and their effects on the critical potential for localized corrosion. Although it is not explicitly stated in agreement CLST 1.12, additional information should be provided by DOE if stress corrosion cracking of Alloy 22 in the presence of lead contamination is confirmed under realistic repository conditions.

4 ENVIRONMENTALLY ASSISTED CRACKING OF DRIP SHIELD MATERIALS

Based on laboratory testing and limited inservice experience until the 1960s, titanium alloys were perceived to be immune to stress corrosion cracking. Field experience and extensive research since then, however, has led to the conclusion that, with certain environment-material combinations, as with most engineering materials, stress corrosion of titanium alloys can occur. Stress corrosion cracking of titanium has generally been explained based on two main theories: (i) hydrogen embrittlement and/or hydrogen-induced cracking; and (ii) mass transport limited kinetics for different species at the crack tip.

In the hydrogen-influenced models, hydrogen has been speculated to influence cracking through either direct or indirect means. In the direct case, hydrogen is absorbed at the crack tip, thereby lowering the surface energy and the fracture stress (Sanderson and Scully, 1968). Hydrogen may also indirectly induce cracking by diffusing into the region ahead of the crack tip and creating conditions more conducive for crack initiation (Beck, 1969). There is experimental evidence in support of the hydrogen-related mechanisms for stress corrosion cracking of titanium alloys. For example, the pH at the crack tip has been measured to be near or less than 1.7, thus serving as the source of atomic hydrogen according to reaction (4-1)

$$H^+ + e^- \rightarrow H_{adsorbed} \rightarrow H_{absorbed} \tag{4-1}$$

This reaction leads to the ingress of hydrogen needed for cracking (Smith, et al., 1970; Brown, et al., 1969). Thermal aging of samples after charging with hydrogen resulted in enhanced diffusion of hydrogen away from the region ahead of the crack and decreases in the cleavage fracture zone (Sanderson and Scully, 1968; Powell and Scully, 1968; Wanhill, 1975). In addition, hydride layers are often found associated with the crack tip region during aqueous stress corrosion cracking experiments (Wang, et al., 1998; Clarke, et al., 1988), and there is extensive evidence that titanium becomes embrittled when the hydrogen concentration exceeds a critical value (Simbi, 1996).

Despite the experimental evidence that supports the hydrogen-related mechanisms, some significant limitations to these mechanisms exist. First, the measured crack growth rates tend to be several orders of magnitude faster than the rate of hydrogen diffusion. This criticism has been countered by arguing that the diffusivity of hydrogen is enhanced in the plastic deformation zone at the crack tip and that, even if the diffusivity is still too slow, the base material may be capable of crack arrest after propagating a relatively short distance following the initial crack burst through the hydride layer (Scully and Powell, 1970; Scully, 1980). In other words, a highly brittle hydride (or at least hydrogen-rich) layer would develop just ahead of the crack tip. The crack then rapidly propagates (bursts) through this layer and into the underlying base material where crack arrest occurs because of crack tip blunting from plastic deformation. The process then begins again with the generation of a new hydride/hydrogen-rich layer. Lending some support to this process has been the observation, in some cases, of somewhat discontinuous crack propagation and the formation of new hydride layers at the base of the crack (Wang, et al., 1998; Scully and Powell, 1970). The second limitation with the hydrogen-related models is the observation of cracking in nonhydrogen-containing environments (e.g., methanolic solutions). These claims, however, do not appear to be well

founded because numerous hydrogen sources may be present as impurities (e.g., water) as explained by Scully and Powell (1970) and Meyn and Sandoz (1969).

The mass transport limited kinetics models basically attempt to explain stress corrosion cracking of titanium alloys using electrochemical theories. In this approach, two primary species have been theorized based on the following reaction

$$Ti + zX^- \rightarrow TiX_z + ze^- \tag{4-2}$$

where

X^- — halide species (usually chloride)
z — the number of halides needed to balance the equation

At the crack tip, Ti^{3+} is assumed to be produced, and z is equal to 3. The mass transport limitation of this reaction is centered around the diffusion of halides into the crack tip. The kinetic aspect relates to the generation of Ti^{3+} (i.e., anodic dissolution of titanium). In these models, crack propagation occurs by essentially continuous anodic dissolution controlled either by mass transport of the halide to the crack tip (Beck, 1974, 1969; Alkire, et al., 1978) or through the dissolution kinetics of titanium to form Ti^{3+} at the crack tip (Beck, 1974). There is some experimental evidence to support the concepts behind these theories. For the halide mass transport model, the halide is proposed to disrupt the repassivation process, thereby enabling dissolution of the bare metal at the crack tip, similar to what occurs at the base of a corrosion pit (Beck, 1974, 1969; Alkire, et al., 1978). Additionally, thermodynamic calculations and experimental measurements have confirmed the presence of Ti^{3+} at the crack tip (Beck, 1974), and the current densities calculated from crack tip measurements are typically approximately 10 A/cm^2 [9,290 A/ft^2], which compares well with crack propagation rates (Beck, 1974). The mass transport kinetics model approach also has some limitations. The most significant limitation of this model is the lack of a clear mechanistic understanding of the processes occurring at the atomic level needed to fully explain and verify the model. In addition, the final disposition of the halide ions that enter the crack tip zone is not clear. One possibility is the formation of a salt film; however, this has not been experimentally determined, and thus halide ions keep entering into the crack tip zone and basically disappear or are ignored as the crack propagates.

Considering the uncertainties in the basic models and the experimental observations supporting these models, it is likely that in some circumstances both mechanisms may be acting together, or some other, as yet unknown, mechanisms may be operable. In any event, there is clear evidence that titanium alloys are prone to stress corrosion cracking in certain conditions. The bulk of the available literature on stress corrosion cracking of titanium alloys is in aerospace and seawater exposure applications, so little information is available for the proposed repository conditions (see Table 4-1). This chapter provides a brief review of the U.S. Department of Energy (DOE) investigations about environmentally assisted cracking that are germane to the materials, environments, or both in question, together with the limited scope experiments conducted at Center for Nuclear Waste Regulatory Analyses (CNWRA).

Table 4-1. Nominal Compositions and Mechanical Properties for Titanium Alloys of Possible Use in the Proposed Repository				
Alloy	**Common Name**	**Major Alloying Elements (wt%)**	**Yield Strength (MPa) [ksi]**	**Tensile Strength (MPa) [ksi]**
Grade 16	Ti–0.05Pd	0.05 Pd	275 [40]	345 [50]
Grade 7	Ti–0.15Pd	0.15 Pd	275 [40]	345 [50]
Grade 24	Ti–6Al–4V–0.05Pd	6.0 Al, 4.0 V, 0.05 Pd	830 [120]	895 [130]
Grade 2*	Commercial purity titanium	None	275 [40]	345 [50]
Grade 5*	Ti–6Al–4V	6.0 Al, 4.0 V	830 [120]	895 [130]
Grade 12*	Ti–0.3Mo–0.8Ni	0.3 Mo, 0.8 Ni	345 [50]	483 [70]
*Included for completeness and comparison but not a candidate material for use in proposed repository				

4.1 The DOE Investigations

Environmentally assisted cracking arising from hydrogen production and ingress has been considered a possible failure mode for the titanium drip shield. DOE examined the possible environments to which the drip shield may be exposed and evaluated the environmentally assisted cracking behavior of titanium alloys in the proposed repository environments. A review of the DOE models to evaluate the effects of environmental conditions on environmentally assisted cracking of the titanium drip shield and assessment of the DOE approach are provided in this section.

4.1.1 Environmentally Assisted Cracking

In reviewing the expected behavior of titanium alloys in the proposed repository, DOE is anticipating that hydrogen-induced cracking will be the main cracking failure mode (CRWMS M&O, 2000k). Based on a review of the literature, it is anticipated that a critical hydrogen concentration is needed to degrade the fracture toughness of titanium. Clarke, et al. (1997, 1994) noted that the fracture behavior of Titanium Grades 2 and 12 changed abruptly at a critical hydrogen concentration changing from predominantly ductile rupture and slow crack growth to fast crack growth. For Titanium Grade 2 this concentration was estimated between 500 and 800 parts per million and, for Grade 12, between 400 and 600 parts per million. More recent work by Ikeda and Quinn (1998) showed that, for Grade 16, the critical hydrogen concentration may be greater than 1,000 parts per million. One concern with these results is the critical hydrogen concentrations were determined based on changes in ductility measured during slow strain rate testing. Hardie and Ouyang (1999), for example, showed that the ductility of Titanium Grade 5, as a function of hydrogen concentration, depended on the strain rate selected. Reducing the strain rate from 5.8×10^{-4} to 2.5×10^{-6} s^{-1} resulted in a decrease of nearly 500 parts per million in the critical hydrogen concentration for

brittle fracture. Similar results were also observed by Wang, et al. (1998) with the crack tip hydride layer thickness increasing with decreasing crosshead speed. Similar reservations concerning the effects of strain rate on cracking results led Nakamura, et al. (2001, 2000) to use constant load testing. Work by Roy, et al. (2000, 1999) using Titanium Grade 12 wedge-open-loaded double cantilever specimens reported stress corrosion cracking in an acidified NaCl brine at 90 °C [194 °F]. By monitoring the crack extension in the specimen side grooves microscopically after testing at K_I levels of 22–27 MPa·m$^{1/2}$ [20–25 ksi·in$^{1/2}$], crack growth rates between 3 and 8 × 10^{-8} m/s [1.2 and 3.1 × 10^{-9} in/s] were noted. At these crack propagation rates, failure of a 1.5-cm [0.59-in] thick titanium drip shield would occur in less than 17 years. Examination of the fracture surfaces, however, does not lend clear evidence of stress corrosion cracking but rather seems more indicative of ductile failure (induced when the samples were intentionally pulled apart). Though it is clear that Titanium Grades 2, 5, 12, and 16 may exhibit stress corrosion or hydrogen-induced cracking under some circumstances, only limited efforts to examine the possible cracking behavior of Titanium Grade 7 have been conducted, and no work on Titanium Grade 24 has been performed.

Stress corrosion cracking has been noted in Titanium Grade 7 in tests conducted using compact tension specimens subjected to a low-frequency (0.001 Hz) cyclic load at a load ratio of 0.7 and a K_{max} of 30 MPa·m$^{1/2}$ [27 ksi·in$^{1/2}$] in basic saturated water (pH ~13) at 110 °C [230 °F] (Andresen, et al., 2001). In these tests, crack growth rates (crack length measured using the potential drop method) of between 1.6 and 7.9 × 10^{-8} mm/s [0.6 and 3.1 × 10^{-9} in/s], which translates to penetration of 1.5 cm [0.590 in] in approximately 6 to 30 years, were measured. Stress corrosion cracking of Titanium Grade 7 was also observed in the time-to-failure experiments using constant load tensile specimens tested in basic saturated water at 105 and 125 °C [221 and 257 °F] (Young, et al., 2001). In other tests (Pulvirenti, et al., 2002b), a Titanium Grade 7 U-bend specimen was observed to fail because of cracking that originated at the center of the apex inside a spot weld when exposed to simulated groundwater containing 1 M of chloride and 0.1 M of fluoride at pH 6.5 and 105 °C [221 °F]. Within 155 days of testing, the crack had completely penetrated through the thickness and width of the specimen. Though U-bend specimens can provide some information, these types of tests are limited because the stress level is unknown and not constant during the test and, in many cases, other key parameters of interest, such as the corrosion potential, are not measured. It is clear, however, that the addition of palladium has not resulted in immunity to stress corrosion cracking of titanium at least in fluoride-containing environments. It should be noted that Scully, et al. (1990) did observe a marked improvement in the hydrogen embrittlement resistance of precipitation-hardened PH 13-8 stainless steels when palladium was added. Based on extensive microstructural analysis, it was determined that the improvement gained was the result of the formation of palladium-aluminum precipitates in the steel that then served as hydrogen trap sites. In the case of Titanium Grade 7, however, the palladium is present as a solid solution rather than as discrete precipitates in a titanium matrix. Furthermore, palladium is a known catalyst for the hydrogen evolution reaction with an exchange current density of 10^{-3} A/cm^2 [0.93 A/ft^2] {compared to 6 × 10^{-9} A/cm^2 [5.6 × 10^{-6} A/ft^2] for titanium} being reported (Bockris and Reddy, 1970). Thus, the hydrogen evolution reaction on Titanium Grade 7 could be enhanced by the presence of palladium as has been speculated to explain the corrosion behavior of Titanium Grade 7 (Brossia and Cragnolino, 2001a; Brossia, et al., 2001). Considering the well-recognized detrimental effects of fluoride on titanium, additional testing to evaluate the susceptibility of Titanium Grade 7 to

stress corrosion cracking in fluoride-containing environments is needed. Also of importance is an examination of the possibility for cracking of Titanium Grade 24 for use as mechanical structural members of the drip shield in the proposed repository.

4.1.2 The DOE Model Abstraction

DOE considers the primary cracking mode for the titanium drip shield to be induced by hydrogen absorption leading to embrittlement (CRWMS M&O, 2000i). Stress corrosion cracking was evaluated as a possible failure mode invoking the slip dissolution/film rupture model as a way to abstract the results to facilitate performance predictions using total system performance assessment (CRWMS M&O, 2000d). Stress corrosion cracking was excluded from further consideration for two main reasons: (i) the drip shield is assumed to be fully annealed prior to emplacement and is thus free from residual stresses needed to initiate stress corrosion cracking (CRWMS M&O, 2000i); and (ii) in the case of rockfall-induced stresses, any cracks that do develop will be tight and quickly filled with oxide corrosion products thereby plugging them and preventing any solution flow through the drip shield (CRWMS M&O, 2000d).

Hydrogen-induced cracking is also considered a possible failure mode for the drip shield (CRWMS M&O, 2000l). Hydrogen is anticipated to be formed as a result of corrosion processes via the corresponding cathodic reaction balancing anodic (passive or galvanic)[1] dissolution, via the following reaction sequence

$$Ti + 2H_2O \rightarrow TiO_2 + 2H_2 \tag{4-3}$$

Of the hydrogen produced during corrosion, a fraction, assumed to be between 2 and 10 percent, will be absorbed into titanium and once, the concentration exceeds a critical value, cracking is considered possible. For Titanium Grade 7, the critical concentration of hydrogen is considered to be at least 1,000 parts per million based on the results obtained in slow strain rate tests using Titanium Grade 16, as discussed previously (Ikeda and Quinn, 1998). Based on the assumption that the dominant corrosion mode is passive dissolution, the following expression was developed to calculate the hydrogen concentration in the material at any given time (CRWMS M&O, 2000l)

$$H_A = \frac{4 \times 10^6 f_h R_{uc} t}{M_{Ti}(d_0 - R_{uc} t)} \tag{4-4}$$

where

H_A	—	hydrogen concentration (parts per million)
f_h	—	fractional efficiency of hydrogen absorption
R_{uc}	—	rate of passive corrosion (mm/yr)
t	—	time (year)

[1]Galvanic corrosion inducing hydrogen-induced cracking was considered to be of limited consequence primarily because of the small contact area involved (CRWMS M&O, 2000d).

M_{Ti} — atomic mass of titanium
d_0 — original thickness of drip shield (mm)

Using a worst-case approach, where a corrosion rate of 1.0×10^{-4} mm/yr [3.9×10^{-6} in/yr] based on the 90th percentile value for the corrosion rates measured in the long-term corrosion test facility using weight-loss coupons (CRWMS M&O, 2000m), an initial thickness of 15 mm [0.590 in], and a fractional absorption efficiency of 10 percent, a hydrogen concentration of ~600 parts per million is estimated after 10,000 years. This concentration is well below the threshold value of 1,000 parts per million assumed to be the critical concentration. Based on an analysis of this type, it was concluded that hydrogen-induced cracking of the drip shield was not a limiting degradation process affecting the functionality of the drip shield.

4.1.3 Assessment of the DOE Approach

There are three overarching concerns about the current DOE approach and modeling efforts in environmentally assisted cracking of titanium as the drip shield. First, there has been no experimental effort to examine the stress corrosion cracking susceptibility of Titanium Grade 24 and little for Titanium Grade 7. Second, the DOE approach relies on corrosion rates determined using weight-loss methods and neglects the well-known accelerating effects of fluoride. Third, DOE uses slow strain rate methods to determine the critical hydrogen concentration for embrittlement and assumes that palladium additions increase this concentration.

Many of the results regarding the susceptibility of titanium alloys to stress corrosion cracking used by DOE in performance assessment were based on materials other than those anticipated for use as the drip shield. As discussed previously, stress corrosion cracking of Titanium Grade 7 has been observed and thus remains a viable failure mechanism. Furthermore, since titanium cracking susceptibility, in most cases, is related to the strength of the alloy, Titanium Grade 24 will most likely be more susceptible to stress corrosion cracking than either Titanium Grades 2, 7, 16, or 12 and, in fact, may behave similar to Titanium Grade 5. Titanium Grade 5 has been shown to suffer from stress corrosion cracking in a number of environments with varied loading conditions (Schutz, 1992). Therefore, the susceptibility of Titanium Grades 7 and 24 to rapid stress corrosion cracking needs to be evaluated further. DOE agreed to provide additional information on environmental assisted cracking of titanium alloys in agreements CLST 1.14 and CLST 6.01.

Although the general approach for hydrogen-induced cracking used by DOE is reasonable, concerns remain for the corrosion rates used and the effect of fluoride. In general, there are significant limitations using weight-loss methods to determine corrosion rates for passive materials (Pensado, et al., 2002). These methods include complications arising from competing processes, such as corrosion product deposition, oxide formation and growth, deposition of other precipitates, the possible confounding effects of cleaning procedures, and the need for highly sensitive measures of small changes in weight. Thus, the use of corrosion rates that may be artificially low because of competing reactions and processes will lead to nonconservative estimates of the hydrogen concentration at a given time. Related to this is the enhancement in the corrosion rate of titanium alloys observed in the presence of fluoride. Numerous investigations have shown a significant increase in the corrosion rate (in many cases by several orders of magnitude) at fluoride concentrations in the range of 10^{-3} to 10^{-2} M

(Huang, 2002; Pulvirenti, et al., 2002b; Brossia and Cragnolino, 2001a,b; Brossia, et al., 2001). Because of these observed increases, the calculated hydrogen concentration at any given time may be underestimated for titanium alloys exposed to fluoride. Thus, better estimates for titanium corrosion rates and the effect of fluoride on these rates are needed to improve the technical basis for this approach. DOE agreed to provide additional information on corrosion rate measurements and the effect of fluoride on corrosion rate of titanium alloys in agreements CLST 1.05 and CLST 6.01.

A key aspect of the DOE approach to model hydrogen-induced cracking is the critical hydrogen concentration. Uncertainties regarding the effects of strain rate sensitivity encountered in slow strain rate experiments have not been captured by DOE. Because the critical hydrogen concentration necessary to observe brittle failure was shown to be dependent on the strain rate (Hardie and Ouyang, 1999; Wang, et al., 1998), an examination is needed of the possibility that the assumed value for the critical hydrogen concentration may be overestimated leading to a nonconservative determination of possible titanium drip shield cracking. Furthermore, the hydrogen concentration for cracking is also assumed to be influenced by palladium. Although this may be the case, it is far from clear that palladium additions will be beneficial. Considering the known catalytic nature of palladium for the hydrogen evolution reaction (Bockris and Reddy, 1970) and the higher solubility of hydrogen in palladium (Gileadi, 1993), it is possible that palladium additions to Titanium Grade 7 will increase the concentration of hydrogen in the metal compared to Titanium Grade 2. It should also be noted that Gibbs free energy-of-formation calculations show that the formation of titanium hydride is favored over palladium hydride (Greene, et al., 2001). Thus, from a thermodynamics perspective, any hydrogen present in the metal lattice of Titanium Grade 7 would prefer to be associated with titanium rather than palladium. The effects of these factors on anticipated performance need further evaluation according to the U.S. Nuclear Regulatory Commission (NRC) review of the DOE documents pertaining to Container Life and Source Term Issue agreements.[2] DOE agreed to provide additional information about critical hydrogen concentration for environmental assisted cracking of the drip shield in agreements CLST 6.01 through 6.03.

Stress corrosion cracking caused by residual stresses arising from fabrication processes and applied stresses resulting from rockfall or drift collapse is a possible failure mode for the drip shield. DOE reported the occurrence of stress corrosion cracking of Titanium Grade 7 in tests conducted in basic saturated water (Andresen, et al., 2001; Young, et al., 2001). The susceptibility of Titanium Grade 7 to stress corrosion cracking under realistic repository conditions led the DOE Waste Package Materials Performance Peer Review Panel to recommend the selection of an alternative material if such observation is confirmed.[3] DOE, however, considers stress corrosion cracking of the drip shield as having a low consequence because of presumed crack plugging by corrosion deposits. This assertion needs to be evaluated further because it is unclear how corrosion product buildup will occur so any cracks that develop are plugged with corrosion products. DOE has neither extensively evaluated the rockfall effect on stress corrosion cracking of titanium alloys nor considered the consequence of the crack presence on subsequent rockfall events where an existing crack acts as the

---

[2]Reamer, C.W Letter (December 21) to S. Brocoum, DOE. Washington, DC: NRC 2001.

[3]Beavers, J.A "Stress Corrosion Cracking" *Presentation to the Waste Package Materials Performance Peer Review Panel March 18–19, 2002.* Las Vegas, Nevada 2002.

nucleation point for a substantial opening in the drip shield. DOE agreed to provide additional information in agreement CLST 2.08 about evaluation of the effect of rockfall or drift collapse on environmentally assisted cracking of the drip shield.

4.2 The CNWRA Investigations

Review of the DOE approach for environmentally assisted cracking of the drip shield indicated that the role of fluoride in the groundwater and the cracking behavior of Titanium Grade 7 have not been adequately considered by DOE. To evaluate the environmentally assisted cracking susceptibility of Titanium Grade 7, as well as other titanium alloys, in the presence of fluoride, preliminary scoping experiments were conducted using the slow strain rate test method. The test solutions were selected based on the localized and uniform corrosion studies conducted at CNWRA (Brossia, et al., 2001).

The chemical compositions of Titanium Grades 2, 5, and 7 used in this study are provided in Table 4-2. All alloys were obtained in the form of hot-rolled and annealed plates 9.52 mm [0.375 in], 7.92 mm [0.312 in], and 25.4 mm [1.0 in] thick. Notched slow strain rate specimens with a diameter of 6.35 mm [0.250 in] and a circumferential notch were machined from the as-received plates. The notch used to facilitate crack initiation was 1.588 mm [0.0625 in] deep with an included angle of 60° and a maximum radius of 61 μm [0.002 in]. The notched specimens were stressed either parallel or perpendicular to the rolling direction, designated as longitudinal (L) and transverse (T) specimens. The slow strain rate tests were conducted using a six-specimen test machine within an autoclave made of Type 316L SS. An extension rate of 1.8×10^{-5} mm/s [7.1×10^{-7} in/s] was used for all tests. The environmentally assisted cracking susceptibility of the titanium alloys was evaluated in 1.0 M NaCl solutions with and without the addition of 0.1 M NaF at 95 °C [203 °F], in addition to a set of baseline tests in air. The solutions used in these tests were fully deaerated with nitrogen. All tests were conducted under open-circuit conditions with an Ag/AgCl (0.1 M KCl) reference electrode. Specimens were connected to a computer-controlled multichannel potentiostat. The potential and current were monitored on one specimen and checked periodically on the rest of the specimens. Load cells and linear variable differential transformers were used to measure the load on each of the specimens and the displacement of the pull rods. After failure, the fracture surfaces of all specimens tested were examined with an optical microscope. Selected specimens were further examined using the scanning electron microscope.

Table 4-2. Chemical Composition of the Titanium Alloys Used in This Study (wt%)

Material	Ti	C	N	Fe	O	H	Al	V	Pd
Grade 2	Balance	0.011	0.016	0.111	0.141	0.001	—	—	—
Grade 5	Balance	0.030	0.007	0.140	0.186	0.012	6.180	4.050	—
Grade 7	Balance	0.009	0.007	0.115	0.140	0 005	—	—	0.155

Table 4-3 summarizes the results of the two sets of slow strain rate tests conducted in deaerated 1.0 M NaCl solutions with and without the addition of 0.1 M NaF at 95 °C [203 °F]. For each of the specimens, the reduction in area was calculated by measuring the area of the fracture surface and dividing by the initial cross-sectional area of the test specimen. As shown in Table 4-3, the reduction in area data varied from 15.7 percent for specimen TiGr5–1(L) to 36.4 percent for specimen TiGr2–1(T) with exception of the TiGr5–1(T) specimen in which failure occurred at the thread of the specimen. There is no general trend in changes in reduction in area with respect to titanium grade and test environment. Gordon[4] reported a value of an approximately 50-percent reduction in area for ductile failure of Titanium Grade 7. The experiments were conducted in 5 wt% NaCl (0.9 M chloride) at pH 2.7 and 90 °C [194 °F] using smooth tensile specimens with a strain rate of 3.3×10^{-6} s^{-1}. The reduction in area of the specimens tested in air, however, was in the same range of those tested in solutions. The low reduction in area values measured for all the specimens tested, regardless of the testing environment, may be the nature of slow strain rate testing of the circumferentially notched, round tensile specimens where failure occurs in a fast manner without an appreciable plastic deformation once crack is initiated at the notch.

Table 4-3. Results of Slow Strain Rate Tests of Titanium Alloys in Chloride Solutions

Specimen (Orientation)	Test Solution	Time to Failure (Hours)	Reduction in Area (Percent)	Test Results
TiGr2–1(L)	1.0 M NaCl + 0.1 M NaF 95 °C [203 °F], N_2 deaerated	21.5	21.5	Environmentally assisted cracking
TiGr2–1(T)	1.0 M NaCl + 0.1 M NaF 95 °C [203 °F], N_2 deaerated	25.3	36.4	Environmentally assisted cracking
TiGr5–1(L)	1.0 M NaCl + 0.1 M NaF 95 °C [203 °F], N_2 deaerated	26.4	15.7	Environmentally assisted cracking
TiGr5–1(T)	1.0 M NaCl + 0.1 M NaF 95 °C [203 °F], N_2 deaerated	—	—	Failed at thread
TiGr7–1(L)	1.0 M NaCl + 0.1 M NaF 95 °C [203 °F], N_2 deaerated	25.8	25.9	Environmentally assisted cracking
TiGr7–1(T)	1.0 M NaCl + 0.1 M NaF 95 °C [203 °F], N_2 deaerated	21.3	35 4	Environmentally assisted cracking
TiGr2–2(L)	1.0 M NaCl 95 °C [203 °F], N_2 deaerated	24.6	28.2	Ductile failure
TiGr2–2(T)	1.0 M NaCl 95 °C [203 °F], N_2 deaerated	24.6	32.6	Ductile failure
TiGr5–2(L)	1.0 M NaCl 95 °C [203 °F], N_2 deaerated	25 0	19.6	Ductile failure
TiGr5–2(T)	1.0 M NaCl 95 °C [203 °F], N_2 deaerated	24.6	18.0	Ductile failure
TiGr7–2(L)	1.0 M NaCl 95 °C [203 °F], N_2 deaerated	23.8	33.1	Ductile failure

[4]Gordon, G. "Stress Corrosion Cracking (SCC) and Hydrogen Induced Cracking (HIC) Modeling and Experimental Program Status" *Presentation to the DOE and NRC CLST Appendix 7 Meeting July 7–8, 1999* Livermore, California CRWMS M&O. 1999

Scanning electron micrographs taken from the fracture surfaces of the longitudinal specimens for all three titanium alloys tested in both solutions are shown in Figure 4-1. Fracture surfaces of all alloys tested in chloride-only solution showed metallic appearance, whereas those tested in the fluoride-chloride solution were covered with corrosion products, probably in the form of TiO_2 because of titanium dissolution. The Titanium Grade 7 specimens tested in the fluoride-chloride solution have much less corrosion products coverage, suggesting the possible effect of palladium addition for reducing the passive corrosion rates. Figure 4-2 shows the typical appearance of the fracture surfaces. It clearly shows microvoids, typical features of ductile fracture, in all specimens tested in chloride-only solution. Similar fracture surface features were also observed in the specimens tested in air. In contrast, brittle fracture features such as facets, slip bands, and voids were observed on the fracture surfaces of the specimens tested in the fluoride-chloride solution. Although failure of the specimens tested in chloride-only solution appeared to be ductile, the values of reduction in area were only slightly larger than those measured in the fluoride-chloride solution in most of the cases.

The measured potentials ranged from -790 to -730 mV with respect to Ag/AgCl (0.1 M KCl) [-839 to -779 mV_{SCE}] in 1.0 M NaCl + 0.1 M NaF solution, whereas they were from -510 to -420 mV with respect to Ag/AgCl (0.1 M KCl) [-559 to -469 mV_{SCE}] in 1.0 M NaCl solution. The potential values measured in the fluoride-chloride solution are below the critical cathodic potential of approximately -700 mV_{SCE} for hydride formation for Titanium Grade 2 in 6-percent NaCl solution (pH 1) at 70 °C [158 °F] (Wang, et al., 1998). It is anticipated that, at these cathodic potentials, hydrides can be formed and, thus, decrease the cracking susceptibility of titanium alloys. Furthermore, hydrogen-induced cracking susceptibility generally increases with decreasing strain rate because the hydrogen has more time to diffuse into the crack tip region. Thus, decreasing strain rate may enhance hydrogen-induced cracking of titanium alloys. Additional metallurgical analysis on the cross sections of the test specimens, as well as testing at low extension rates, are under way to verify hydrides formation and the strain rate effect for the environmental conditions used in this study.

Of these three titanium grades, Titanium Grade 5 generally showed a significant ductility loss and was more susceptible to environmentally assisted cracking, as evidenced by small values of reduction in area. Wang, et al. (1998) reported that Titanium Grade 3 is more susceptible to hydrogen embrittlement than Titanium Grade 2. They attributed the increased susceptibility to the formation of additional hydrides in the interior because of the higher oxygen content in Titanium Grade 3. Increased yield strength also tends to increase susceptibility to hydrogen embrittlement because it allows for a sharp crack to be maintained more easily. It is possible that the observed high susceptibility of Titanium Grade 5 to environmentally assisted cracking may be attributed to a combined effect of its high oxygen content and high yield strength.

For the effect of specimen orientation, current results obtained from slow strain rate testing of three titanium alloys in both longitudinal and transverse orientations are insufficient to determine its effect. Clarke, et al. (1997) evaluated hydrogen-induced cracking of commercial purity titanium using slow straining of compact tension specimens. They reported that specimen orientation in terms of the distribution of residual β-phase and the texture of the fabricated plate may greatly affect the susceptibility of titanium alloys to fast fracture. The specimen orientation with the rolling plane and rolling direction parallel to the applied tensile stress exhibited least resistance to embrittlement by hydrogen. The effect of specimen orientation needs further evaluation.

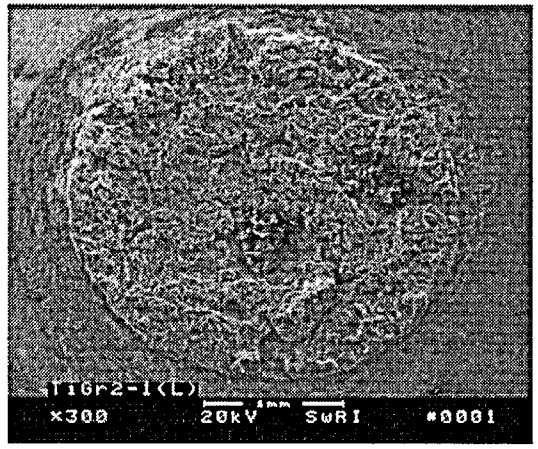

TiGr2–1(L)

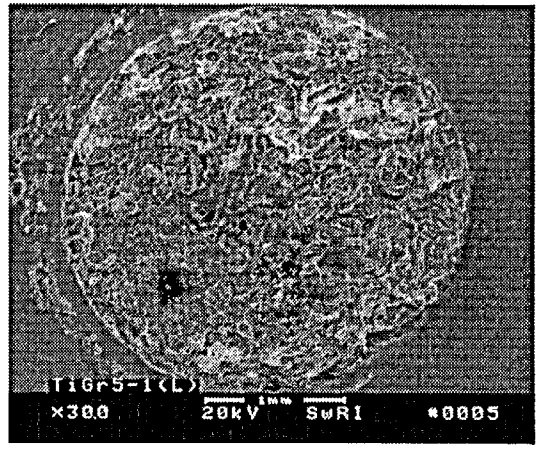

TiGr5–1(L)

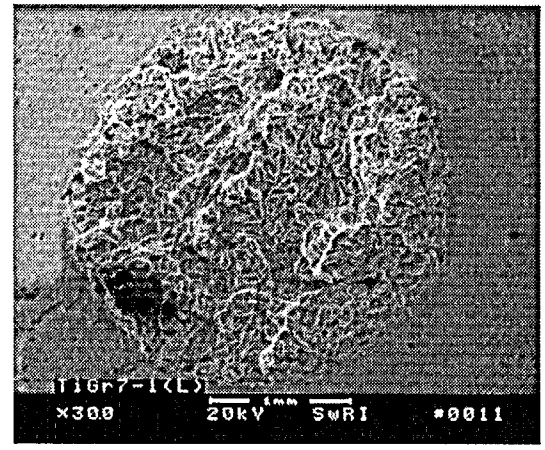

TiGr7–1(L)

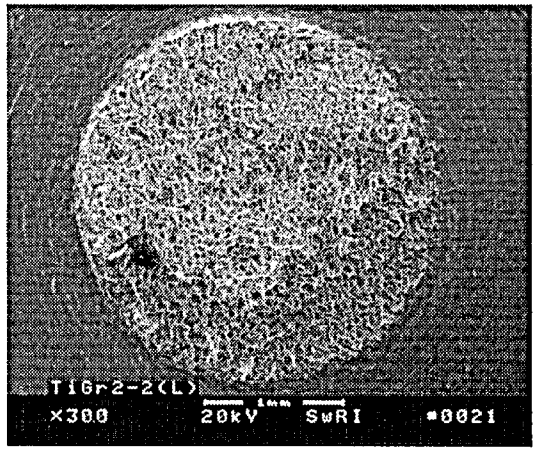

TiGr2–2(L)

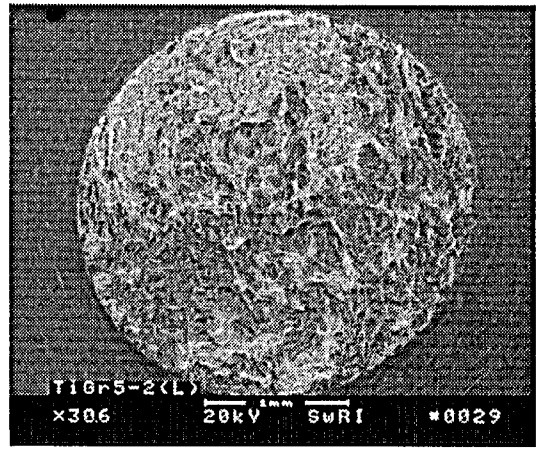

TiGr5–2(L)

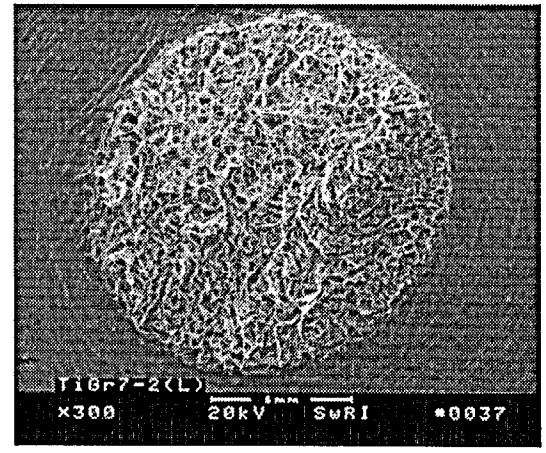

TiGr7–2(L)

Figure 4-1. Scanning Electron Micrographs of Fracture Surfaces of Titanium Slow Strain Rate Specimens Tested in Fluoride-Chloride Solution (Top Row) and in Chloride-Only Solution (Bottom Row) at 95 °C [230 °F]

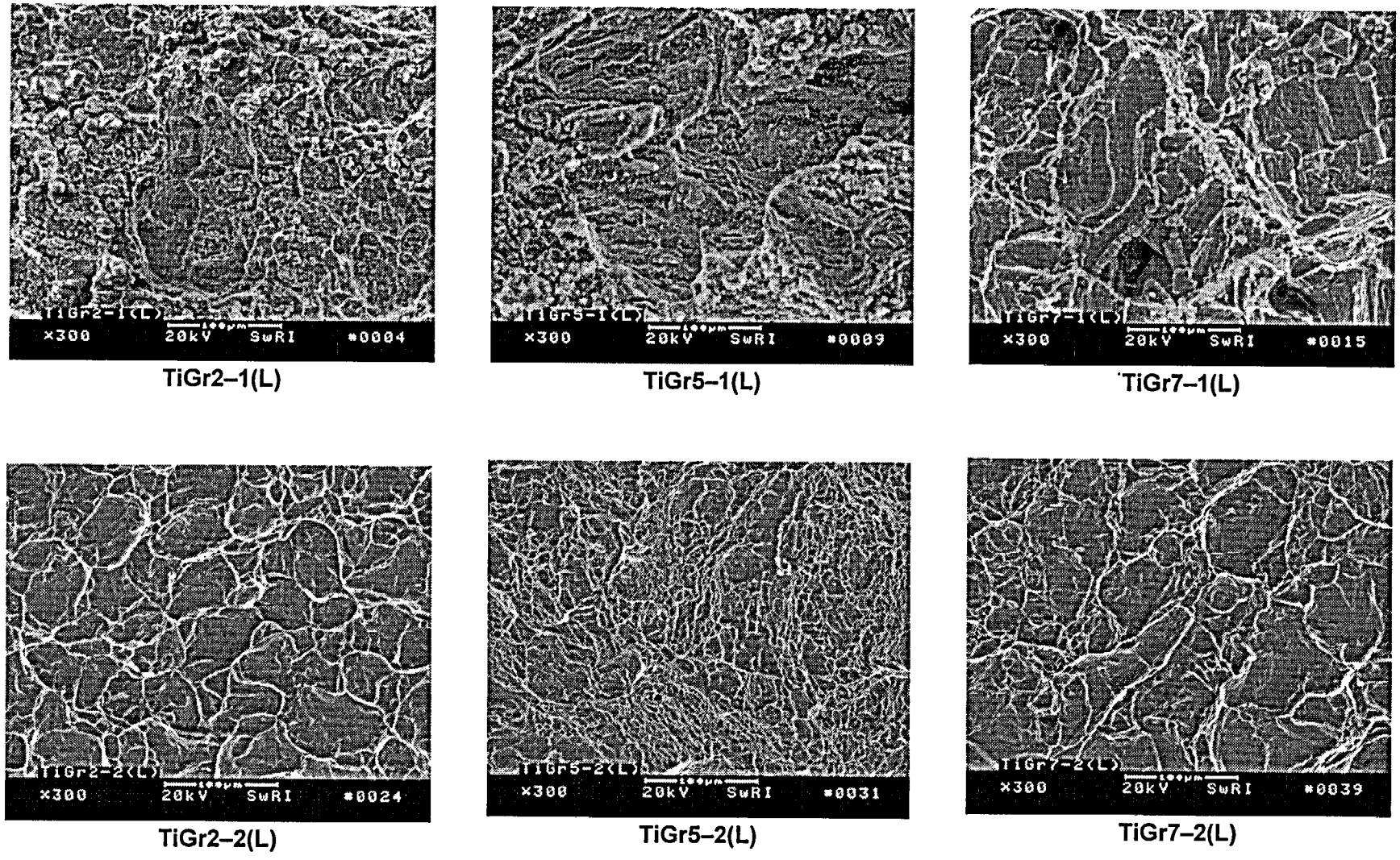

Figure 4-2. Scanning Electron Micrographs of Fracture Surfaces of Titanium Slow Strain Rate Specimens Showing Brittle Fracture Features Tested in Fluoride-Chloride Solution (Top Row) and Microvoids Resulting from Ductile Fracture in Chloride-Only Solution (Bottom Row) at 95 °C [230 °F]

4.3 Summary

DOE considered the primary environmentally assisted cracking process for the titanium drip shield is caused by hydrogen absorption leading to embrittlement. DOE evaluated the susceptibility of the drip shield to hydrogen-induced cracking using a critical threshold hydrogen concentration of 1,000 parts per million as a criterion for failure and concluded that hydrogen-induced cracking is not a limiting degradation process affecting the function of the drip shield. This analysis was based on the corrosion rate measured from the weight loss of coupons tested in the long-term corrosion test facility to calculate the hydrogen generated by the associated cathodic reaction and several assumptions involved in estimating the fraction of hydrogen absorbed into the metal. Review of the DOE approach for environmentally assisted cracking of drip shield indicated that the critical hydrogen concentration chosen needs to be evaluated further for Titanium Grade 7 because it is based on results for a different titanium alloy. In addition, reliance on the corrosion rates measured from weight loss may lead to a nonconservative estimate of the quantity of hydrogen absorbed. Furthermore, the possible detrimental effects of fluoride on hydrogen uptake and its potential accelerating influence on subsequent hydrogen-induced cracking have not been evaluated. On the other hand, the susceptibility of Titanium Grade 7 to stress corrosion cracking in basic saturated water, as observed in the DOE-sponsored work at General Electric, has led the DOE Waste Package Materials Performance Peer Review Panel to recommend the selection of an alternative material if such observation is confirmed.

CNWRA performed limited experiments to evaluate the environmentally assisted cracking susceptibility of Titanium Grade 7 and other titanium alloys in the presence of fluoride using the slow strain rate test method. Tests were conducted in 1.0 M NaCl solutions with and without the addition of 0.1 M NaF at 95 °C [203 °F]. These test solutions were selected based on previous CNWRA studies on localized and uniform corrosion of Titanium Grade 7. Preliminary results indicated that the presence of fluoride may lead to an enhanced susceptibility to environmentally assisted cracking, as characterized by the brittle fracture features observed on the circumferentially notched, round tensile specimens.

These preliminary slow strain rate test results indicate that Titanium Grade 7 may be susceptible to environmentally assisted cracking in the presence of fluoride. This concern has not been adequately considered by DOE. The critical threshold hydrogen concentration and the fraction of hydrogen absorbed considering the catalytic properties of palladium for hydrogen generation, also need to be experimentally determined or justified by DOE to validate the anticipated performance of the drip shield from the hydrogen-induced cracking model. DOE agreed to provide additional information for the selection of values of the critical hydrogen concentration leading to embrittlement and the assumed range of corrosion rates and fraction of hydrogen absorption, according to agreements CLST 6.02, and CLST 6.03. Also, according to agreement CLST 6.01, DOE will conduct stress corrosion cracking tests of titanium using a similar approach to that adopted for Alloy 22. The tests will cover a wide range of environmental conditions, including the confirmation that no detrimental effects can be expected from the presence of fluoride in the aqueous environment. Evaluation of the effect of rockfall or drift collapse on environmentally assisted cracking of the drip shield will be provided by DOE according to agreement CLST 2.08.

5 SUMMARY, CONCLUSIONS, AND RECOMMENDATIONS

Environmentally assisted cracking of container and drip shield materials, including stress corrosion cracking and hydrogen embrittlement, is considered an important degradation process that may strongly influence the lifetimes of the waste package and the drip shield. Several deficiencies and limitations are identified in the current U.S. Department of Energy (DOE) approach and in the technical bases provided for the evaluation of stress corrosion cracking of the Alloy 22 outer container and environmentally assisted cracking of the Titanium Grade 7 drip shield. These deficiencies include the effects of environmental factors and fabrication processes on the susceptibility of Alloy 22 to stress corrosion cracking, the effect of minor environmental species on stress corrosion cracking of Alloy 22, and the effect of fluoride on the environmentally assisted cracking susceptibility of titanium alloys.

5.1 Stress Corrosion Cracking of Container Materials

The DOE evaluation of the flaw sizes and distributions, residual stresses as a result of fabrication processes, and stress mitigation methods rely on many assumptions that need to be verified. The present models are not based on the current waste package design or fabrication method. Verification of important assumptions, such as residual stresses after solution annealing and quenching of the disposal container stress profiles after laser peening and induction annealing, is necessary to determine the adequacy of the DOE assessment. Tests performed by DOE indicate Alloy 22 is resistant to chloride stress corrosion cracking. For conditions where stress corrosion cracking has been initiated, the crack propagation rates are low, and crack propagation ceases below the critical stress intensity for stress corrosion cracking. The effects of potential and solution chemistry on stress corrosion cracking susceptibility have been explored mostly using slow strain rate tests, but these variables have not been evaluated for crack propagation rates or critical stress intensities for stress corrosion cracking. DOE models for stress corrosion crack initiation and propagation do not consider the important effects of environmental composition and potential.

Center for Nuclear Waste Regulatory Analyses (CNWRA) conducted experiments to evaluate the stress corrosion cracking susceptibility of Alloy 22 and Type 316L SS in concentrated chloride solutions. Type 316 L SS was found to be susceptible to stress corrosion cracking when the potential of the specimen was above the crevice corrosion repassivation potential. In contrast, the initiation of stress corrosion cracking was prevented when the potential was less than the crevice corrosion repassivation potential. When the potential of the specimen was reduced below the repassivation potential after crack initiation and propagation, the crack propagation rate was substantially reduced as implied by changes in the crack opening displacement and compliance. It is not possible, however, to conclude that stress corrosion cracking is completely arrested when the specimen potential is reduced below the repassivation potential because the sensitivity of the crack growth rate measurements is limited to 3.3×10^{-9} mm/s [1.3×10^{-10} in/s]. In these studies, Alloy 22 was found to be very resistant to stress corrosion cracking in concentrated chloride solutions. No conclusive determination of Alloy 22 stress corrosion cracking susceptibility could be made from the results of the tests conducted in this investigation. Additional tests in progress will help to establish the relationship between the crevice corrosion repassivation potential and the stress corrosion cracking susceptibility of Alloy 22.

The effects of waste package fabrication and stress mitigation processes, material composition and material property variations, and environmental variations on stress corrosion cracking of Alloy 22 have not been adequately considered in the DOE model abstraction. The possible detrimental effects of variations in the environmental composition and fabrication effects on the stress corrosion cracking susceptibility of Alloy 22 need to be investigated. DOE has agreed to provide additional information in agreements CLST 1.12 through 1.16 to address the effects of waste package environments, fabrication and welding, compositional variation, and thermal aging on stress corrosion cracking of Alloy 22. In addition, release of radionuclides from waste packages that fail from stress corrosion cracking may be determined by the geometry of the crack openings and the deposition of corrosion products and mineral deposits. DOE agreed to provide the technical basis for crack plugging and arrest that may alter the release of radionuclides according to agreement TSPAI 3.03.

5.2 Effect of Minor Species on Stress Corrosion Cracking of Container Materials

Studies sponsored by the State of Nevada indicated that the resistance of the Alloy 22 outer container to localized corrosion and stress corrosion cracking may be affected by the presence of impurities, such as lead, mercury, and arsenic, in the water contacting the waste packages. Stress corrosion cracking of Alloy 22 was reported to occur at 250 °C [482 °F] in a 1,000× J–13 Well water containing 5,000 parts per million of lead (as lead acetate) and acidified by the addition of HCl to pH 0.5. The State of Nevada investigators, however, could not reproduce this preliminary result. Limited data on stress corrosion cracking of Alloy 22 in lead-containing environments have been reported by DOE. No stress corrosion cracking was observed in slow strain rate tests in water containing 1 percent $PbCl_2$ (7,450 parts per million of lead) at 95 °C [203 °F]. It should be noted that the test solutions used in both the DOE and the State of Nevada investigations were not properly characterized in terms of the lead speciation.

CNWRA conducted a limited analysis to evaluate lead solution chemistry and its effect on the anodic polarization behavior and stress corrosion cracking of Alloy 22. Speciation calculations revealed the formation of Pb^{2+} cations and Pb-Cl complexes in $PbCl_2$ solutions. The presence of lead species in a supersaturated $PbCl_2$ solution (16,300 parts per million of lead) with pH 0.5 by the addition of HCl promotes the occurrence of a pronounced anodic oxidation peak (also observed on platinum) and simultaneously enhances the dissolution of Alloy 22. This enhanced dissolution in a crevice specimen was characterized by the presence of randomly distributed etch pits. No localized corrosion was observed in crevice specimens tested in solutions with lead concentrations ranging from 1,500 to 5,400 parts per million. In addition, no stress corrosion cracking was observed at an applied potential of −100 mV_{SCE}, which is a potential corresponding to the anodic oxidation peak, when both single and double U-bend specimens were tested in super-saturated $PbCl_2$ solutions (9,500–11,900 parts per million of lead) with pH 0.5 at 95 °C [203 °F].

These results suggest that Alloy 22 is resistant to stress corrosion cracking in supersaturated $PbCl_2$ solutions even at the extremely high lead concentrations and low pH used in the tests. Moreover, no deleterious effect of lead species on localized corrosion was observed in crevice specimens for a wide range of lead concentrations with the exception of supersaturated $PbCl_2$ solutions. Based on these preliminary results and provided these high lead concentrations are not attainable in the anticipated repository environments, Alloy 22 is unlikely to be susceptible to

stress corrosion cracking or localized corrosion. DOE agreed to provide additional information in agreements CLST 1.01 and CLST 1.10 for the range of concentrations of minor species expected to evolve in Yucca Mountain waters and their effects on the critical potential for localized corrosion. Although it is not explicitly stated in agreement CLST 1.12, additional information should be provided by DOE if stress corrosion cracking of Alloy 22 in the presence of lead contamination is confirmed in realistic repository conditions.

5.3 Environmentally Assisted Cracking of Drip Shield Materials

DOE considered the primary environmentally assisted cracking process for the titanium drip shield is caused by hydrogen absorption leading to embrittlement. DOE evaluated the susceptibility of the drip shield to hydrogen-induced cracking using a critical threshold hydrogen concentration of 1,000 parts per million as a criterion for failure and concluded that hydrogen-induced cracking is not a limiting degradation process affecting the functionality of the drip shield. This analysis was based on the corrosion rate measured from weight loss of coupons tested in the long-term corrosion test facility to calculate the hydrogen generated by the associated cathodic reaction and several assumptions involved in estimating the fraction of hydrogen absorbed into the metal. Review of the DOE approach for environmentally assisted cracking of drip shield indicated that the critical hydrogen concentration chosen needs to be evaluated further for Titanium Grade 7 because it is based on results for a different titanium alloy. In addition, reliance on the corrosion rates measured from weight loss may lead to a nonconservative estimate of the quantity of hydrogen absorbed. Furthermore, the possible detrimental effects of fluoride on hydrogen uptake and its potential accelerating influence on subsequent hydrogen-induced cracking have not been evaluated. On the other hand, the susceptibility of Titanium Grade 7 to stress corrosion cracking in basic saturated water as observed in the DOE-sponsored work at General Electric has led the DOE Waste Package Materials Performance Peer Review Panel to recommend the selection of an alternative material for drip shield construction if such observation is confirmed.

CNWRA performed limited experiments to evaluate the environmentally assisted cracking susceptibility of Titanium Grade 7 and other titanium alloys in the presence of fluoride using the slow strain rate test method. Tests were conducted in 1.0 M NaCl solutions with and without the addition of 0.1 M NaF at 95 °C [203 °F]. These test solutions were selected based on previous CNWRA studies on localized and uniform corrosion of Titanium Grade 7. Preliminary results indicated that the presence of fluoride may lead to an enhanced susceptibility to environmentally assisted cracking, as characterized by brittle fracture features observed on the circumferentially notched, round tensile specimens.

These preliminary slow strain rate test results indicate that Titanium Grade 7 appears to be susceptible to environmentally assisted cracking in the presence of fluoride. This concern has not been adequately considered by DOE. The critical threshold hydrogen concentration and the fraction of hydrogen absorbed considering the catalytic properties of palladium for hydrogen generation, also need to be experimentally determined or justified by DOE to validate the anticipated performance of the drip shield from the hydrogen-induced cracking model. DOE agreed to provide additional information for the selection of values of the critical hydrogen concentration leading to embrittlement and the assumed range of corrosion rates and fraction of hydrogen absorption, according to agreements CLST 6.02 and CLST 6.03. Also, according to agreement CLST 6.01, DOE will conduct stress corrosion cracking tests of titanium using a

similar approach to that adopted for Alloy 22. The tests will cover a wide range of relevant environmental conditions, including the confirmation that no detrimental effects can be expected from the presence of fluoride in the aqueous environment. Evaluation of the effect of rockfall or drift collapse on environmentally assisted cracking of the drip shield will be provided by DOE according to agreement CLST 2.08.

5.4 Future Work

Evaluation of the susceptibility of container and drip shield materials to stress corrosion cracking and environmentally assisted cracking is necessary to assess the lifetimes of the waste package and the drip shield. DOE models evaluated stress corrosion cracking susceptibility of Alloy 22 using model parameters based on limited experimental work. The effects of waste package environments (including minor environmental species), fabrication and welding, compositional variation, and thermal aging on stress corrosion cracking of Alloy 22 need to be properly considered by DOE as indicated in the DOE and the U.S. Nuclear Regulatory Commission (NRC) agreements. Additional experimental work and simulations that consider ranges of repository environments, compositional variations, and fabrication processes are needed for DOE to complete the evaluation.

If the relationship between crevice corrosion repassivation potential and critical potential for stress corrosion cracking of Alloy 22 in chloride-containing solutions can be demonstrated, an appropriate model abstraction can be readily incorporated into a new version of the TPA code developed by NRC. Then, performance calculations and sensitivity analyses can be used to evaluate the consequences of these technical concerns in a quantitative risk-insight context.

The critical hydrogen concentration for the onset of cracking in Titanium Grade 7 should be evaluated by considering the possibility of enhanced hydrogen uptake and absorption in the presence of fluoride. Experimental measurements of the critical threshold hydrogen concentration and the fraction of hydrogen absorbed are needed to validate the anticipated performance of drip shield. The possibility of stress corrosion cracking in simulated concentrated solutions should be fully explored by DOE to confirm the use of Titanium Grade 7 as the drip shield material.

6 REFERENCES

Agrawal, A.K. and J.P.N. Paine. "Lead Cracking of Alloy 600—A Review." Proceedings of the Fourth International Conference on Environmental Degradation of Materials in Nuclear Power Systems—Water Reactors. Houston, Texas: NACE International. 1990.

Alkire, R., D. Ernsberger, and T.R. Beck. "Occurrence of Salt Films During Repassivation of Newly Generated Metal Surfaces." *Journal of the Electrochemical Society.* Vol. 125. pp. 1,382–1,388. 1978.

American Society for Metals. "Nondestructive Inspection and Quality Control Ultrasonic Inspection." *Metals Handbook.* Vol. 11. Metals Park, Ohio: American Society for Metals. pp. 161–198. 1976.

American Society of Mechanical Engineers. "Nondestructive Examination—Section V." *American Society of Mechanical Engineers Boiler and Pressure Vessel Code.* New York City, New York: American Society of Mechanical Engineers. 1995.

Anderson, T.L. *Fracture Mechanics—Fundamentals and Applications.* Boca Raton, Florida: CRC Press. 1991.

Andresen, P.L. and F.P. Ford. "Fundamental Modeling of Environment Cracking for Improved Design and Lifetime Evaluation of BWRs." *International Journal of Pressure Vessels and Piping.* Vol. 59, No. 1-3. pp. 61–70. 1994.

Andresen, P.L., P.W. Emigh, L.M. Young, and G.M. Gordon. "Stress Corrosion Cracking of Annealed and Cold Worked Titanium Grade 7 and Alloy 22 in 110 °C Concentrated Salt Environments." Proceedings of the CORROSION 2001 Conference. Paper No. 01130. Houston, Texas: NACE International. 2001.

ASTM International. "Standard Specification for Low-Carbon Nickel-Molybdenum-Chromium, Low-Carbon Nickel-Chromium-Molybdenum, Low-Carbon Nickel-Chromium-Molybdenum-Copper, Low-Carbon Nickel-Chromium-Molybdenum-Tantalum, and Low-Carbon Nickel-Chromium-Molybdenum-Tungsten Alloy Plate, Sheet, and Strip." *ASTM B–575–99a: Annual Book of Standards. Vol. 3.02: Wear and Erosion—Metal Corrosion.* West Conshohocken, Pennsylvania: ASTM International. 2001a.

———. "Standard Test Method for Conducting Cyclic Potentiodynamic Polarization Measurements for Localized Corrosion Susceptibility of Iron-, Nickel-, or Cobalt-Based Alloys." *ASTM G61–86: Annual Book of Standards. Vol. 3.02: Wear and Erosion—Metal Corrosion.* West Conshohocken, Pennsylvania: ASTM International. 2001b.

———. "Standard Practice for Making and Using U-Bend Stress-Corrosion Test Specimens." *ASTM G30–97: Annual Book of Standards. Vol. 3.02: Wear and Erosion—Metal Corrosion.* West Conshohocken, Pennsylvania: ASTM International. 2001c.

———. "Standard Test Method for Plane-Strain Fracture Toughness of Metallic Materials." *ASTM E399–90: Annual Book of Standards. Vol. 3.01: Metallography Metals—Mechanical Testing: Elevated and Low-Temperature Tests.* West Conshohocken, Pennsylvania: ASTM International. pp. 422–452. 1999.

Beck, T.R. "A Review: Pitting Attack of Titanium Alloys." *Localized Corrosion.* NACE–3. Houston, Texas: NACE International. pp. 644–652. 1974.

———. "Electrochemical Aspects of Titanium Stress Corrosion Cracking." *Fundamental Aspects of Stress Corrosion Cracking.* R.W. Staehle, A.J. Forty, and D. Van Rooyen, eds. Houston, Texas: NACE International. pp. 605–619. 1969.

Bockris, J.O.'M. and A.K.N. Reddy. *Modern Electrochemistry.* New York City, New York: Plenum Press. 1970.

Bromley, L.A. "Approximate Individual Ion Values of β in Extended Debye-Huckel Theory for Uni-Univalent Aqueous Solutions at 298.15 K" *Journal of Chemical Thermodynamics.* Vol. 4. pp. 669–673. 1972.

Brossia, C.S. and G.A. Cragnolino. "Effect of Palladium on the Localized and Passive Dissolution of Titanium." Proceedings of the CORROSION 2001 Conference. Paper No. 01127. Houston, Texas: NACE International. 2001a.

Brossia, C.S. and G.A. Cragnolino. "Effects of Environmental and Metallurgical Conditions on the Passive and Localized Dissolution of Ti-0.15%Pd." *Corrosion.* Vol. 57. pp. 768–776. 2001b.

Brossia, C.S., L.B. Browning, D.S. Dunn, O.C. Moghissi, O. Pensado, and L. Yang. "Effect of Environment on the Corrosion of Waste Package and Drip Shield Materials." CNWRA 2001-003. San Antonio, Texas: CNWRA. 2001.

Brown, B.F., C.T. Fujii, and E.P. Dahlberg. "Methods for Studying the Solution Chemistry Within Stress Corrosion Cracks." *Journal of the Electrochemical Society.* Vol. 116. pp. 218–219. 1969.

Carlos, B.A., S.J. Chipera, and D.L. Bish. "Distribution and Chemistry of Fracture-Lining Minerals at Yucca Mountain, Nevada." LA–12977–MS. Los Alamos, New Mexico: Los Alamos National Laboratory. 1995.

Clarke, C.F., D. Hardie, and B.M. Ikeda. "Hydrogen-Induced Cracking of Commercial Purity Titanium." *Corrosion Science.* Vol. 39. pp. 1,545–1,559. 1997.

Clarke, C.F., D. Hardie, and B.M. Ikeda. "The Effect of Hydrogen Content on the Fracture of Precracked Titanium Specimens." *Corrosion Science.* Vol. 36. pp. 487–509. 1994.

Clarke, C.F., B.M. Ikeda, and D. Hardie. "Effect of Crevice Corrosion on Hydrogen Embrittlement of Titanium." *Environment-Induced Cracking of Metals.* NACE–10. Houston, Texas: NACE International. pp. 419–424. 1988.

Copson, H.R. "Effect of Composition on Stress Corrosion Cracking of Some Alloys Containing Nickel." *Physical Metallurgy of Stress Corrosion Cracking*. T.N. Rhodin, ed. New York City, New York: Interscience Publishers. pp. 247–269. 1959.

Copson, H.R. and S.W. Dean. "Effect of Contaminants on Resistance to Stress Corrosion Cracking of Ni-Cr Alloy 600 in Pressurized Water." *Corrosion*. Vol. 21. pp. 1–8. 1965.

Costa, D., H. Talah, P. Marcus, M. Calvar, and A. Gelpi. "Interaction of Lead with Nickel-Base Alloys 600 and 690." Proceedings of the Seventh International Conference on Environmental Degradation of Materials in Nuclear Power Systems—Water Reactors. Houston, Texas: NACE International. pp. 199–208. 1995.

Cragnolino, G.A. and N. Sridhar. "A Review of Stress Corrosion Cracking of High-Level Nuclear Waste Container Materials—I." CNWRA 92-021. San Antonio, Texas: CNWRA. 1992.

Cragnolino, G.A., D.S. Dunn, Y.-M. Pan, and N. Sridhar. "The Critical Potential for the Stress Corrosion Cracking of Fe-Cr-Ni Alloys and Its Mechanistic Implications." Chemistry and Electrochemistry of Corrosion and Stress Corrosion Cracking: A Symposium Honoring the Contributions of R.W. Staehle. R.H. Jones, ed. Warrendale, Pennsylvania: The Minerals, Metals, and Materials Society. pp. 83–104. 2001a.

Cragnolino, G.A., D.S. Dunn, Y.-M. Pan, and O. Pensado. "Corrosion Processes Affecting the Performance of Alloy 22 as a High-Level Radioactive Waste Container Material." Scientific Basis for Nuclear Waste Management XXIV. K.P. Hart and G.R. Lumpkin, eds. Symposium Proceedings 663. Pittsburgh, Pennsylvania: Materials Research Society. pp. 507–514. 2001b.

Cragnolino, G.A., D.S. Dunn, C.S. Brossia, V. Jain, and K. Chan. "Assessment of Performance Issues Related to Alternate EBS Materials and Design Options." CNWRA 99-003. San Antonio, Texas: CNWRA. 1999.

Cragnolino, G.A., D.S. Dunn, and N. Sridhar. "Environmental Effects on Stress Corrosion Cracking of Type 316L Stainless Steel and Alloy 825 as High-Level Nuclear Waste Container Materials." CNWRA 94-028. San Antonio, Texas: CNWRA. 1994.

CRWMS M&O. "Waste Package Project FY–01 Closure Methods Report." TER–EBS–ND–000006. Rev. 00. Las Vegas, Nevada: CRWMS M&O. 2001a.

———. "Waste Package Operations Fabrication Process Report." TDR–EBS–ND–000003. Rev. 02. Las Vegas, Nevada: CRWMS M&O. 2001b.

———. "Repository Safety Strategy: Plan to Prepare the Safety Case to Support Yucca Mountain Site Recommendation and Licensing Considerations." TDR–WIS–RL–000001. Rev. 04 ICN 01. Las Vegas, Nevada: CRWMS M&O. 2000a.

———. "Total System Performance Assessment for the Site Recommendation." TDR–WIS–PA–000001. Rev. 00 ICN 01. Las Vegas, Nevada: CRWMS M&O. 2000b.

———. "Waste Package Degradation Process Model Report." TDR–WDS–MD–000002. Rev. 00 ICN 01. Las Vegas, Nevada: CRWMS M&O. 2000c.

———. "Stress Corrosion Cracking of the Drip Shield, the Waste Package Outer Barrier, and the Stainless Steel Structural Material." ANL–EBS–MD–000005. Rev. 00 ICN 01. Las Vegas, Nevada: CRWMS M&O. 2000d.

———. "Design Analysis for the Ex-Container Components." ANL–XCS–ME–00001. Rev. 00. Las Vegas, Nevada: CRWMS M&O. 2000e.

———. "Design Analysis for UCF Waste Packages." ANL–UDC–MD–000001. Rev. 00. Las Vegas, Nevada: CRWMS M&O. 2000f.

———. "Update to the EIS Engineering File for the Waste Package in Support of the Final EIS." TDR–EBS–MD–000010. Rev. 00 ICN 01. Las Vegas, Nevada: CRWMS M&O. 2000g.

———. "General Corrosion and Localized Corrosion of Waste Package Outer Barrier." ANL–EBS–MD–000003. Rev. 00. Las Vegas, Nevada: CRWMS M&O. 2000h.

———. "Abstraction of Models of Stress Corrosion Cracking of Drip Shield and Waste Package Outer Barrier, and Hydrogen Induced Cracking of the Drip Shield." ANL–EBS–PA–000004. Rev. 00 ICN 01. Las Vegas, Nevada: CRWMS M&O. 2000i.

———. "Analysis of Mechanisms for Early Waste Package Failure." ANL–EBS–MD–000023. Rev. 00. Las Vegas, Nevada: CRWMS M&O. 2000j.

———. "Review of the Expected Behavior of Alpha Titanium Alloys Under Yucca Mountain Conditions." TDR–EBS–MD–000015. Rev. 00. Las Vegas, Nevada: CRWMS M&O. 2000k.

———. "Hydrogen Induced Cracking of Drip Shield." ANL–EBS–MD–000006. Rev. 00 ICN 01. Las Vegas, Nevada: CRWMS M&O. 2000l.

———. "General Corrosion and Localized Corrosion of the Drip Shield." ANL–EBS–MD–000004. Rev. 00. Las Vegas, Nevada: CRWMS M&O. 2000m.

Dunn, D.S., Y.-M. Pan, and G.A. Cragnolino. "Stress Corrosion Cracking of Nickel-Chromium-Molybdenum Alloys in Chloride Solutions." Proceedings of the CORROSION 2002 Conference. Paper No. 425. Houston, Texas: NACE International. 2002.

Dunn, D.S., Y.-M. Pan, and G.A. Cragnolino. "Stress Corrosion Cracking, Passive, and Localized Corrosion of Alloy 22 High-Level Radioactive Waste Containers." Proceedings of the CORROSION 2000 Conference. Paper No. 206. Houston, Texas: NACE International. 2000.

Dunn, D.S., Y.-M. Pan, and G.A. Cragnolino. "Effects of Environmental Factors on the Aqueous Corrosion of High-Level Radioactive Waste Containers—Experimental Results and Models." CNWRA 99-004. San Antonio, Texas: CNWRA. 1999.

Eremias, B. and V.V. Marichev. "Environmental Aspects of Stress Corrosion Cracking Growth in Austenitic Stainless Steel." *Corrosion Science*. Vol. 20. pp. 307–312. 1980.

Estill, J.C., K.J. King, D.V. Fix, D.G. Spurlock, G.A. Hurst, S.R. Gordon, R.D. Mccright, and R.B. Rebak. "Susceptibility of Alloy 22 to Environmentally Assisted Cracking in Yucca Mountain Relevant Environments." Proceedings of the CORROSION 2002 Conference. Paper No. 535. Houston, Texas: NACE International. 2002.

Ford, F.P. and P.L. Andresen. "Development and Use of a Predictive Model of Crack Propagation in 304/316L, A533B/A508 and Inconel 600/182 Alloys in 288 °C Water." Proceedings of the Third International Conference on Environmental Degradation of Materials in Nuclear Power Systems—Water Reactors. G.J. Theus and J.R. Weeks, eds. Warrendale, Pennsylvania: The Metallurgical Society. pp. 798–800. 1988.

Gileadi, E. *Electrode Kinetics for Chemists, Chemical Engineers, and Materials Scientists.* New York City, New York: VCH Publishers. 1993.

Greene, C.A., A.J. Henry, C.S. Brossia, and T.M. Ahn. "Evaluation of the Possible Susceptibility of Titanium Grade 7 to Hydrogen Embrittlement in a Geologic Repository Environment." Proceedings of the Materials Research Society Conference. Symposium Proceedings 663. Pittsburgh, Pennsylvania: Materials Research Society. pp. 515–523. 2001.

Hardie, D. and S. Ouyang. "Effect of Hydrogen and Strain Rate upon the Ductility of Mill-Annealed Ti6Al4V." *Corrosion Science.* Vol. 41. pp. 155–177. 1999.

Helgeson, H.C., D.H. Kirkham, and G.C. Flowers. "Theoretical Prediction of the Thermodynamic Behavior of Aqueous Electrolytes at High Pressures and Temperatures: IV. Calculation of Activity Coefficients, Osmotic Coefficients, and Apparent Molal and Standard and Relative Partial Molal Properties to 600 °C and 5 kb." *American Journal of Science.* Vol. 281. pp. 1,249–1,516. 1981.

Helie, M., I. Lambert, and G. Santarini. "Some Considerations about the Possible Mechanisms of Lead Assisted Stress Corrosion Cracking of Steam Generator Tubing." Proceedings of the Seventh International Conference on Environmental Degradation of Materials in Nuclear Power Systems—Water Reactors. Houston, Texas: NACE International. 1995.

Heubner, U.L., E. Altpeter, M.B. Rockel, and E. Wallis. "Electrochemical Behavior and Its Relation to Composition and Sensitization of NiCrMo Alloys in ASTM G–28 Solution." *Corrosion.* Vol. 45, No. 3 pp. 249–259. 1989.

Huang, H-H. "Electrochemical Impedance Spectroscopy Study of Strained Titanium in Fluoride Media." *Electrochimica Acta.* Vol. 47. pp. 2,311–2,318. 2002.

Ikeda, B.M and M.J. Quinn. "Hydrogen Assisted Cracking of Grade-16 Titanum: A Preliminary Examination of Behavior at Room Temperature." 06819–REP–01200–0039. Rev. 00. Toronto, Ontario, Canada: Ontario Hydro. 1998.

Ilevbare, G.O., T. Lian, and J.C. Farmer. "Environmental Considerations in the Studies of Corrosion Resistant Alloys for High-level Radioactive Waste Containment Considered for High-Level Nuclear Waste Containment." Proceedings of the CORROSION 2002 Conference. Paper No. 539. Houston, Texas: NACE International. 2002.

Ives, M.B. "Etch Pitting—Theory and Observation." *Localized Corrosion*. NACE–3. Houston, Texas: NACE International. pp. 78–103. 1974.

Jones, R.H. and S.M. Bruemmer. "Environment-Induced Crack Growth Processes in Nickel-Base Alloys." *Environment-Induced Cracking of Metals*. NACE–10. Houston, Texas: NACE International. pp. 287–310. 1990.

Khaleel, M.A., O.J.V. Chapman, D.O. Harris, and F A. Simonen. "Flaw Size Distribution and Flaw Existence Frequencies in Nuclear Piping." *Probabilistic and Environmental Aspects of Fracture and Fatigue*. New York City, New York: American Society of Mechanical Engineers. 1999.

King, K.J., J.C. Estill, and R.B. Rebak. "Characterization of the Resistance of Alloy 22 to Stress Corrosion Cracking." Proceedings of the Pressure Vessels and Piping Conference. Paper No. 03E–02. New York City, New York: American Society of Mechanical Engineers. 2002.

McCright, R.D. "Engineered Materials Characterization, Corrosion Data and Modeling—Update for the Viability Assessment." UCRL–ID–119564. Vol. 3. Rev. 1.1. Livermore, California: Lawrence Livermore National Laboratory. 1998.

McCright, D., G. Ilevbare, J. Estill, and R. Rebak. "Studies of Corrosion Resistant Materials Being Considered for High-Level Nuclear Waste Containment in Yucca Mountain Relevant Environments." Proceedings of the CORROSION 2002 Conference. Paper No. 537. Houston, Texas: NACE International. 2002.

Meyn, A. and G. Sandoz. "Fractography and Crystallography of Subcritical Crack Propagation in High Strength Titanium Alloys." *Transactions of the Metallurgical Society of AIME*. Vol. 245. pp 1,253–1,258. 1969.

NACE International. *Testing of Metals for Resistance to Sulfide Stress Cracking at Ambient Temperatures*. NACE Standard TM0177–96. Houston, Texas: NACE International. 1996.

Nakamura, N., Y. Fukaya, G. Nakayama, T. Kimoto, H. Ueda, and M. Akashi. "Initiation and Propagation of Stress-Corrosion Crack in Alpha-Titanium Alloys as Candidate Container Materials for the HLW Disposal." Chemistry and Electrochemistry of Corrosion and Stress Corrosion Cracking: A Symposium Honoring the Contributions of R.W. Staehle. R.H. Jones, ed. Warrendale, Pennsylvania: The Minerals, Metals, and Materials Society. pp. 615–633. 2001.

Nakamura, N., M. Akashi, Y. Fukaya, G. Nakayama, and H. Ueda. "Stress Corrosion Crack Initiation Behavior in α-Titanium Used for Nuclear Waste Disposal Overpack." Proceedings of the CORROSION 2000 Conference. Paper No. 00195. Houston, Texas: NACE International. 2000.

NRC. NUREG–1762, "Integrated Issue Resolution Status Report." Rev. 0. Washington, DC: NRC. August 2002.

———. "Issue Resolution Status Report, Key Technical Issue: Container Life and Source Term." Rev. 3b. Washington, DC: NRC. 2001.

Pan, Y.-M., D.S. Dunn, and G.A. Cragnolino. "Effects of Environmental Factors and Potential on Stress Corrosion Cracking of Fe-Ni-Cr-Mo Alloys in Chloride Solutions." Environmentally Assisted Cracking: Prediction Methods for Risk Assessment and Evaluation of Materials, Equipment, and Structures. R.D. Kane, ed. ASTM STP 1401. West Conshohocken, Pennsylvania: ASTM International. pp. 273–288. 2000.

Payer, J.H., J.A. Beavers, T.M. Devine, G.S. Frankel, R.H. Jones, R.G. Kelly, and R.M. Latanision. "Peer Review of the Waste Package Materials Performance Final Report." Las Vegas, Nevada: DOE. 2002.

Pensado, O., D.S. Dunn, G.A. Cragnolino, and V. Jain. "Passive Dissolution of Container Materials—Modeling and Experiments." CNWRA Report. San Antonio, Texas: CNWRA. 2002.

Perfect, D.L., C.C. Faunt, W.C. Steinkampf, and A.K. Turner. "Hydrochemical Data Base for the Death Valley Region, California and Nevada." U.S. Geological Survey Open-File Report 94-305. 1995.

Pitzer, K.S. "Ion Interaction Approach: Theory and Data Correlation." *Activity Coefficients in Electrolyte Solutions*. K.S. Pitzer, ed. Boca Raton, Florida: CRC Press. pp. 75–153. 1991.

———. "Thermodynamics of Electrolytes 1: Theoretical Basis and General Equations." *Journal of Physical Chemistry*. Vol. 77. pp. 268–277.

Powell, D.T. and J.C. Scully. "Stress Corrosion Cracking of Alpha Titanium Alloys at Room Temperature." *Corrosion*. Vol. 24. pp. 151–158. 1968.

Pulvirenti, A.L., K.M. Needham, M.A. Adel-Hadadi, C.R. Marks, J.A. Gorman, and A. Barkatt. "Effects of Lead, Mercury, and Reduced Sulfur Species on the Corrosion of Alloy 22 in Concentrated Groundwaters as a Function of pH and Temperature." Proceedings of the Materials Research Society Conference. Symposium Proceedings 713. Paper No. JJ11.6 Warrendale, Pennsylvania: Materials Research Society. 2002a.

Pulvirenti, A.L., K.M. Needham, M.A. Adel-Hadadi, A. Barkatt, C.R. Marks, and J.A. Gorman. "Corrosion of Titanium Grade 7 in Solutions Containing Fluoride and Chloride Salts." Proceedings of the CORROSION 2002 Conference. Paper No. 02552. Houston, Texas: NACE International. 2002b.

Roy, A.K., D.C. Freeman, and M.K. Spragge. "Stress Corrosion Cracking Evaluation of Candidate Container Alloys by Double Cantilever Beam Method." Proceedings of the CORROSION 2000 Conference. Paper No. 00189. Houston, Texas: NACE International. 2000.

Roy, A.K., D.L. Flemming, D.C. Freeman, and B.Y. Lum. "Stress Corrosion Cracking of Alloy C-22 and Ti Gr-12 Using Double-Cantilever-Beam Technique." *Micron.* Vol. 30. pp. 649–654. 1999.

Roy, A.K., D.L. Fleming, and B.Y. Lum. Stress Corrosion Cracking of Fe-Ni-Cr-Mo, Ni-Cr-Mo, and Ti Alloys in 90 °C Acidic Brine." Proceedings of the CORROSION '98 Conference. Paper No. 157. Houston, Texas: NACE International. 1998.

Russell, A.J. and D. Tromans. "A Fracture Mechanics Study of Stress Corrosion Cracking of Type 316L Austenitic Steel." *Metallurgical Transactions.* Vol. 10A. pp. 1,229–1,238. 1979.

Sakai, T., K. Aoki, T. Shigemitsu, and Y. Kishi. "Effect of Lead Water Chemistry on Oxide Thin Film of Alloy 600." *Corrosion.* Vol. 48. pp. 745–750. 1992.

Sanderson, G. and J.C. Scully. "The Stress Corrosion of Ti Alloys in Methanolic Solutions." *Corrosion Science.* Vol. 8. pp. 541–578. 1968.

Schutz, R.W. "Stress Corrosion Cracking of Titanium Alloys." *Stress Corrosion Cracking: Materials Performance and Evaluation.* Materials Park, Ohio: ASM International. pp. 265–297. 1992.

Scully, J.C. "The Function of Hydrogen in Stress Corrosion Crack Propagation." *Supplement to Transactions of JIM.* Vol. 21. pp. 581–588. 1980.

Scully, J.C. and D.T. Powell. "The Stress Corrosion Cracking Mechanism of α-Titanium Alloys at Room Temperature." *Corrosion Science.* Vol. 10. pp. 713–733. 1970.

Scully, J.R., J.A. Van Den Avyle, M.J. Cieslak, and C.R. Hills. "Hydrogen Assisted Cracking of Palladium Modified PH 13-8 Stainless Steel." *Hydrogen Effects on Material Behavior.* Warrendale, Pennsylvania: The Minerals, Metals, and Materials Society. pp. 755–764. 1990.

Silcock, J.M. "Nucleation and Growth of Stress Corrosion Cracks in Austenitic Steels with Varying Ni and Mo Contents." *Corrosion.* Vol. 38, No. 3. pp. 144–156. 1982.

Simbi, D.J. "Stress Corrosion Cracking of Titanium and Its Alloys in Halide Containing Environments—A Mechanistic Review." *Corrosion Reviews.* Vol. 14. pp. 343–374. 1996.

Smith, J.A., M.H. Peterson, and B.F. Brown. "Electrochemical Conditions at the Tip of an Advancing Stress Corrosion Crack in AISI 4340 Steel." *Corrosion.* Vol. 26. pp. 539–542. 1970.

Speidel, M.O. "Stress Corrosion Cracking on Stainless Steels in NaCl Solutions." *Metallurgical Transactions.* Vol. 12A. pp. 779–789. 1981.

———. "Stress Corrosion Crack Growth in Austenitic Stainless Steel." *Corrosion.* Vol. 33. pp. 199–203. 1977.

———. "Stress Corrosion Cracking in Fe-Mn-Cr Alloys" *Corrosion.* Vol. 32. pp. 187–190. 1976

Sridhar, N. and G.A. Cragnolino. "Stress-Corrosion Cracking of Nickel-Base Alloys." *Stress Corrosion Cracking.* R.H. Jones, ed. Metals Park, Ohio: ASM International. pp. 131–179. 1992.

Sridhar, N. and D.S. Dunn. "Effect of Applied Potential on Changes in Solution Chemistry Inside Crevices on Type 304 Stainless Steel and Alloy 825." *Corrosion.* Vol. 50, No. 11. pp. 857–872. 1994.

Sridhar, N., G.A. Cragnolino, and D.S. Dunn. "Experimental Investigations of Failure Processes of High-Level Waste Radioactive Waste Container Materials." CNWRA 95-010. San Antonio, Texas: CNWRA. 1995

Sridhar, N., J.C. Walton, G.A. Cragnolino, and P.K. Nair. "Engineered Barrier System Performance Assessment Codes (EBSPAC) Progress Report." CNWRA 93-021. San Antonio, Texas: CNWRA. 1993.

Staehle, R.W. *Theory of Stress Corrosion Cracking in Alloys.* J.C. Scully, ed. Brussels, Belgium: North Atlantic Treaty Organization. pp. 223–288. 1971.

Staehle, R.W., J.J. Royuela, T.L. Raredon, E. Serrate, C.R. Morin, and R.V. Farrar. "Effect of Alloy Composition on Stress Corrosion Cracking of Fe-Cr-Ni Base Alloys." *Corrosion.* Vol. 26, No. 11. pp. 451–486. 1970.

Tamaki, K., S. Tsujikawa, and Y. Hisamatsu. "Development of a New Test Method for Chloride Stress Corrosion Cracking of Stainless Steel in Dilute NaCl Solutions." *Advances in Localized Corrosion.* NACE–9. Houston, Texas: NACE International. pp. 207–214. 1990.

Wang, Z.F., C.L. Briant, and K.S. Kumar. "Hydrogen Embrittlement of Grade 2 and Grade 3 Titanium in 6% Sodium Chloride Solution." *Corrosion.* Vol. 54. pp. 553–560. 1998.

Wanhill, R.J.H. "Aqueous Stress Corrosion in Titanium Alloys." *British Corrosion Journal.* Vol. 10. pp. 69–78. 1975.

Young, L.M., P.L. Andresen, and G.M. Gordon. "The Probabilistic Nature of Environmental Cracking in Candidate Waste Package Materials." Proceedings of the Tenth International Conference on Environmental Degradation of Materials in Nuclear Power Systems—Water Reactors. Paper No. 109. Houston, Texas: NACE International. 2001.